Academic Year 2021 DISSERTATION

A universal failure rate calculation method for single event burnout in high power semiconductor devices

Srikanth Gollapudi

Graduate School of Life Science and Systems Engineering
Kyushu Institute of Technology
2-4 Hibikino, Wakamatsu-ku, Kitakyushu, 808-0196, Japan

A dissertation submitted for in partial fulfilment of the requirements
for the degree of Doctor of Philosophy in Engineering

Acknowledgement

This thesis has become a reality with the kind support and help of many individuals. I would like extend my sincere thanks to all of them for the contribution both directly and indirectly.

With immense pleasure and deep sense of gratitude, I wish to express sincere thanks to my supervisor Prof. Ichiro Omura for introducing me to the world of semiconductors. It was only due to his motivation, enthusiasm, immense knowledge, and valuable suggestions that has helped me all the time of research and writing of this thesis. I could not have imagined having a better advisor and mentor for my Ph.D. study. I am deeply thankful and blessed to get a chance to work under his guidance.

I express sincere thanks to my thesis committee members, Prof. Tsuyoshi Hanamoto, Prof. Kazuhiro Toyoda, and Prof. Shyam S. Pandey for the encouragement, insightful comments and the patience in reading my draft dissertation. I am thankful to their suggestions in making dissertation more effective.

My heartfelt thanks to Prof. Shyam S. Pandey for introducing me to Prof. Ichiro Omura, which ultimately helped me in getting into Omura laboratory. Moreover, thank you so much for being the pillar of support for all Indian students in Kyutech in all means. I am also very thankful to my M.Tech supervisor Prof.R.K.Srivastava, IITBHU for the continuous encouragement and great support.

I wish to express my sincere thanks to Ms. Miyo Iwahori for being supportive, helpful and part of every step of the way in all these three years in the laboratory. Your help and motivation for my family during all difficult times helped me hugely.

I express my sincere thanks to Neelima mam for the unconditional support in all aspects of life especially during hard times. It is only because of your support that made us feel safe and secure.

I would like to thank my friend Dr. Atul Mani Tripathi for introducing me to Prof. Shyam S. Pandey and Kyutech. I like to acknowledge the support rendered by my colleagues Prof.

Abstract

Power semiconductor devices are susceptible to catastrophic failures when exposed to energetic particles present in cosmic radiation. The most serious failure mechanism is single event burnout (SEB). SEB in terrestrial operating condition is a widely recognized problem due to the usage of high Power semiconductor devices in many terrestrial applications. However, the recent increase in the aircraft power requirement and subsequent demand for high power semiconductor devices in avionics indicates the importance of expanding SEB study to higher altitudes. Moreover, the SEB failure rate in avionic system is many times higher than terrestrial electronics due to the increase in cosmic ray flux at high altitudes. The calculation of SEB failure rate of power devices plays critical role in power device selection to make the system robust against cosmic radiation. The failure rate calculation using modeling approaches is very easy and offers many advantages compare to real life tests and accelerated tests. However, empirical formula proposed by Zeller from the accelerating testing result can only be applicable to evaluate the failure rate at sea level. In this research, a universal failure calculation method is proposed to evaluate the failure rate of any high power semiconductor device. Unique feature of decoupling between failure cross section and cosmic ray flux spectrum in the proposed method makes it possible to calculate the failure rate in any radiation condition like terrestrial conditions, aviation altitudes, space environment etc. The failure rate results shown for PiN diodes of 100 μm (1) and 300 μm (3) due to the interaction of cosmic ray neutrons up an altitude of 60 km.

First chapter provides the basic introduction about purpose of this work, the research objectives and importance of proposed failure rate calculation method.

Second chapter describes the origin of radiation along with the radiation environment. The interaction of radiation with the matter and in particular the discovery of Single Event Effects in electronic integrated circuits is discussed. Moreover, we discussed the reason for considering the cosmic ray neutrons in the present work.

Third chapter presents the literature review about energetic particle interaction with the high power semiconductor devices. The phenomena leading to device destruction also discussed in various power devices in detail.

Fourth chapter describes the Single Event Burnout simulation of PiN diode. The physical process leading to the failure is shown for 300 μm and 100 μm PiN diode using the simulation results. The transient current waveforms are shown to differentiate the burnout and non-burnout situations.

Fifth chapter introduces the proposed universal failure rate calculation method. Various components of the failure calculation method are discussed in detail. The threshold charge for device destruction obtained from simulation results is shown for 300 μm and 100 μm PiN diode.

Sixth chapter presents results obtain from the proposed method. The calculated failure rate at sea level is validated with the Zeller results. Further, altitude dependent failure rate up to 60 km is obtained using the neutron spectrum from EXPACS database. In addition, the cutoff energy dependence on failure rate also briefly discussed.

Table of Contents

1 Introduction

Power semiconductor devices evolved as key components of all power electronic systems after the initial replacement of vacuum tubes by the solid-state devices in 1950s. Power semiconductor devices became a crucial part in many applications ranging from consumer, industrial, medical and transportation sectors etc. and estimated that they control around 50% of total electricity used in the world.

During early nineties, a new failure mechanism observed in high voltage power devices used in railway applications. A catastrophic failure of device occurred due to this failure. Investigation on this indicated that terrestrial cosmic radiation particles are the cause of this failure. After the discovery of cosmic ray induced catastrophic failure in power devices, the power electronic community has started giving attention to cosmic ray ruggedness of power devices during the system design stage. This catastrophic failure of the devices happens during the blocking condition of the device. When the high energetic particle of cosmic radiation interacts with the device, it generates electron-hole pairs along the path. During the conduction state of the device, these extra charge carriers do not affect the device. However, in the blocking state, the plasma of charge carriers shields its interior from electric field. The voltage drop occurs at pronounced electric field spikes at the edges of plasma. When these electric field spikes exceeds the critical electric field of the device material, leads to further generation of carriers due to impact ionization. This phenomena results in a destructive mechanism in power devices called Single Event Burnout (SEB).

SEB in terrestrial operating condition is a widely recognized problem due to the usage of high Power semiconductor devices in many terrestrial applications. However, recently electrically signaled control system replaces the relatively heavy mechanical and hydro mechanical control systems in aircrafts. Therefore, the electric power usage in aircraft has reached 1 MW in recent Boeing 787. The weight reduction priority of the aircraft along with the increased electric power demand encourages the use of increased bus voltage and there by high power semiconductor devices in avionics. This suggests the necessity of expansion in SEB failure study of power semiconductor devices from terrestrial electronics to avionics.

Earlier inflight experiments to observe the device failure shows cosmic ray neutrons present in the atmosphere plays key role in device upsets. The intensity of neutron flux changes with altitude and reaching a maximum between 15 km to 20 km, called Pfotzer maximum where the neutron intensity is 300 times higher than sea level. Therefore, the sensitivity of SEB failure is many times higher in avionics compare to terrestrial electronics.

It is very important to know SEB failure rate in high power semiconductor devices operating in terrestrial electronics and avionics. The knowledge of failure rate helps the design engineers in choosing the semiconductor device rating in particular operating radiation condition to sustain from SEB failure. The failure rate usually measured in FIT. One FIT corresponds to a failure in one billion hours of device operation.

There are different approaches to calculate SEB failure rate.

- The Real life testing is conducted by exposing the power semiconductor devices to actual radiation. This method gives the precise results due to actual operating environment. However, huge number of devices have to be tested for very long time to obtain the failure rate.

- The ground radiation testing is conducted using accelerating testing facilities to obtain the failure rate very quickly compare to real life testing methods. However, the limitation of flux spectrum of radiation facility, difference in the facility spectrum compare to actual radiation environment along with limited experiment facility poses some disadvantages of this method.

- The failure rate calculation using failure-modeling approach is very easy and offers many advantages compare to above methods. Zeller has proposed a phenomenological method to calculate failure rate using device parameters. However, this empirical formula proposed by Zeller from the accelerating testing result can only applicable to evaluate the failure rate at sea level.

Therefore, this demonstrates the requirement of an easy mathematical approach to calculate the failure rate not only at terrestrial radiation conditions but also at high altitude radiation environments.

2

1.1 Objectives of thesis

- Develop a cosmic ray induced failure calculation method applicable to all kinds of power devices used in terrestrial, aviation and space environments without any fitting parameters

- Introduction of new formulation in the proposed method so that the method is applicable to any radiation environment.

- Simulate the SEB failure phenomena of 100 μm and 300 μm PiN diode using Sentaurus TCAD and obtain threshold charge for device destruction. Which is the failure criteria of proposed method.

  - ➤ Calculate the failure rate of 100 μm and 300 μm PiN diode due to the interaction of sea level neutrons using the proposed method and validate the results with Zeller empirical method

  - ➤ Calculate the failure rate of 100 μm and 300 μm PiN diode due to the impact of cosmic ray neutron up to an altitude of 60 km

  - ➤ Evaluate the under estimation factor of failure rate due to the maximum cutoff energy limitation of neutron spectrum in accelerated testing facilities.

2 Radiation and its effects on Electronics

In this chapter, the discovery of cosmic radiation and its interaction with the semiconductor material are discussed in detail. The initial discovery of single event effects in microelectronic circuits due to the interaction of cosmic ray particles also discussed. Moreover, of the cosmic ray particles, neutrons show significant effects on the operation of semiconductor devices.

2.1 Discovery of radiation

The history of cosmic rays would not have started without the understanding of electric and magnetic phenomena, and the phenomena of radiation. The scientific theory of electrical and magnetic phenomena was developed at the end of 18th century and in the 19th century by many researchers, such as Coulomb, Volta, Ampere, Oersted, Ohm and Faraday etc. Finally, in 1865, James Clerk Maxwell established the mathematical framework referred to as classical theory of electromagnetism.

The theory of electromagnetism provided the mathematical tools to investigate related phenomena such as radiation at the end of 18th century by H. Herz, P. Lenard and W. Roentgen. Initially it was considered as form of electromagnetic radiation predicted by Maxwell, but soon it showed different properties so that it required the better understanding of properties.

In 1785, Charles Augustin de Coulomb reported that the torsion balance electrometer invented by him discharges spontaneously due to the action of air rather than defective insulation. This was later confirmed by M. Faraday and W. Crookes and further improved the experiment. The reason for the discharge was known to be caused by some sort of radiation that ionizes the air inside the electroscope, but the source of this radiation was unknown.

H. Hertz conducted series of experiments during 1886 to 1889 to discover electromagnetic waves and his student P. Lenard expanded this experiments only focusing on cathode rays. Wilhelm Roentgen used photographic plate while experimenting with cathode tubes and found X-rays in 1895 [1]. A year later, Henri Becquerel investigated further Roentgen rays using photographic plate and found penetrating radiation emitted by uranium salts. This was a new form of radiation with different properties than X-rays. The continuation of this work by Pierre and Marie Curie lead to discovery of radioactivity and showed the ionization of air due to the radiation emitted by radioactive elements.

The simplest explanation of Coulombs observation of discharge in electroscope at that point was due to ionization of air by the radiation emitted by radioactive elements. The other possibilities were that it originates from atmosphere or it has some extra terrestrial source, which was predicted by Nikola Tesla in his patent about the method of utilizing radiant energy in 1901.

2.2 Search for source of radiation

In the beginning of 20th century, Julius Elster and Hans Geitel conducted series of measurments by isolating the electroscopes with thick metal box, where again they observed the same phenomena and lead to the conclusion that the radiation has high penetrating power.

Until then, it was believed that the radioactive elements in the Earth causes the discharge in electrometer. Further, radioactive radiation is absorbed in the air. Hence, the intensity decreases with the distance of its sources. In order to investigate the dependence of radiation on altitude, in 1909, Theodor Wulf developed most precise electrometer and conducted the experiments at 300 meter elevation of the Eiffel tower. Unknowing the fact that the metal of the tower also contribute to radioactivity, unfortunately his measurements were inconclusive regarding whether radiation decreases or increases with the altitude.

In order to confirm the Earth`s crust as the source of radiation, Dominico Pacini conducted series of experiments on and below the sea surface. If radiation coming from Earth`s crust, the body of water should reduce the radiation intensity of radiation by absorption. The radiation on the surface of sea did not show any reduction of intensity of radiation and observed 20 % decrease in discharge at 3 m depth in water compare to surface. From these experiments, he concluded that radiation was coming from above and was penetrating in water.

The first experiments using balloon flight was conducted by Albert Gockel by ascending to 4500 meters above sea level. He found no decrease in ionization rate with altitude as expected and confirmed the Pacinis conclusion. Finally, balloon flights conducted by Victor Hess in 1911 and 1912 up to 5000 meters gave enough precise experimental results. His results shown a small decrease in intensity of radiation in the first few hundred meters above the earth surface. Increase in intensity observed at high altitudes and at 5200 meter, the intensity was measured to be higher than at surface. From these results, Hess concluded that the radiation was of extraterrestrial origin. For this experiment, Victor Hess has won the Nobel Prize in 1936. Later these experimental results were confirmed by Kolhorster even at higher altitudes up to 9300 meters.

In 1926, Mallikan and Cameron carried out absorption measurements of radiation at various depths in lakes at higher altitudes. Based on absorption coefficient and altitude dependence of radiation, they concluded that the radiation was high-energy gamma rays and they shoot through space equally in all directions and named them "Cosmic rays". However, the conclusion was proved to be wrong but the name styed to this date.

2.3 Natural radiation environment

When the semiconductor devices exposed to natural radiation, it results in failure during certain operating environments. In order to understand the effect clearly, it is essential to know the environment of cosmic radiation. A primary distinction of radiation can be made between space and atmospheric ones.

2.3.1 Space radiation environment

Space radiation characterized by wide range of particles that generated due to several radioactive phenomena.

The cosmic rays in space are divide in to follwoing categories.

➢ **Sun Activities**: Solar flares and coronal mass ejections (CMEs) are the main components of this. Solar flares seen as sudden brightening in the photosphere near sunspots. They result in intense release of energy involving tearing and reconnection of strong magnetic fields lines. They are the largest explosive events of solar system. Large increase in solar wind density in the interplanetary space is observed immediately after the occurrence of solar flares because the energy released from solar flares accelerated the particles in the solar plasma to higher energies. CMEs occur in the layers outside the sun in photosphere and chromosphere and release approximately 1017 grams of plasma into interplanetary space.

➢ **Solar wind**: In the suns outer atmosphere, the corona extends several solar diameters in to planetary space. This corona continuously emits a stream of protons (95%), electrons (<1%), doubly charged helium ions (~4%) and small amount of heavy ions, collectively known as solar wind.

➢ **Galactic Cosmic Radiation (GCR)**: The GCR originate outside solar system and contains ions of all elements of the periodic table and the composed of protons (83%), alpha particles (13%), electrons (3%) and other heavier nuclei. The flux levels of

galactic cosmic rays are hazardous to spacecraft electronics because their energies make them extremely penetrating. The Earth`s magnetic field provides some protection from galactic cosmic rays by deflecting the particles as they arrive in magnetosphere.

➢ **Earth`s magnetosphere**: The interaction of solar wind and its associated magnetic field with the earth's magnetic field defines the Earth`s magnetosphere. The lower boundary of the magnetosphere is ionosphere and the upper boundary is magnetopause. As the charge particles in the solar wind move around the earth, some of the particles cross Earth`s magnetic field lines and leak in to magnetosphere. Some particles trapped by the Earth`s magnetic field and contribute to the formation of Van Allen belts. Others collect in the magneto tail and create poles of opposite charges, producing generator that transport particles along magnetic field lines at the poles. The particles trapped in the near Earth`s environment composed of protons, electrons and heavy ions. These trapped particles pose significant threat to electronics.
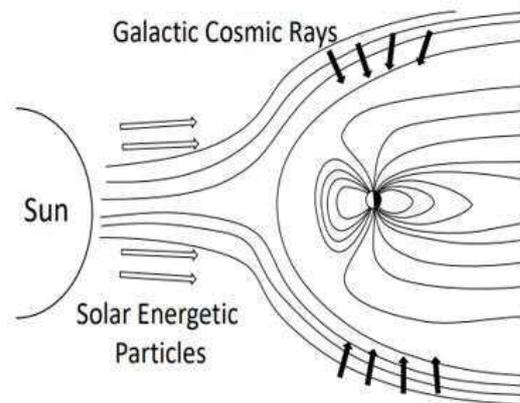
Figure 2-1: Sources of Ionizing radiation

2.3.2 Atmospheric radiation environment

The atmosphere shields the most of the space radiation. When cosmic rays and solar particles enter the Earth`s atmosphere, they are in fact attenuated by interaction of oxygen and nitrogen atoms in the atmosphere. This results in secondary particles and further attenuation due to interactions. The products of cosmic ray showers are protons, electrons, neutrons, heavier ions, muons, and pions. In terms of most effective particles to cause, upsets in electronic circuits are

neutrons. They are measurable at an altitude of 330 km and their density increases with decrease in altitude reaching a maximum at altitudes between 15 km to 20 km called Pfotzer maximum. Below this altitude, the intensity decreases and at ground, the neutron density is 1/300 of the peak flux. The knowledge of neutron levels comes from balloon, aircraft and ground based measurements. The energy of neutrons in the ground level reach hundreds of MeV.

2.4 Discovery of Single Event Upsets (SEU)

In the year 1962, Wallmark and Marcus predicted that cosmic rays would start upsetting the microelectronic circuits when the feature size becomes small[2]. Later in 1975, Binder, Smith, and Holman of Hughes Corp., observed the upsets in digital flip-flops circuits in space satellites[3] and claimed that the upsets were due to cosmic rays in the iron group. In 1978, for the first time upsets were observed at sea level in dynamic RAMs by May and Woods[4] and concluded that upsets were due to alpha particles emitted from trace amounts of thorium and uranium that used to fabricate the electronic devices. In 1978, Pickel and Blandford developed a model to predict cosmic ray bit error rate in NMOS RAMs used in satellite memory[5]. The upsets were explained to be due to cosmic rays in iron and aluminum groups.

In 1978, for the first time the upsets were observed in dynamic RAMs due to the nuclear reaction of energetic neutrons and protons[6]. It was the first that the field of SEUs (Single Event Upsets) started. Also in 1979, McNulty et al. reported soft errors due to the nuclear reaction induced by proton[7]. For the first time in 1979, the upset experiments conducted on static RAMs with heavy ions from accelerator facility and cosmic ray latch up observed in the devices[8].

The single event effects in high power devices were observed for the first time in Power MOSFET in 1986. The subsequent literature of single event effects high power devices is discussed in chapter 4.

2.5 Interaction between radiation and matter

When the solid material interacts with the radiation, the local properties of the material changes due to the deposition of energy by the radiation in to the material. The type of the interaction depends on various parameters such as mass, charge, kinetic energy of the particle or the mass, charge and density of the target material. When the energetic particles such as protons, neutrons and heavy ions interact with the semiconductor devices, various failures occurs ranging from degradation to the catastrophic failure.

When an energetic particle interacts with matter, they lose part or whole energy through different mechanisms. The most important mechanism is electronic stopping. It refers to electromagnetic scattering of particles through elastic collisions between the particles and the field of atomic electrons in the material. This causes excitation of electrons in the target atoms and results in direct ionization. However, the electrons remain in same position because the energy transfer is lower than the energy required releasing it from the bond between the atom and its neighboring atoms. However, the imparting particle continue its path in the target material until all of its energy is lost in creating the ionizing track of electrons and holes pairs.

The parameter used to characterize the penetration of particles in to material is the average energy (E) lost per unit length (-dE/dx), which is termed as stopping power or stopping force. The variation of this mostly commonly used is the mass stopping force, called Liner Energy Transfer (LET) and is defined as the average energy deposited by imparting particle in the target material per unit length and is shown in equation 1.

$$LET = -\frac{1}{\rho}\frac{\partial E}{\partial x} \qquad (1.1)$$

Where ρ is the density of target material. The unit of LET is MeV.cm^2/mg.

LET depends on both the nature of particle and density of target material like silicon. The value of LET of various ions inside any target material can be calculated by Stopping and Range of Ions in Matter (SRIM) developed by Ziegler [9]. the Monte Carlo based FLUKA [10] and Geant4 [11] also can be used to calculate LET.

9

The typical shaper of LET along the ion track is as shown in Figure 2-2. This shows the amount of ionization created by the incoming particle along its path in the material[12]. The figure clearly indicates that most of the energy is deposited near the end of the track called Bragg peak. Due to the slowdown of the particle in the matter due to the loss of kinetic energy, it gets sufficient time for energy loss, so the rate of energy loss increases.
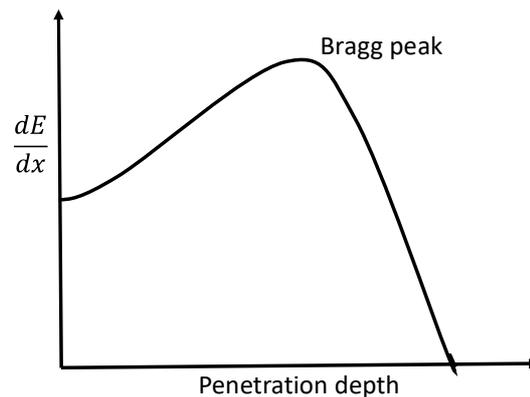

Figure 2-2. Bragg curve showing the variation of dE/dx with particle penetration depth

On the other hand, if the incoming particle interacts with the atomic nucleus of target material, the results in nuclear interactions, which takes place for neutrons, protons and heavy ions. Nuclear reactions divided mainly in to three categories: elastic scattering, inelastic scattering, and transmutation.

In an elastic collision, the incoming particles imparts some of its energy to atom of the target material. This atom dislodges from its position if the imparting energy is greater than energy required for displacement (approximately 25 eV for most materials). The dislodged atom is referred as primary recoil and the recoiling nuclei along with other fragment travels through the semiconductor material, losing energy along its via stopping force and cause secondary ionization of the material.

During inelastic neutron or proton collision, the energetic particle is captured by the nucleus of the target. As a result, the nucleus is left in an excited state and returns to normal state by the emission of gamma ray. Inelastic collision can also cause dislocation of target atom.

The transmutation involves the capturing of incident proton or neutron by the target nucleus and subsequent emission of another particle such as proton or alpha particle. The remaining

10

atoms is thereby transmuted, i.e., converted in to another element. The nature of reaction products depends on target material. For example, when a proton or neutron interacts with silicon, they can generate a variety of different ions ranging from hydrogen to phosphorous.

2.5.1 Useful terminology

In order to explain the effects of radiation on electronics, it is essential to introduce some fundamental definitions that are commonly used.

➢ Absorbed dose: it measures the amount of energy absorbed by the target material per unit mass. The absorbed dose is measured in *Gray* and sometimes in *rad*.

1 Gray (Gy) = 1 Joule/kg.

1 rad=0.01 Gy.

Absorbed dose does not indicate the rate of occurrence or type of irradiation.

➢ Range: This describes the distance travelled by the energetic particle in the target material before losing all its energy. This depends on the type of the target material (density) and the type, and energy of the particle. Range is calculated based on the initial energy of the particle and the energy lost per unit length in the material.

➢ Flux: this gives the rate of incidence of particles in a material. The unit of measurement is particles/cm^2/sec.

➢ Fluence: the time integral of flux over a period measured in Particles/cm^2.

2.6 Overview of radiation effects on electronics

The effects of radiation on the behavior of electronic components or systems is divided into two main categories: Cumulative and stochastic events.

Cumulative effects are gradual events that takes place during the entire lifetime of device when exposed to radiation environment. The electronic devices exhibit the failure when the total accumulated fluence reaches the device tolerance limit. Cumulative effects are demonstrated via two ways: Total ionizing Dose Effects and Displacement Damage Effects.

On the other hand, the stochastic events are the single event effects. Which causes change in the behavior of electronic devices or systems because of passing of single energetic particle.

2.6.1 Total ionizing dose effects

These are cumulative radiation effects caused by the ionization of insulating film used in semiconductor devices. Therefore, MOS devices undergoes this effect due to the presence of silicon dioxide film and results threshold voltage shift and degradation in channel mobility. Here, the process leads to TID effect in n-channel MOS device is explained[13]. When the gate is positive biased, an electric field is created along the gate oxide and an inversion layer of minority carriers formed below Si-SiO$_2$ interface as shown in Figure 2-3. The time dependent response of the device to radiation is explained below.
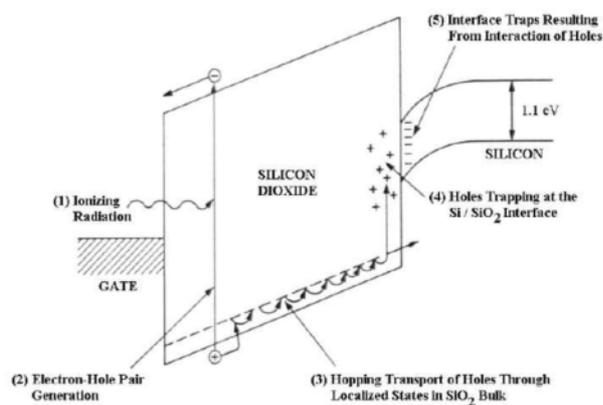

Figure 2-3: Total Ionizing effect in MOS structure[13]

1. Radiation causes the creation of e-h pairs in SiO$_2$. Some of them recombine immediately. Due to the presence of electric field, some of the electrons swept out of oxide and are collected by gate electrode. Due to the lower mobility of holes, they appear relatively immobile. Because of hole accumulation, a smaller gate voltage is required to create the inversion layer of electrons, thus results in threshold voltage shift.

2. Holes starts to move slowly toward Si-SiO$_2$ interface. This stochastic, hopping transport of holes happens over milliseconds to seconds depending on the temperature, applied field and oxide thickness.

3. When the holes reach the Si-SiO$_2$ interface, the bulk silicon collects some of them. However, some of them are captured by deep, long living trap states. These trapped holes causes voltage shift that can persist for hours to years.

4. The radiation induced traps right at the Si-SiO$_2$ interface. These traps are localized traps with energy levels in the Si bandgap and it is observed that they are negatively charge. These interface traps highly dependent on oxide processing.

The main effects of TID on behavior of MOS devices is that the threshold voltage is majorly affected. The threshold voltage shift occurs in both n-channel and p-channel MOS devices. In P-channel case, the buildup of positive charge in gate oxide requires higher negative voltage to be applied to gate in order to create inversion layer. On the other hand, in case of n-channel, the buildup of positive charge makes it easy to create inversion layer, resulting in lower threshold voltage as the radiation dose is increased. Lastly, the mobility of the channel degrades due to TID, which is mainly evident at high ionizing dose. This is caused by the presence of both trapped oxide charge near Si-SiO$_2$ interface and interface states that leads to additional scattering of carriers when transported along the channel.

2.6.2 Displacement Damage Effects

Displacement Damage (DD) effects also cumulative radiation effects that relates to dislodging of lattice atoms from their original position when energetic particles interaction takes place. DD effects due to neutrons are particularly important because they do not interact directly with electrons in the target material; instead, they lose their energy through nuclear reaction. After the atom dislodge, the recoiled atom and the scattered primary particle continue to lose energy in the material, resulting in cascade of secondary displaced secondary atoms. Displacement damage mainly affect the silicon body of bipolar and MOS devices. However, the effects on MOS devices significant for fluence above 10^5 neutrons/cm^2. The displacement effects in bipolar devices mainly results in degradation of bi polar gain and lifetime.

A minimum of 25 MeV energy deposition in nucleus is sufficient to dislodge an atom from the original positon. The absence of an atom in its actual lattice position is called vacancy, while the dislodged atom stops and occupies non-lattice position called interstitial. A region contains a relatively closely spaced defects is called defect cluster. The presence of disturbance in lattice periodicity introduces new energy levels in the bandgap, which alters the electrical properties of the device. The effects of presence of radiation induced defect centers in the silicon bandgap are summarized as:

1. Generation of e-h pairs through a level close to mid gap. Which results in increase in leakage current in silicon device.

2. Recombination of electron hole pairs, where the defect captures a carrier of one polarity, followed by the capture of carrier with opposite polarity. Which causes reduction in lifetime of minority carriers and results gain degradation in bi-polar transistor.

3. Temporary capture of carriers at a shallow level, results in transfer inefficiency in charge coupled devices.

4. Compensation of donors or acceptors by the radiation induced defects results in reduction of majority carrier concentration. This causes increase in internal resistance of the device.

5. Tunneling of carriers through potential barrier by means of defect levels. This defect assisted or trap assisted tunneling process results in increase of device currents.

2.6.3 Single Event Effects

Single Event Effects (SEE) are stochastic effects, which causes perturbation in device behavior due to the interaction of single energetic particle. When an energetic particle interacts with a device, it deposits part of or all of its energy through direct or indirect ionization and generates column of electron-hole pairs along its track in the material. SEEs usually happens in reverse biased p-n junctions of the devices, where, due to the presence of high electric field, the electron hole pairs moves in opposite direction instead of recombining. Finally, these e-h pairs collected into circuit nodes in the form of transient currents and initiates the failure mechanisms. Depending on the variety of parameters related to both device technology and irradiation condition, the caused failures distinguished as soft failures or hard failures.

➢ **Soft SEEs**: These are non-destructive in nature that can be reset by applying correct signal to the device. The most commonly observed soft SEEs are:
  ➢ Single Event Upsets (SEUs): These related to a bit flip in digital storage elements such as memories and flip flops when interacted with single particle. The charge induced by the energetic particle introduces changes in the charge stored on the nodes (capacitors) of the storage element. This leads to change in logic state of the element and change in the value of bit. This event does not cause any damage to the element and the changes can be re written with the right value.
  ➢ Multiple Cell Upset (MCU) and Multiple Bit Upsets (MBU): it is possible that a single particle can upset multiple cells in a digital storage element. Lateral

diffusion of charge deposited by the energetic particle is responsible for multiple cell upset. The diffused charge is collected by the sensitive volumes around the strike location results in corruption of bit information. Multiple Cell Upsets (MCU) occur when two or more bits corrupted. If these corrupted bits belongs to same logical word, then is termed as Multiple Bit Upset (MBU). MBUs are more dangerous because Error Correction Code (ECC) no longer works properly when the number of errors in same word exceeds the limitation of the ECC.

➢ Single Event Transient (SET): This is a short tem voltage spike results from the electric field separation of charge generated by a particle passing through or near a circuit junction. This voltage pulse may propagate in analog, digital or mixed mode circuitry, competing with the legitimate signal flow. This propagating voltage pulse does not involve in state change, so one can differentiate between SET and SEU.

➢ **Hard SEEs**: These failures are destructive in nature and usually related to increased current through the device, which is sufficient for metal traces to vaporize, bond wires to fuse open, and silicon regions to melt due to thermal runaway. The most commonly observed hard errors are:

➢ Single Event Latch up (SEL): This catastrophic failure mechanism affects multilayered pnpn structures such as thyristors or CMOS technologies. An interconnected two-transistor model demonstrates simple model of SEL phenomena. In this, the collector current of each transistor feed the base current of the other. In such structure, an increase in pnp collector current gives an increase in the npn base current. This in turn increase the collector current of npn and thereby the base current of pnp.

Any event of turning on any of the transistor due to a particle strike, if this positive feedback gain of thyristors pnpn is high enough, then parasitic BJT structures can trigger the latch up. Thereby, a low resistive path is developed between power supply and ground terminal of the device which remains even after the removal of triggering event. So, once latched high current condition will remain until the removal of the power supply or catastrophic failure of the device.

The use of current monitoring circuit allows removal of the power supply immediately after initiation of latch up to protect the devices against thermal destruction.

➢ Single Event Burnout (SEB): This is observed in high power semiconductor devices such as MOSFET, IGBT, and Diode etc. during the reverse biased condition. In case of MOSFET and IGBT, the current transient induced by the energetic particle turns on the parasitic transistor inherent to the device. At this point, a regenerative feedback mechanism is initiated which causes an increase in current until the device destruction. However, different phenomena observed in power diode for destruction due to the absence of bipolar transistor. Ion induced charge multiplication due to avalanche phenomena is the main cause of failure in case of power diode.

➢ Single Event Gate Rupture (SEGR): This is observed in Power MOSFETs when energetic particles pass through neck region and creates conducting path in gate oxide during the off state. These particle-induced charges creates dangerously high electric fields across dielectric. If it exceeds a critical value, a localized gate rupture occurs. Once this happens, current flow through the gate oxide to poly silicon of gate and results in thermal runaway, locally melting of silicon, poly silicon and dielectric.

2.7 Dominance of neutrons on single event effects

The atmospheric radiation environment that affect the operation of power devices consists of neutrons, protons, muons and pions. They are generated due to the interaction of galactic cosmic rays, which are 83 % protons, 16 % alpha particles and 1% heavy ions[14] with the atmospheric atoms that consists of nitrogen (78%) and oxygen(21%)[15]. Every cosmic ray creates showers of secondary due to this interaction and generates further cascades that results in complex radiation environment. The created secondary cascades do not continue to increase in number as they penetrate earth atmosphere because there is also absorption processes. Pions have a mean lifetime of nanoseconds and muons have microseconds. Therefore, they decay spontaneously. Therefore, neutrons are the main particles that trigger the failure in high power semiconductor devices, as they indirectly ionize the atoms inside the device by nuclear reaction.

Atmospheric neutrons have been identified as main cause of SEEs at elevated altitudes[16]. They extend in energy more than 1000 MeV. The neutrons in the atmosphere vary with both latitude and altitude. The altitude variation is resulted from various production and removal processes. This results in maximum neutron flux at about 60000 feet, called Pfotzer maximum. The sea level neutron flux is several hundred times lower than that in Pfotzer maximum.

The atmospheric neutrons appeared to follow a form that combines both exponential and trigonometry with altitude[17]. During 1988 and 1989, IBM flew a series of proprietary experiments on three different flights in which upsets observed in 64-k static RAMs. A few years later, IBM and Boeing carried joint research sponsored by Defence Nuclear Agency (DNA) and Naval Research Laboratory (NRL). This study confirms the SEUs in avionics and measured inflight failures correlates with the atmospheric neutron flux as shown in Figure 2-4 and Figure 2-5.
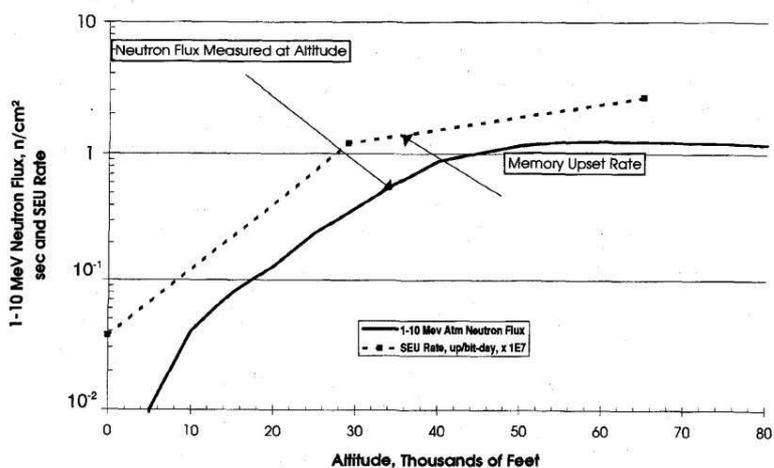

Figure 2-4: correlation of SEU rate in IMS 1601 RAM with atmospheric neutron flux as function of altitude[16]

Attributing the in-flight upset rates to neutrons based on several factors. From the upset data available, Taber and Normand, plotted the measured upset data against altitude and latitude. These upset rates correlated with atmospheric neutron curves as function of altitude and latitude and shows good agreement. The inflight upsets as function of altitude and latitude directly following the variation of neutron flux with altitude and latitude. From this, it is clear that atmospheric neutrons are dominating in causing the upsets in electronics.
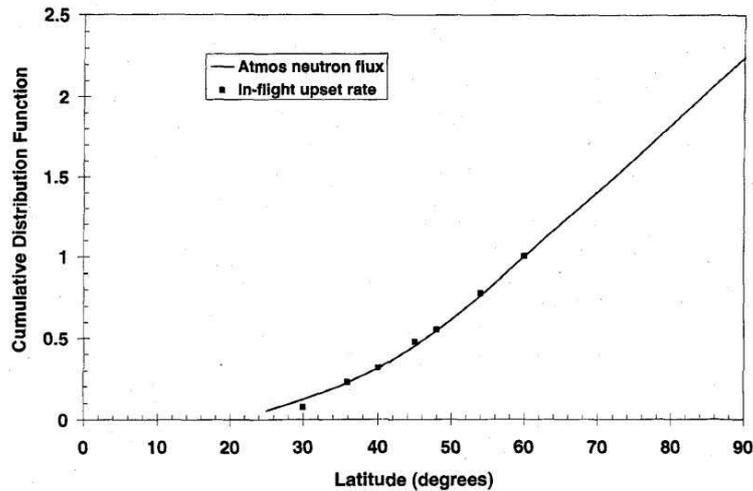
Figure 2-5: Correlation of upsets in IMS 1601 RAM with atmospheric neutron flux as function of geographic latitude[18]

An early study also showed that when large number of memory devices monitored for single event upset at three different locations with varying altitudes, the upset rate observed to decrease with elevation, indicating that atmospheric neutrons are main cause for the upsets in the devices.

2.8 Notable neutron spectrum measurements in atmosphere

Two sets of bonner spheres spectrometers are primarily involved in the measurement of secondary neutron spectrum. One is the de facto Japan standard Bonner sphere spectrometer[19] and the other is that used in the National Aeronautics and Space Administration (NASA) ER-2 project[20], [21].

The notable neutron spectrum measurements in 1990s are the NASA ER-2 program and the life testing at New York as measured by International Business Machines (IBM). One of the main aim of NASA ER-2 programs is to characterize the dosage of atmospheric cosmic radiation to aircrews. ER-2 High Altitude Airborne Science Aircraft intensively flew the bonner sphere spectrometer to 65000 feet altitude, where there is a peak atmospheric neutron flux. The measurements provided valuable scientific data to many further projects. For instance, the data was used to verify the predictions of QinetiQ Atomospheric Radiation Model (QRAM) [22] and useful conclusions were given by Goldhagen et al.[20], [21]. At high altitudes, geometric latitude observed to have little effect on the shape of neutron spectrum, but it strongly effects the flux density. The shape of the spectrum varies slightly at high altitude (12 km to 20 km) , but there is

18

significant difference at sea level. Three peaks (at 10^{-8} MeV, 1 MeV, and 100 MeV) were observed in the spectrum at sea level, but the thermal neutron peak in the spectrum is not observed at high altitudes.

The spectrometer was used at IBM T.J.Watson Research Center for 10 months to measure neutron spectrum at New York[23]. The spectrum measured at New York become part of the JEDEC JESD89A standard.

Many experiments conducted in Japan and Germany using Bonner sphere spectrometer to measure the neutron spectrum. In Japan, Nakamure et al.[24] and Kowatar et al.[25] have measured the spectrum at several different altitudes on a mountain. The neutron spectra at different altitudes of mountain were found to have similar shape.

The PTB Neutron MUltisphere Spectrometer (MEMUS) of Wiegel and Alevra is an extended Bonner sphere spectrometer with 16 spheres from 3 inch to 18 inch diameter[26]. Four out of 16 spheres were loaded with high Z-material to obtain good response at high energy. A battery powered version of this spectrometer which relying on four C-sized batteries that can operate for 7 days was also introduced. This enables the measurement of neutron flux spectrum at remote locations.

2.9 Conclusion

In this chapter, the discovery of cosmic rays and its interaction with the semiconductor is discussed in detail. Moreover, the first identification of single event effects in microelectronic circuits is discussed along with the other effects caused by cosmic rays on semiconductors. In the next chapter, the effects induced by the cosmic rays in high power semiconductor devices is discussed.

3 SEB in High power semiconductor devices

The previous chapter presents the discussion about the history of research on cosmic ray discovery and the effect caused by cosmic ray particles on microelectronic circuits and computer memories. Finally, neutrons were observed to be most dangerous particles in triggering the failure in semiconductor devices. In this chapter, the destructive phenomena of single event effect in high power devices discussed. Traditionally the static blocking capability of the power devices is limited by the avalanche breakdown phenomena. However, failures in power devices observed for voltages much lower than their breakdown capability. The reason for the failure was attributed to the cosmic rays present in the atmosphere. This failure is destructive in nature and termed as Single Event Burnout (SEB).

3.1 Literature review on SEB of Power MOSFET

For the first time in 1985, a destructive latch up effect was observed in several n-type Power MOSFETs from different manufacturers[27] during the experiment conducted by exposing the devices to fission flux from Cf-252, and the destructive failure observed in the devices when the drain to source voltage exceeds about 50% of the power device blocking capability. The failure was attributed to the turn on of parasitic transistor. During the heavy ion exposure of IRF 150 transistor, Burnout was observed in the drain region of a single cell [28]. It was estimated in 1987 that, some 300 IRF 150 type MOSFETS were using in ten spacecraft in orbit. However, there were no reports of or-orbit failures due to SEB in these devices due to harder parts being used in the space qualified units [29].

Nondestructive heavy ion experiments conducted for the first time in 1987 by Oberg et al.[30] and Fischer [31]using a technique of limiting current with a series resistor removing power within 1 μs of detecting high current condition. This allows the usage of single part for multiple experiments. Oberg et al. observed the decrease the threshold drain to source voltage with increase in LET of the heavy ion. Also observed the decrease in failure cross section with increase in angle of incidence of heavy ion except when V_{DS} is above the threshold. In 1987, Richter et al. demonstrated that simulation of SEB is possible in silicon using focused laser beam as long as there were optically sensitive regions in the device[32]. The experiment was conducted on IRF 120 n-MOSFETs using a pulsed Nd:Yg laser at 1060 nm wavelength with

>700 μm penetration depth in silicon. The results from this experiments in comparison with previous results from Oberg et al. [30].

Several researchers developed the models to understand the physics of single event burnout. Nondestructive heavy ion experiments to observe the drain current were conducted by Fisher[31] on n-channel and complementary p-channel MOSFETs of similar rating. The thermal runaway of the device was prevented by controlling the power available to the device by setting the value of input capacitor. The results indicated that, N-channel devices failed at V_{DS} corresponding to 22% to 90% of rated breakdown voltage, while P-channel devices did not undergo any failure. This is consistent with a model for current induced avalanche (CIA) leading to secondary breakdown developed by Wrobel et al[33].

In a model developed by Hohl and Galloway [34] determined the electric field intensity in the lightly doped epi-layer as the main contributor for SEB sensitivity. A dense plasma of electrons and holes were generated when the heavy ion strikes through the source (emitter) region of the device. Electrons flow to the drain (collector) region while the excess holes swept in to the p-body (base) diffusion. These excess holes while move through p-body (base) spreading resistance to ground contact a voltage drop develops that forward biases the parasitic base-emitter junction formed by the p-body and source junction. Due to this, further injection of electrons into lightly doped epi region occurs. This causes increase in electric field due to further generated holes through avalanche multiplication. Apparently, the current in the epi-layer increases generatively until the device enters second breakdown and thermal runaway.

Hohl and Johnson[35] explored effect of change in electric field intensity on single event burnout(SEB). It was observed that, with increase in collector current, the peak electric field moves from near the base-collector junction to the epi-substrate with a rapid increase in hole generation at this location. This is consistent with the current induced avalanche model proposed by Wrobel [33].

The investigation of power MOSFET hardening against SEB was carried by Titus et al.[36]. The approach was to reduce the NPN bipolar action by suppressing turn on, reducing peak electric field in the epi region. They demonstrated the devices that do not undergo burnout until 94% of V_{DS} and with additional changes; devices were not susceptible to SEB with ions up to 63

MeV-cm^2/mg. This improvement came with some reduction in electric performance i.e. a 20-time increment in on resistance.

For the first time in 1991, Titus et al. [37] experimentally verified the SEB in bipolar transistors. Due to the presence of lightly doped epitaxial structure similar to MOSFET, avalanche mechanism has initiated the SEB. Moreover, the threshold voltage is observed to be below BV_{CEO}, which until then considered as highest safest operating condition for bipolar transistors.

In the early 1990s, SEB research continued to investigate the effect of heavy ion range on SEB sensitivity. Stassinopouols et al. showed SEB at fixed bias depends on the charge along the ion track and not just on the surface LET of the ion[28]. Moreover, the charge generation at least up to the epi substrate junction leads to single event burnout. In addition, it was found that heavy ion energy dependence on critical charge to device burnout, with high-energy ion having lower threshold than low energy ion with similar LET. Meanwhile, kuboyama et al.[38] conducted experiments to measure the critical charge to device destruction using charge sensitive pre-amplifier and pulse height analyzer similar to that used in ion beam charge collection experiments[39], [40]. Critical charge along with the dimension of device sensitive volume are key to estimate the failure rates in space environments. The critical charge (Q_{th}) stays constant under any condition that cause SEB. This indicates it depends only on the device design and not the operating conditions or heavy ion.

Power devices using Silicon Carbide (SiC) have shown improved characteristics in high voltage and high temperature applications than Silicon. Therefore, research carried out towards SiC hardening against cosmic radiation. Hiroaki Asai et al. tested 1200 V SiC MOSFETs from different manufacturers by exposing to white neutron irradiation[41]. The results shows the SEB probability increases exponentially with applied voltage. The Monte Carlo simulation shows the energetic carbon and alpha particles have enough range to pass the whole drift region and cause punch through breakdown that resulted in increased SEB cross section in SiC power devices.

Witulski et al. investigated the heavy ion induced Single event burnout mechanism in 1200 V SiC Power MOSFET[42]. The threshold voltage for initiation of burnout observed to decrease significantly for particles with Linear Energy Transfers greater than 10 MeV/cm^2/mg. TCAD simulation confirms turn on mechanism of parasitic transistor drives avalanche mechanism

similar to silicon MOSFET. The heavy ion experiments by Ball et al. suggests ion induced, highly localized energy pulses responsible for catastrophic failure in 1200 V SiC Power MOSFET with lower energy pulse responsible for device degradation[43]. A 3D TCAD simulation identifies a resistive shunt effect capable of generating very high-localized current and subsequent high energy dissipation during the ion interaction.

Qiumei Li etc al. performed 2-D simulations of SEB failure mechanism in SiC VDMOSFET. The results shows large transient current initiates the burnout of the device[44]. The magnitude of the transient current related to Liner Energy Transfer (LET) and the operating voltage of MOSFET. The middle of gate found to be the sensitive region in the device.

Investigation of SEB mechanism on 650 V SiC Double Trench MOSFETs by Zhou etc. showed the very low threshold voltage at high LET[45]. Moreover, Single Event Gate Rupture (SEGR) observed to be more severe in SiC DT-MOSFET.

Accelerated neutron irradiation experiment carried out by Martinella et al. on different commercial SiC power MOSFETs with planar, trench and double trench architecture[46]. Enhanced gate drain leakage observed in some devices without any destruction. In particular, planar and trench devices shown partial gate rupture whereas complete gate rupture observed in double trench architecture.

3.2 Literature review on SEB of Power IGBT

McDonald et al. measured the destructive single event effects on three different IGBTs from Omnirel, Infinion and semikron with rated voltage from 600 V to 1200 V[47]. Even though all devices experienced SEB and SEGR, the estimated events in geosynchronous orbit were quite small. Which enables the usage of these devices in many applications.

Shoji et al. performed white neutron irradiation experiments on IGBT and observed the sharp increase in failure rate when collector voltage increasing beyond threshold voltage[48]. This was attributed to the latch up of parasitic thyristors by the onset of impact ionization at n^- drift $/n^+$ buffer junction. Moreover, it was experimentally confirmed that the threshold voltage could be controlled by designing bipolar gain through increasing n-drift thickness.

Zerarka et al. investigated the new design of planar IGBT aimed at improving SEB robustness against cosmic radiation[49]. The TCAD simulation results shows, addition of deep

23

P$^+$ diverter region in the IGBT cell significantly increases the threshold voltage to trigger the burnout. The reduction in hole current moving under emitter effectively reduced the failure rate of the new structure compared to the conventional.

Foro et al., reported the first evaluation of 1200 V trench gate field stop IGBT susceptibility to 50 MeV, 80 MeV, 150 MeV and 180 MeV quasi energetic neutrons[50]. They used rectangular parallelepiped sensitive volume (RPP) in which critical charge deposited leads to the failure. This was justified by the fact that space charge region of P-well and N$^-$ epi layer supports all the electric field thus considered as a sensitive volume.

3.3 Literature review on SEB of High voltage power diode

During the early 1990s, European and Japanese manufacturers observed some field failures of high voltage power devices used in train engines[51], [52]. These includes GTOs and diodes that were rated 4500 V that developed to operate for >35 years at 50-60% of the rated voltage in terrestrial applications.

A salt mine experiment was conducted to investigate the failure mode[51]. The voltage stress experiment conducted at 4000 V with 18 diode of 4500 V rating with 6.5 cm diameter at three different altitudes. In the first phase, experiment conducted at top floor laboratory with tin roof and six failures observed over a period of 700 device-hr as shown in Figure 3-1. In the second phase, the devices tested in a salt mine with 500 feet below ground, and no failures of the devices observed over 7000 device-hr. In the third phase, experiment conducted again at top floor laboratory, and three failure recorded in 300 device-hr as in phase 1. In the last phase, diodes tested in basement, and two failures recorded in 1000 device-hrs. From these observations, naturally occurring cosmic rays found to be the reason for failure of devices in train engines.
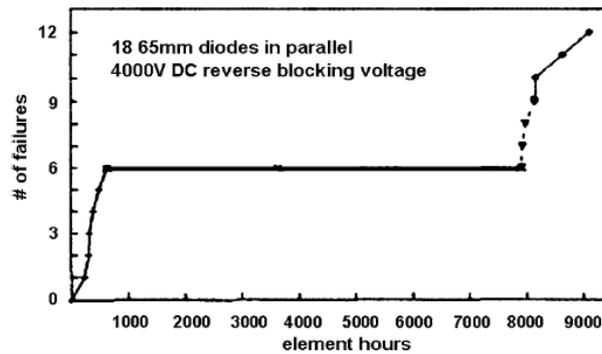
Figure 3-1: Results of salt mine experiment showing device failure rate vs time[51]

Similar experiment conducted in japan using GTOs operating at 4300 V with different concrete shielding configurations[52]. In this case, a decrease in failure rate observed with GTOS when the concrete shielding changed from 0 feet to 6.7 feet.

In the same year in 1994, ABB semiconductors measured the failures in GTOs , diodes and thyristors rated 2.5 kV and 4.5 kV[53]. The failure consists of localized breakdown in the bulk of the device and the failure has occurred within few nanoseconds without any precursor. The study has shown that the direct energy deposition from the high-energy particle could not induce the device burnout unless there is particle-induced nuclear reaction leading to high local electric field sufficient for impact ionization. The authors predicted the applied voltage of the device and the n-base resistivity of the device are the phenomenological parameters for estimating the failure rate of the device.

The failure phenomena in Power diode believed to be different from MOSFET due to the absence of inherent BJT as in case of MOSFET. Peter Voss et al., reported the heavy ion experiments of high voltage power diodes with blocking voltage ranging from 4500 V to 6000 V with C12 ions[54]. Even the heavy ion could initiates the failure only if it undergoes nuclear collision with lattice atom. Once interaction happens, a self-supporting multiplication phenomena is initiated which depends on location of the collision and the field strength in the vicinity. The failure probability is highest at the PN junction where the electric field is maximum.

After knowing the catastrophic failure of power devices due to the nuclear reaction of cosmic ray particles and subsequent formation of cascade of heavier ions such as silicon and aluminum, many irradiation experiments with heavy ions [55], [56] were conducted to approach the failure

25

experimentally. Irradiation experiments with protons[57] and neutrons[58] have also produced the burnout failure in power diodes.

High-energy neutrons with spectrum similar to atmosphere were observed to induce the failure in High voltage power devices for operating voltages as low as 50% of rated voltage. Eugene Normand et al., conducted neutron irradiation experiment on 4.5 kV disk diodes at Weapons Neutron Research facility at Los Alamos National Lab[59]. The measured failures were in close agreement with the field failures measured by Kabza et al., in Europe[51].

Avalanche multiplication believed to be the reason for the initiation of device burnout. To confirm this, Maier et al. investigated the charge multiplication phenomena by nondestructive charge measurement using charge sensitive preamplifier[56]. For this, a 4 kV diode was irradiated by 90 MeV Kr ions to observe the collected charge spectrum shown in Figure 3-2. For the voltages below 850 V, a single peak corresponding to the charge deposited by the heavy ion was observed. This peak broadens and shifts to higher charge with increase in voltage. Maier et al. interpreted this shift as slight amplification of collected charge and incomplete charge collection at low voltage. At 875 V, a second peak appears because of avalanche multiplication at high electric fields. The charge corresponding to second peak is over twenty times than that of charge in first peak. The charge in second peak increases with voltages due to avalanche multiplication at high electric fields. The diminishing of first peak at 1100 V indicates all incoming charge undergoes avalanche multiplication.
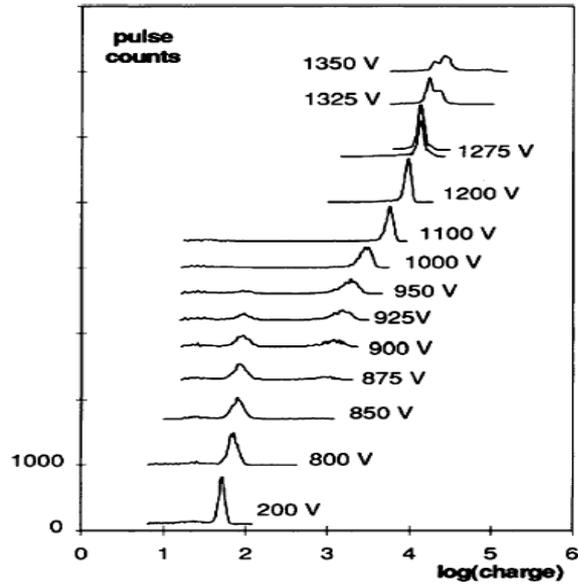
Figure 3-2: Charge spectrum of 4 kV diode due to bombardment of 90 MeV Kr ions showing number of events as function of total generated charge[56]

Similar charge multiplication observed for the same diode irradiated also with Si and C ions of different energies. Maier et al. also reported that charge amplification onsets suddenly at a threshold voltage as shown in Figure 3-3. The amplification triggered at low voltage for Kr irradiation, however the avalanche multiplied charge is only two to ten times the ion deposited charge. The amplification started at higher voltages (1500-1800V) when irradiated with Si ion and avalanche multiplied charge is 100 to 1000 times higher than ion deposited charge. Nearly similar results obtained for 17 MeV C ion and 13.5 MeV Si ion. Interestingly the amplification triggered at higher voltage when 17 MeV C ion incident at an angle 30^0 compared to 90^0. These results indicated that threshold voltage for the onset of amplification depends on the type of the ion, its energy, its angle of incidence on the device and the impact location on the device. The track of the ion in the direction of electric field and the impact location at high electric field region are most effective to charge multiplication at lower threshold voltage.
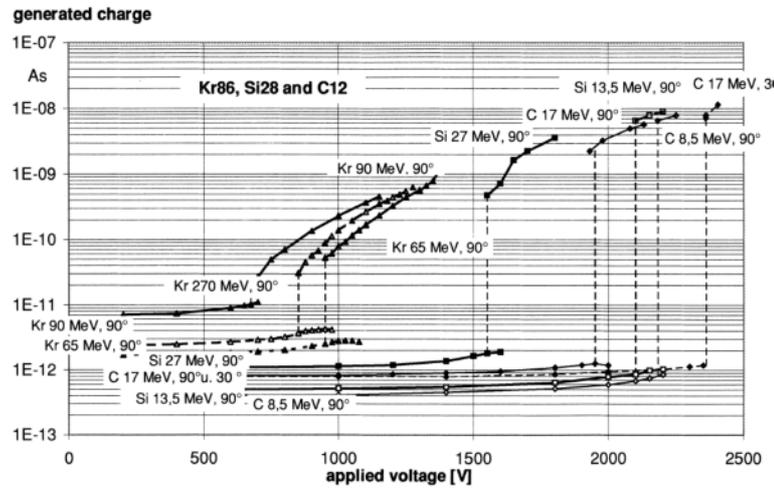
Figure 3-3: Avalanche multiplication summary of 4 kV diode irradiated with Kr, Si, C showing generated charge as function of applied voltage [56]

Busatto G et al., reported completely different results of charge multiplication triggered at low voltage for lower energy [55]. However, this effect is attributed to different penetration depth of heavy ion in diode. The Bragg peak for 108 MeV ions is at 38 μm (Electric field of 100 kV/cm) while it is 60 μm (Electric field of 80 kV/cm) for 156 MeV ions as shown in Figure 3-4. The avalanche multiplication maximized when the Bragg peak occurs at maximum electric field position. This indicates the burnout of power devices depends on the charge induced in the high electric field region rather than total deposited charge by heavy ion.
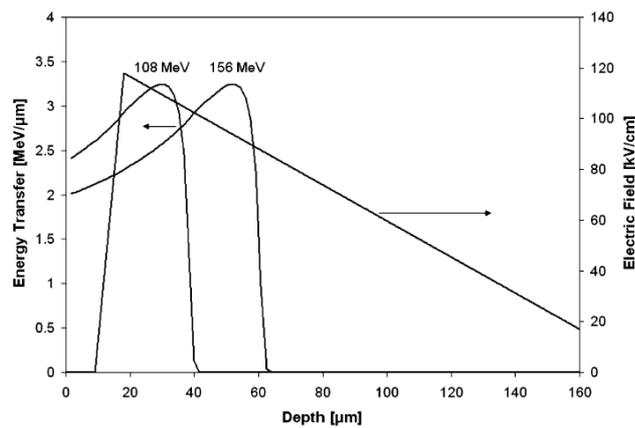
Figure 3-4: LET of silicon ions at 108 MeV and 156 MeV inside silicon crystal along with electric field[55]

Research progress to analyze the current waveforms of the diode during destruction to understand the physical mechanism for device burnout[57], [60]. Hallen et al. done experiments on 2.7 kV diode at Uppasala tandem accelerator using 30 MeV C ions to investigate the effect of ion fluence on failure occurrence[60]. A fluence of 10^6 ions has not resulted in device failure when operating at 1.8 kV. However, a fluence of 10^4 ions itself resulted in failure at 2 kV, which was observed by sudden increase in current. The experimental results with various ion fluence at different operating voltages showed that only few incident ions are sufficient to induce the device failure at high voltages.

Soelkner et al. using magnetic probe measurement and direct measurement detected current waveforms in a 4 kV power diode irradiated with 70 MeV protons[57]. An initial current pulse of 4 A due to avalanche multiplication was flown by sharp rise in current after 100 ns as shown in Figure 3-5. The second rise of current indicates the device destruction. Moreover, they investigated the temperature dependence on the onset of charge multiplication in 4 kV diode in the range of 22^0C to 120^0 C for 17MeV C12 irradiation. The onset voltage for carrier multiplication increased over 20% for the considered temperature range. This is because; the impact ionization coefficients are temperature dependent, which decreases with temperature because of reduction in scattering length of the carriers. Therefore, the probability of device burnout decreases with temperature.
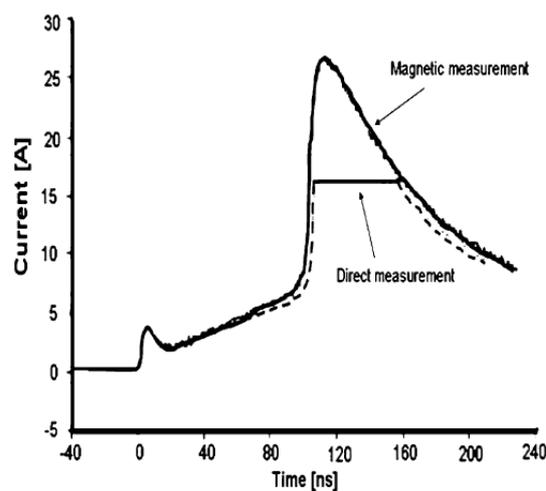
Figure 3-5: Current signal during destructive event in 4 kV diode with 70 MeV proton irradiation[57]

29

Numerical simulation is very useful to model the electrical characteristics of semiconductor devices. Moreover, transient simulations certainly helpful in understanding the time dependence of mechanism leading to device burnout. A 2-D simulation is mostly carried out because a dense mesh along ion strike and very small temporal steps in 3-D simulation leads to very long computing times. Electrical characteristics during SEB are obtained by solving poison's equation along with continuity equation for holes and electrons. The impact ionization model plays crucial role in describing ion-induced breakdown.

First attempts of modeling SEB of power devices using numerical simulation was by Kabza et al[51]. They performed simulation of cylindrical diode by depositing radiation-generated carriers along the center axis of the diode. The transient simulations shown two peaks of output current. The first peak corresponds to charge collected from the radiation deposited charge and the second peak corresponding to avalanche generated charge. After that, current goes back to zero because of absence of destructive part of the event in the model considered.

The simulation model by kaindl et al[61] focused on temporal and special evolution of electric field and electron current density along the particle track. They performed cylindrical symmetrical simulation of 3.5 kV diode for 17 MeV C ion when the device operating at 1900 V and 2000 V. the spatial and temporal distribution of electric field is shown in Figure 3-6 along the axis of symmetry. The electric field peak moves throughout the device while electron density expands in response to the ion strike. In case of 1900 V, the electric field diminishes with time means there is no avalanche multiplication and non-destruction of power device. Therefore, the collected charge corresponds to ion deposited charge alone. However, in case of 2000 V, the electric field peak moves from anode to cathode causing significant avalanche multiplication of charge carriers. This is similar to second break down in power diode in response to the application of high voltage pulse[62]. In this case, the electron density becomes large throughout the diode indicates the initiation of device destruction.
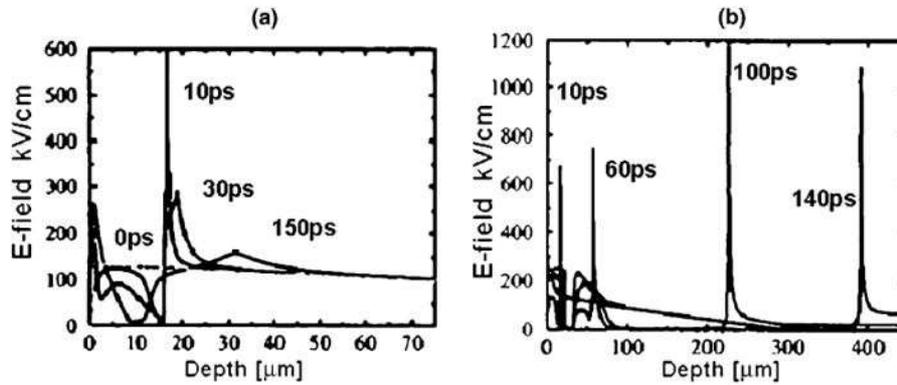
Figure 3-6: Spatial and temporal distribution of electric field in 3.5 kV diode due to the impact of 17 MeV C ion at a) 1900 V   b) 2000 V [61]

Kaindl et al. also performed simulation study to identify the robustness of diode structure against energetic particles. They carried out the simulation of PT and NPT structure of the diode and results confirms PT diodes are more robust against cosmic radiation over NPT diodes.

Albadri et al. performed non isothermal simulation to observe the electrical and thermal effect on device burnout[63]. A 3500 V power diode exposed to 17 MeV C ions when operating at high voltages ($\geq$ 2700 V). Occurrence of high temperature around melting point of the constituent material of diode identified as the reason for the actual failure of the device. Moreover thermal effects plays crucial role in describing the failure mechanism prediction.

Silicon Carbide (SiC) has improved characteristics than Silicon at high voltage and high temperature applications of power device. Hiroaki Asai et al. evaluated the variation in SEB tolerance of 600 V SiC diodes from two different manufacturers by exposing the devices to neutron irradiation at Research Center for Nuclear Physics at Osaka University[64]. The neutron tolerance is different by an order of magnitude for two manufacturers. Monte Carlo simulation results indicates the secondary carbon from nuclear reaction plays crucial role in initiating the burnout mechanism in SiC diodes.

Tomoyuki Shoji et al. performed white neutron irradiation experiments on SiC power diodes at RCNP facility and observed rapid increase in temperature leading to the formation of crown shaped aluminum[65]. The SEB simulation results indicates peak temperature located at n^-/n^+ junction and anode contact where hammock shaped electric field is observed due to space charge effect. Moreover, the peak temperature location in simulation closely agrees with the destruction

location observed in irradiation experiment. The simulation results also shows the failure mechanism in SiC power diode is similar to that of Si power diodes.

3.4 SEB failure phenomena in Power MOSFET, IGBT, Diode

Power devices subjected to burnout phenomena during blocking operation. High number of charge carriers are deposited in the device due to the interaction of energetic particle. During the forward bias condition, these charge carriers does not affect the operation of power device. However, during the blocking condition, the high electric field present the power device causes movement of charge carriers in opposite direction instead of recombining. While doing so, the charge carriers shields its interior from the electric field resulting in the appearing of peaks in the electric field. If this peak electric field exceeds critical electric field of device material, then impact ionization is initiated and further charge carriers are generated. The power devices that contain the pn-junction are most sensitive to burnout phenomena.

SEB initially observed in Power MOSFETs, and the failure attributed to the turn on of parasitic transistor that is inherent to the MOSFET structure. The Single Event Burnout later observed in IGBTs and the phenomena for failure in IGBT was similar to the MOSFET. Subsequently, the high voltage power diodes failures observed in 1994 in railway applications[51], [52]. However, the mechanism of failure in Power diode is not same as MOSFET or IGBT because of absence of inherent bipolar structure. The structural similarity of MOSFET, IGBT and PiN diode shown in Figure 3-7. In this section, we will analyze the failure mechanism of different devices due to the interaction of energetic particle.
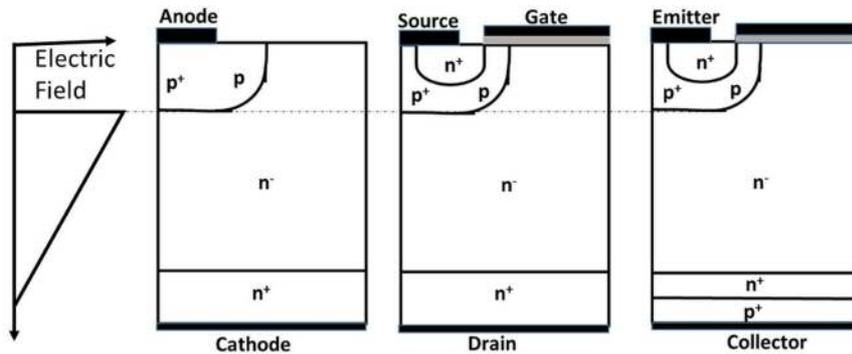
Figure 3-7: Basic structural similarity of PiN diode, MOSFET and IGBT along with internal electric field distribution

3.4.1 Burnout phenomena in MOSFET

When the high energetic particle interact with power MOSFET, electron-hole pairs generated along the track of the particle in the device. During the blocking mode operation, high electric field present in the device. The presence of high electric field separates the charge carriers instead of recombining. Therefore, a current flows due to the movement of the carriers. The holes move towards the source and the electrons move towards the drain terminal and while doing so peaks in the electric field appears. Applying voltage higher than threshold voltage, the formation and propagation of high electric field leads to strong multiplication of ion induced charge carriers. So a highly conductive plasma filament extends from source to drain contact. The charge carriers diffusing out of plasma turn on the parasitic transistor inherent to MOSFET structure. This causes an additional current amplification and subsequent device destruction.

3.4.2 Burnout phenomena in IGBT

The initiation of burnout phenomena in IBGT is similar to that of MOSFET. However, due to the presence of second inherent bipolar transistor in IGBT, the charge diffusing out of plasma filament turns on both the transistors. This results in strong injection of holes from the entire P^+ - emitter in to the drift region. As a result significant hole current density emerging from the entire emitter concentrates towards the cell of IGBT. In contrast, the hole current density is distributed mainly in the track of streamer in case of MOSFET.

3.4.3 Burnout phenomena in Power diode

The power diode operating in the reverse biased condition is prone to failure due to Single Event Burnout. Electric field is supported in the depletion region of the diode. When the high energetic particle interacts with the power device, an electrically neutral plasma is generated along the track of the particle. This charge plasma disturbs the stationary electric field in the device. At the front of plasma, a peak in the electric field is developed. For small voltage, the charge carriers diffuse out of plasma and consequently the electric field peak decreases. The period during which the peak electric field presents is too short for the additional generation of charge carriers by impact ionization. As a result, the charge flowing out of diode is corresponds to charge generated by imparting particle.

A completely different phenomena observed when sufficiently high reverse voltage is applied the diode. At high reverse voltage, a sufficiently higher stationary electric field develops. When the heavy energy particle interacts, the peak in the stationary electric field will be higher than the earlier non-multiplication event. This result in a stable state in which, the peak of the electric field travels through the entire device from anode to the cathode with an undiminished high value. The strong impact ionization caused by this high peak electric field creates highly conductive plasma filament that constitutes short between anode and cathode with a very high current flow. A very high avalanche generated charge of about four orders higher than initial deposited charge of the particle is generated.

3.5 Importance of failure rate calculation

High power semiconductor devices are key components of power electronic systems which used in aerospace, industrial, automation, transportation, renewable energy conversion systems and many other systems which require high reliability. Therefore, power semiconductor devices operates in harsh environment radiation condition. The devices are generally designed to operate near to the breakdown voltage for atlease 25 years. Single event burnout is a catastrophic failure mechanism, which abruptly destructs the device operating in blocking condition. Failure rates are represented in FIT, with 1 FIT corresponds to a failure in billion hours of device operation. Some of the studies have shown that devices operating in avionics should be de rated to 50 % of the maximum voltages in order to keep the failure rate with in the acceptable limits of 100 FIT, the standard set by IEC 62396-2[66] . In addition, a de rating in voltage by additional 10%, improves the cosmic ray rugged ness of the device significantly. Therefore, it is very important

to choose power device for the actual operating voltage of the power device in different radiation environments. Therefore, altitude dependent failure rate calculated in the study gives an overall picture of voltage derating of the power device at different altitudes in order to limit the failure rate with in permissible limits.

Also, power devices that are operating in very sensitive applications, ex. airplane, trains etc. A failure in a particular device results in complete disturbance to the whole system. Therefore, failure rate calculation is very important in the actual operating radiation environment where the device is intended to operate. In the proposed failure rate calculation method, once the failure cross section of the device is known, we can easily calculate the failure rate of the device at any operating condition and there by the derating factor of the device at particular environment to keep the failure rate within limits.

3.6 Conclusion

In this chapter, literature review about the burnout in high power devices is discussed along with the physical phenomena leading to the burnout in detail. Moreover, the importance of failure rate calculation of power device is presented. In the next chapter, we discuss about the simulation of burnout phenomenon in PiN diode in TCAD simulation along with the burnout results in 100 μm and 300 μm PiN diodes.

4 Simulation of Single Event Burnout phenomena of PiN Diode

In this chapter, we will introduce the Technology Computer Aided Design (TCAD) simulation tool for the simulation of PiN diode. Two diode structures are considered for simulation with drift layer thickness of 100 μm 300 μm. The physical process that leads to the device destruction is observed from the simulation results. The results for electric field, electron and hole density profiles after the impact of neutron are shown for non-destructive event and the destructive event, and the transient current profile obtained for different operating voltages due to the impact of energetic neutrons. Finally, generated charge, which is a useful parameter in our proposed failure rate calculation method, is obtained from transient current.

4.1 Introduction to TCAD simulation methodology

Sentaurus TCAD from Synopsys Corporation is a simulation tool used for semiconductor device simulation. It uses finite element method for the characterization of process and devices. This fundamentally finds approximate solution for the boundary value problems that consist of partial difference equations such as diffusion, transport equation etc. The simulated device structure is subdivided into smaller units called finite elements using the meshing algorithm. In each finite element, the equations are solved to find the local state of the element. Finally, the assembly of these elements performed to reflect the complete solution. The simulation of PiN diodes are carried in Sentaurus TCAD from Synopsys Corporation.

The simulation process involves three main steps as shown in Figure 4-1. The initial step is modeling of PiN diode structure using Sentaurus Structure Editor. The simulation of electrical characteristics using Sentaurus Device follows this. The final step is the analysis of results using Sentaurus Visual.

4.1.1 Sentaurus Structure Editor

Sentaurus structure editor is an editor for two-dimensional and three-dimensional structures. The programming language of structure editor is based on scheme like LISP programming language, which differs significantly from conventional programming languages. This language makes it easy to generate parameterized structure for varying design parameters. The process flow of the simulation can be classified into the following steps: generating the device structure,

binding of analytical doping profiles to respective regions, formation of virtual contacts and meshing of device for device simulation.
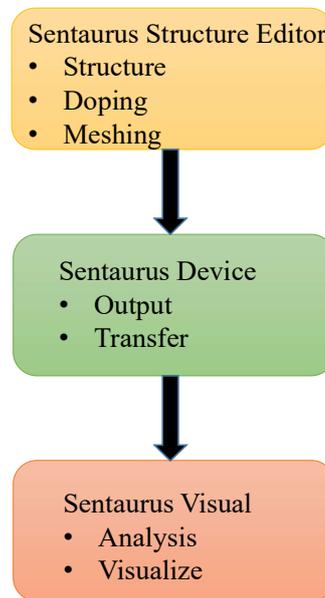
Figure 4-1: Schematic illustrating TCAD simulation process

The two dimensional device structures are formed geometrically using primitives like square, polygon etc. Complex structures can be generated by combining the available primitive elements. The modelling of the structure is similar to making a drawing of the device. Several basic geometrical elements are combined to form the structure. Each of these geometrical elements are also defined in terms of materials Eg. Silicon, nitride, oxide etc.

The Doping distributions are defined using analytical functions. The Sentaurus Structure Editor supports binding of analytical functions or one-dimensional profiles to a refinement window placed on predefined regions. With the virtual contact formation, a virtual pad is formed at the contact regions on the structure based on a placement window.

The final step in the process flow is setting up the meshing configuration for device simulation. The meshing of the device plays crucial role in obtaining the device response close to the actual device. Increasing the mesh density improves the precision in simulation results, however it consumes more time for computation. In general, fine meshing is adapted at position where there is abrupt change in parameters like at the junctions.

4.1.2 Sentaurus Device

Sentaurus Device is a multidimensional, electro thermal, mixed mode device and circuit simulator. It incorporates advanced physical models and robust numerical methods for the simulation. Terminal currents, voltages and charges are computed based on a set of physical device equations that describes the carrier distribution and conduction mechanisms. A real semiconductor device, such as a PiN diode, is represented in the simulator as a virtual device whose physical properties are discretized onto a non-uniform mesh of nodes.

Sentaurus Device simulation is based on semi-classical macroscopic transport models. To solve the transport using semi-classical theory, it requires three coupled equations: the Poisson equation, the continuity equation and the transport equation. Sentaurus Device employs Boltzmann transport equation as the basic theory and uses the Monte Carlo method as a well-established numerical technique to solve the Boltzmann transport equation.

Sentaurus Device solves the device equations, which are essentially a set of partial differential equations self-consistently on the discrete mesh in an iterative fashion. For each iteration, an error is calculated and the Sentaurus Device attempts to converge on a solution that has an acceptably small error. For this, a few settings for the numeric solver is required. This includes selection of solver type and a user defined convergence criterion. For this, a few settings for the numeric solver is required. This includes selection of solver type and a user defined convergence criterion.

4.2 PiN Diode structure and simulated breakdown voltage

In the present work, PiN diode is considered for the simulation, because PiN structure is the basis for all the high voltage semiconductor devices. Two PiN structures of 100 μm and 300 μm length are simulated in the present study. The dimensions and the doping profiles of the 300 μm PiN diode is shown in Figure 4-2 along with the 2D generated meshing of the structure in TCAD simulation. Here only shown 2D simulation because of the huge amount of time considered for simulating with 3D structure. When doing the 2D simulation, the dimension along the Z-axis by default 1 μm. The results for original 3D configuration is obtained from the 2D simulation using the cylindrical command in the Math section of Sentaurus Device. This makes the cylindrical structure for the 2D structure by considering x=0 as the axis of cylinder.
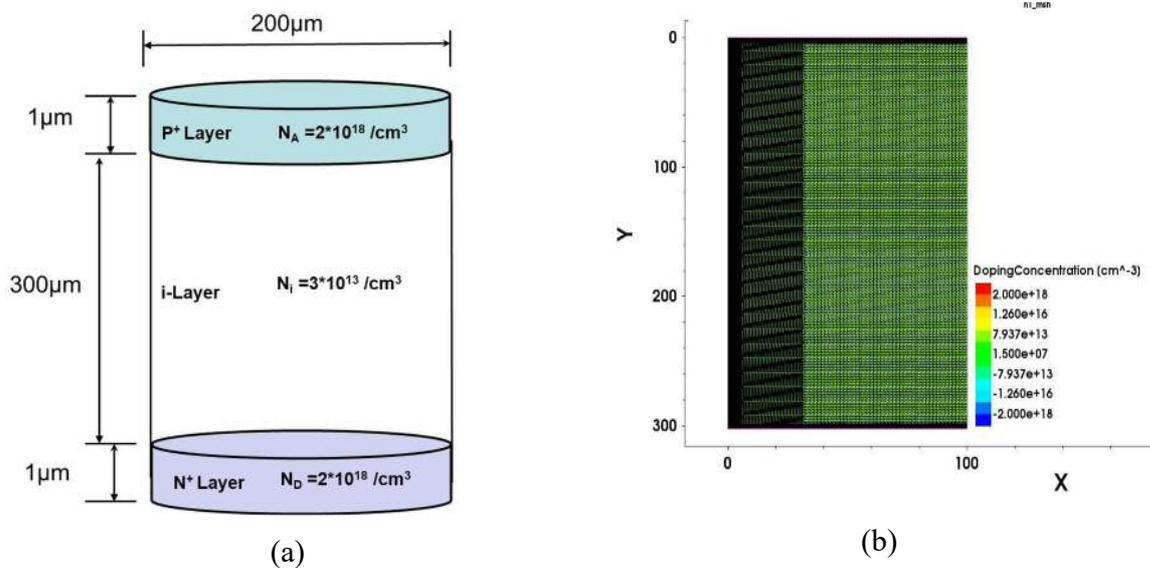
Figure 4-2: a) Schematic structure of PiN diode with 300 μm drift layer b) 2D meshing profile

For the considered 300 μm device, breakdown characteristics are obtained from the simulation and the breakdown voltage obtained as 3 kV as shown in Figure 4-3.
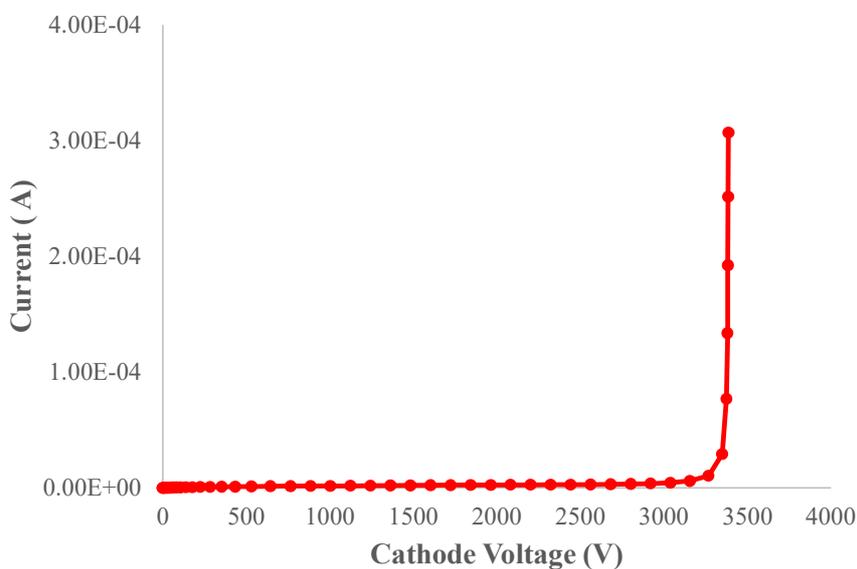
Figure 4-3: Breakdown characteristics of PiN diode with 300 μm drift layer

The dimensions and the doping profiles of the 100 μm drift layer PiN diode is shown in Figure 4-4 along with the meshing profile of the simulated 2D structure.

(a)	(b)
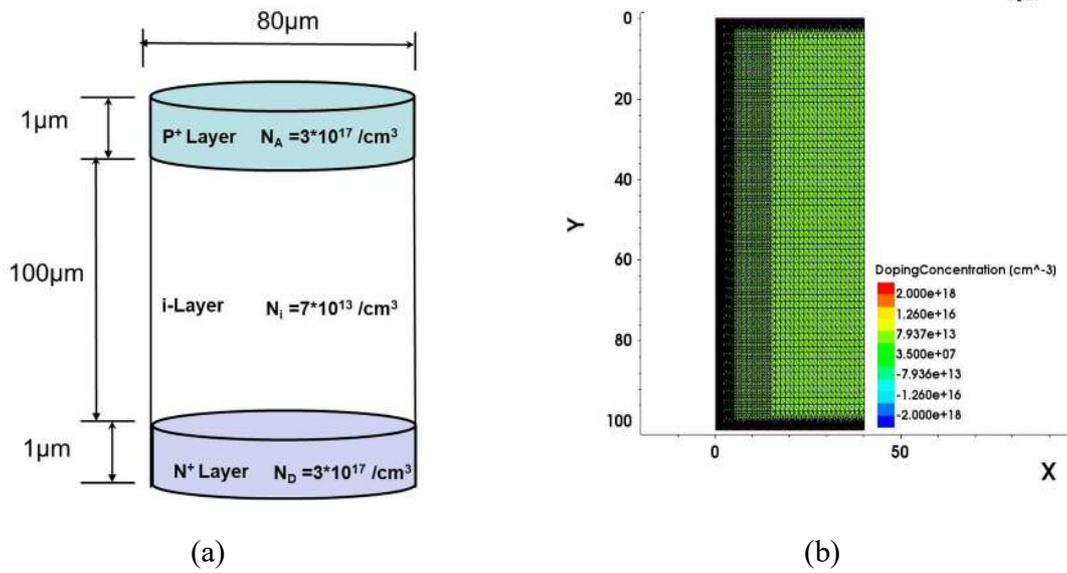
Figure 4-4: a) Schematic structure of PiN diode with 100 μm drift layer b) 2D meshing profile

Similar to 300 μm PiN diode, for the 100 μm PiN structure also simulated to obtain the breakdown characteristics. The breakdown voltage of 100 μm drift layer PiN structure with doping profiles shown in Figure 4-4 is obtained to be 1 kV as shown in Figure 4-5.
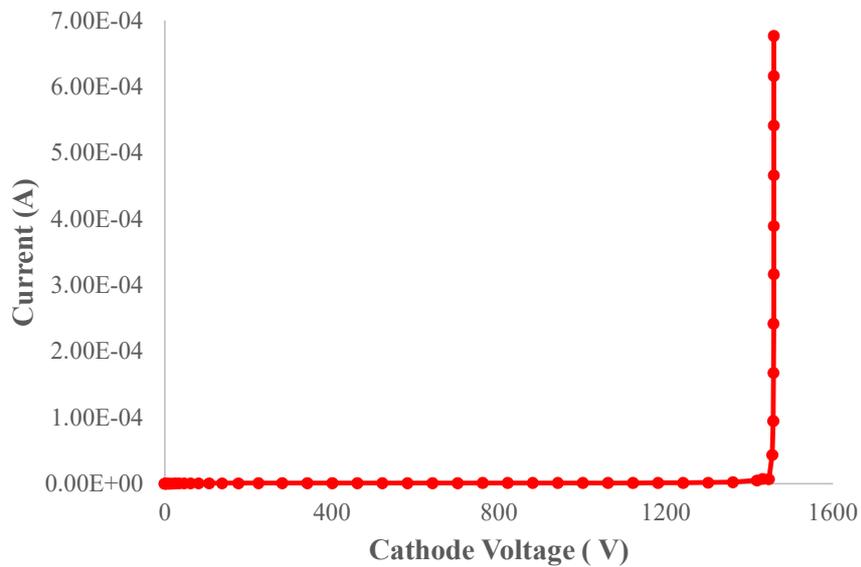
Figure 4-5: Breakdown characteristics of PiN diode with 100 μm drift layer

4.3 Simulation of Burnout phenomena in Sentaurus TCAD

When the high-energy particle of cosmic radiation interacts with the power device, part of incident particle energy is deposited in the device by generating plasma of electron-hole pairs along its path in the device. During the conduction state of device, these extra electron-hole pairs do not affect the device. However, during the blocking state of device, the plasma of charge carriers shields its interior from the high electric field that present in the device. In doing so, the voltage drop occurs at pronounced electric field spikes at the edge of plasma. When the electric field spikes exceeds the critical electric field of the device material, the subsequent impact ionization results in generation of further electron-hole pairs. This is self-sustaining process, and a streamer is developed between anode and cathode with in nanoseconds and device destruction takes place as shown in Figure 4-6.
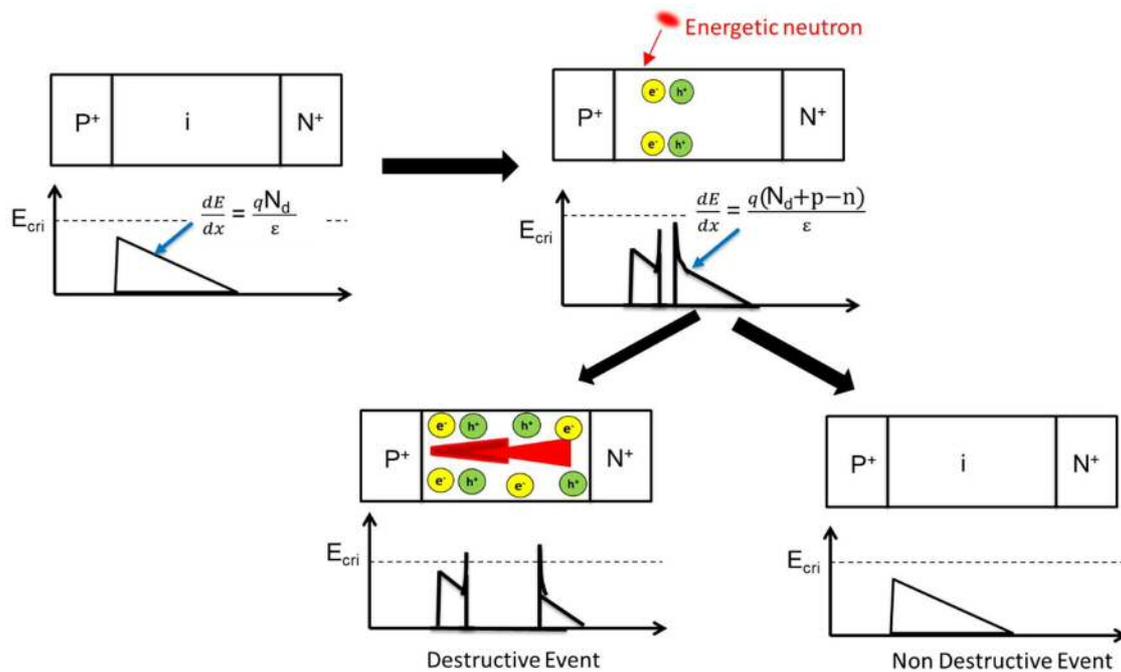
Figure 4-6: Schematic diagram representing the destructive and nondestructive events in PiN diode due to neutron interaction

At low voltages, the impact ionization is not strong enough that the charge carriers diffuse away and finally device comes back to blocking state. However, at higher operating voltages, the strong impact ionization causes the accumulation of charge carriers so quickly that sufficient energy is generated to melt the device locally and the device loses its blocking capability permanently as shown in Figure 4-6.

We have done the simulation of the impact of energetic neutron on PiN diode structures using Heavy Ion model in the Sentaurus TCAD to observe the burnout phenomena. Making a 3D process simulation is the most correct, interesting way, however, for Heavy Ion the computation time is relatively long, and calibration is little more difficult. In order to overcome this, we have done the 2D structure simulation what has relatively short calculation time and reproduced the effect of 3D using cylindrical command in Math section of Sentaurus Device.

The charge corresponds to initiation of catastrophic failure in the device is called threshold charge. The threshold charge for device destruction depends on following factors.

➢ **Operating Voltage**: Electric field, which is responsible for the impact ionization and further avalanche breakdown, depends on operating voltage of device. Therefore, the threshold charge for device destruction is low at high operating voltages.

➢ **Particle energy**: the initial charge deposited by the energetic particle depends on the energy of the particle.

➢ **Impact location on device**: maximum electric field is present near to PN junction. Therefore, the threshold charge for device destruction is low for the interaction near to PN junction.

By considering all the factors that affect the threshold charge for device destruction, numerous TCAD simulations are carried out in order to the obtain the threshold charge for device destruction as function of voltage due to various energetic neutrons at different locations in 300 μm and 100 μm PiN diodes.

4.4 Simulation results for Burnout phenomena in 300 μm PiN diode

TCAD simulation is carried out for 300 μm PiN diodes with different initial deposited charge using Heavy Ion model of TCAD simulation at different locations along the length of the PiN diode. At lower operating voltages, the weak electric field intensity could not support for the impact ionization and subsequent avalanche breakdown of the power device as shown in Figure 4-7. However, at high voltages, the electric field intensity is high enough to cause impact ionization and subsequent generation of electron-hole pairs that forms the filamentation between anode and cathode. The simulation results for destructive burnout and non-destructive events are shown for 300 μm (3 kV) PiN diode.

(a)10 ps

(e) 10 ps

(b) 100 ps

**(f) 100 ps**

(c) 4 ns

(g) 4 ns

(d) 8 ns

(h) 8 ns
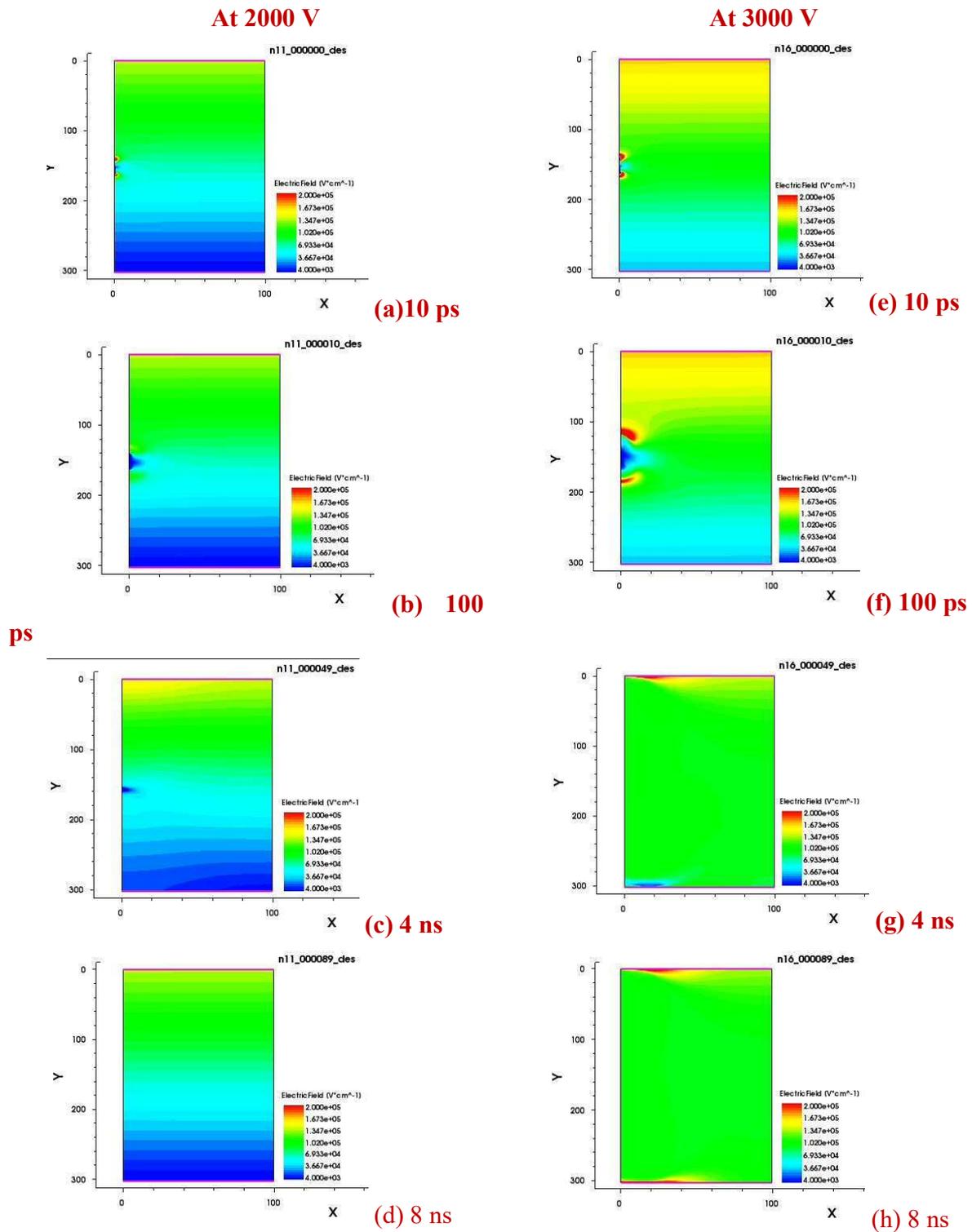
Figure 4-7: Electric field distribution in 300 µm (3 kV) PiN diode (a) ,(b), (c),(d) during 2000 V (e),(f),(g),(h) during 3000 V operation.

43

The simulated results for electric field intensity in 300 μm PiN diode are shown in Figure 4-7 for two different reverse biased voltages of 2000 V and 3000 V when a 300 MeV neutron particle interacts with the device at 141 μm from anode contact. These results clearly indicates the peak in the electric field appears at both ends of the charge plasma due to the shielding of carriers from electric field. The peak of the electric field is high in 3000 V operation compare to 2000 V operation. This is because of high static electric field in the device at 3000 V. As the time passes, the peaks in the electric field moves away towards anode and cathode junctions.

In case of 2000 V operation, the electric field peak diminishes while moving towards anode and cathode junctions. This diminishing electric field peak is lower than the critical electric field of the silicon. Therefore, there is no impact ionization and no further generation of charge carriers. The initially deposited charge carriers diffuse away from the initial deposition position, and the electric field returns to its initial state. Therefore, the device recovers and returns to its normal state. As we can see at 8 ns, the electric field returns to its normal value.

However incase of 3000 V operation, completely different phenomena happens. As the electric field is moving towards anode and cathode junctions, the peak of the electric field is sufficiently higher than critical electric field of silicon. At 8 ns, the peak electric field appears at both anode and cathode junctions which is more than critical electric field of silicon. This causes impact ionization and further generation of electrons and holes and results in the formation of charge streamer between the anode and cathode. The high current causes the burnout of the power device at 3000 V operation.

The temporal and special distribution of electric field due to the impact of 300 MeV neutron at 141 μm from anode contact at 2000 V is shown in Figure 4-8. The result shows, the two peaks appear in the electric field at the ends of plasma and moves towards anode and cathode junctions. At 100 ps, the peak of the electric field becomes lower than the critical electric field of the silicon and results in no impact ionization and no further electron hole generation. The initially deposited charge carriers diffuse away and at 7 ns, the electric field returns to initial state and device recovery takes place without any damage.
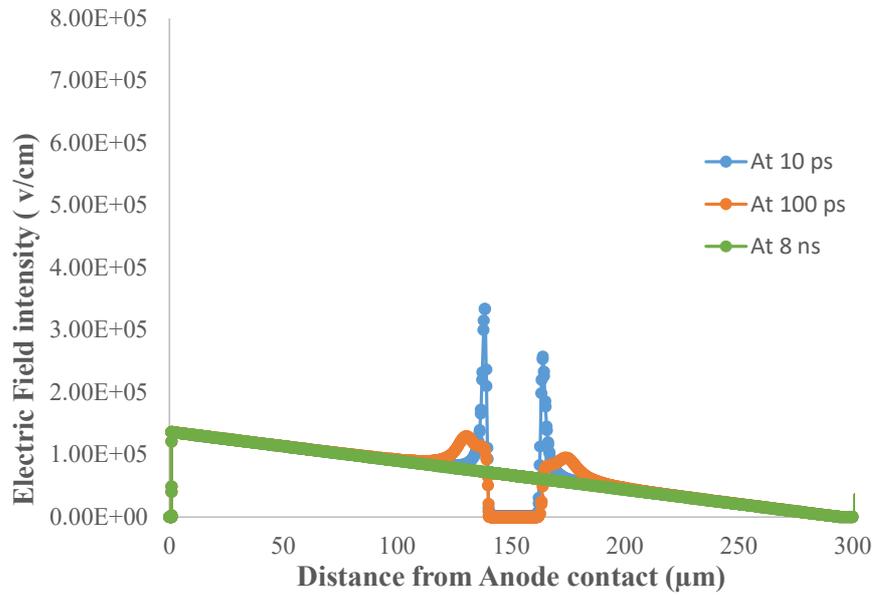
Figure 4-8: Temporal and Spatial distribution of Electric field in 300 µm (3 kV)PiN diode at 2000 V operation

The temporal and special distribution of electric field at 3000 V is shown in Figure 4-9 when 300 MeV neutron interacts with the device at 141 µm from anode contact. Unlike in 2000 V case, in 3000 V operation, the peak electric field at 100 ps is more than the critical electric field of silicon. This results in impact ionization and subsequent generation of electron- hole pairs. This
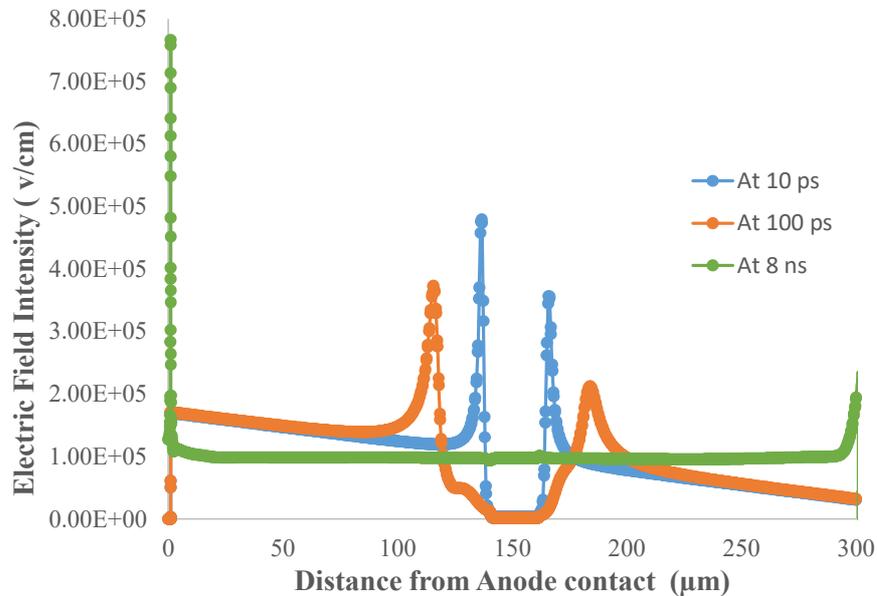
Figure 4-9: Temporal and Spatial distribution of Electric field in 300 µm (3 kV) PiN diode at 3000 V operation

further increases the electric field peak, and is more than critical electric field even after reaching anode and cathode junctions at 7 ns. The generation of electron hole pairs due to impact ionization causes the formation of charge filament between anode and cathode and results in short circuit between the contacts. Finally, the device burnout takes place.

The electron density distribution computed from TCAD simulation is shown in Figure 4-10 due to the impact of 300 MeV neutron at 141 μm from anode contact when operating at 2000 V and 3000 V. As we can see at 100 ps and 4 ns the initially deposited electrons move towards cathode due to the reverse biased operation. In case of 2000 V, due to the absence of impact ionization, no extra electrons generated at the anode side due to the movement of holes. Therefore, all the deposited charge diffused away and the diode returns to normal state at 8 ns.

In case of 3000 V operation, we can see the moving of deposited electrons towards cathode at 100 ps same as in 2000 V operation. However, at 4 ns, the impact ionization and further creation of electrons towards the anode side as well is observed. This results in the formation of electron plasma between the anode and cathode contacts that can be observed at 8 ns. Therefore, the short circuit between the anode and cathode causes high current that generates temperature enough to melt the silicon and subsequent burnout of the PiN diode.

The temporal and spatial distribution of electron density at 2000 V due to the impact of 300 MeV neutron at 141 μm from anode contact is shown in Figure 4-11. Due to the presence of low electric field in case of 2000 V operation, the initial deposited electrons diffuse away from the impact location without any further generation due to the absence of impact ionization. At 10 ns, it is clear from the results that the electron density reaches to its normal state indicating the regain of blocking capability of PiN diode without any damage.

However in case of 3000 V operation, due to the presence of high electric field, further generation of electrons takes place as shown in Figure 4-12. This continuous generation of electrons due to impact ionization results in the formation of electron filament between the anode and cathode contacts at 7 ns. This leads to short circuit between anode and cathode, result in very high current. This high current increases the device temperature more than melting point of silicon and device failure happens. Finally, the PiN diode loses it blocking capability due to the impact of 300 MeV neutron at 141 μm from anode contact when operating at 3000 V and device destruction takes place.

At 2000 V   **At 3000 V**

(a)10ps   **(e) 10 ps**

(b)100ps   **(f)100 ps**

(c) 4 ns   **(g) 4 ns**

(d) 8 ns   **(h) 8 ns**
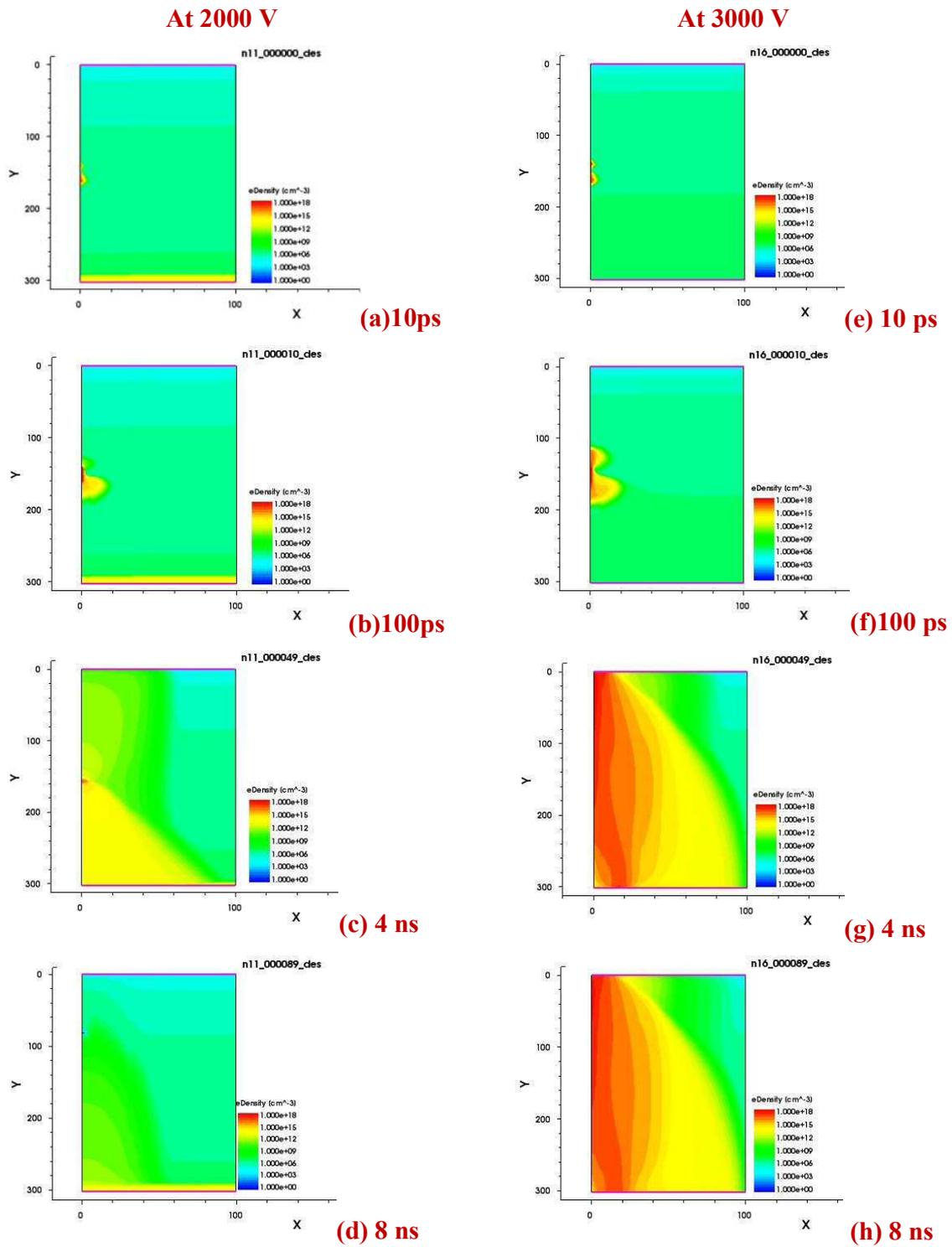
Figure 4-10: Electron density distribution in 300 μm (3 kV) PiN diode (a) ,(b), (c),(d) during 2000 V (e),(f),(g),(h) during 3000 V operation.
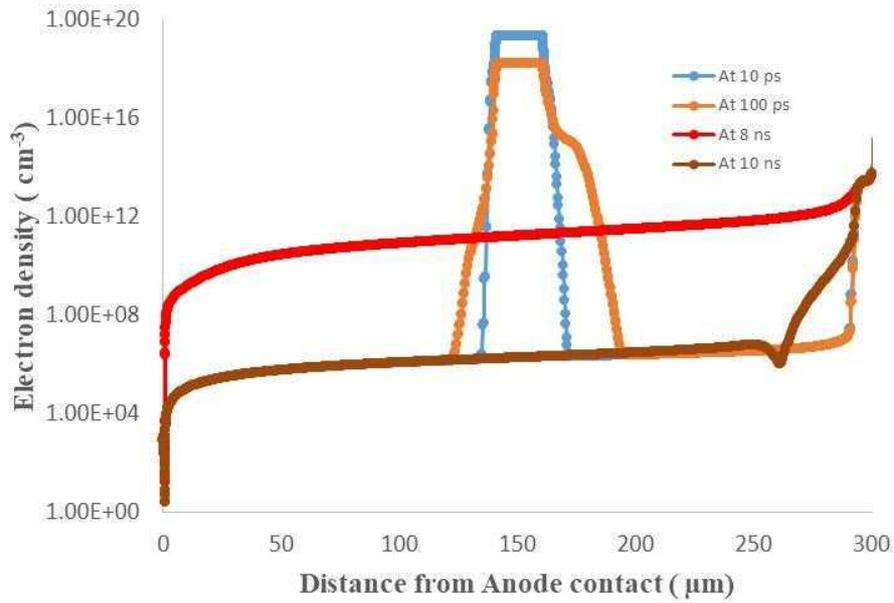
Figure 4-11: Temporal and Spatial distribution of Electron density in 300 μm (3 kV) PiN diode at 2000 V operation
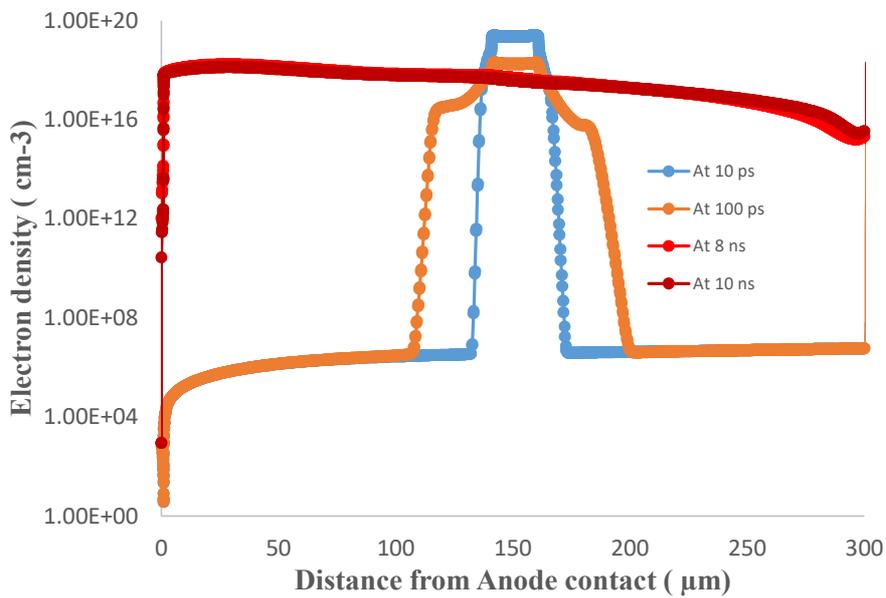
Figure 4-12: Temporal and Spatial distribution of Electron density in 300 μm (3 kV) PiN diode at 3000 V operation

Similarly, the hole distribution in the PiN structure due the impact of 300 MeV neutron at 141 μm from anode contact is shown in Figure 4-13.

At 2000 V **At 3000 V**

(a)10 ps

(b) 100 ps

(c) 4 ns

(d) 8 ns

(e) 10 ps

(f) 100 ps

(g) 4 ns

(h) 8 ns
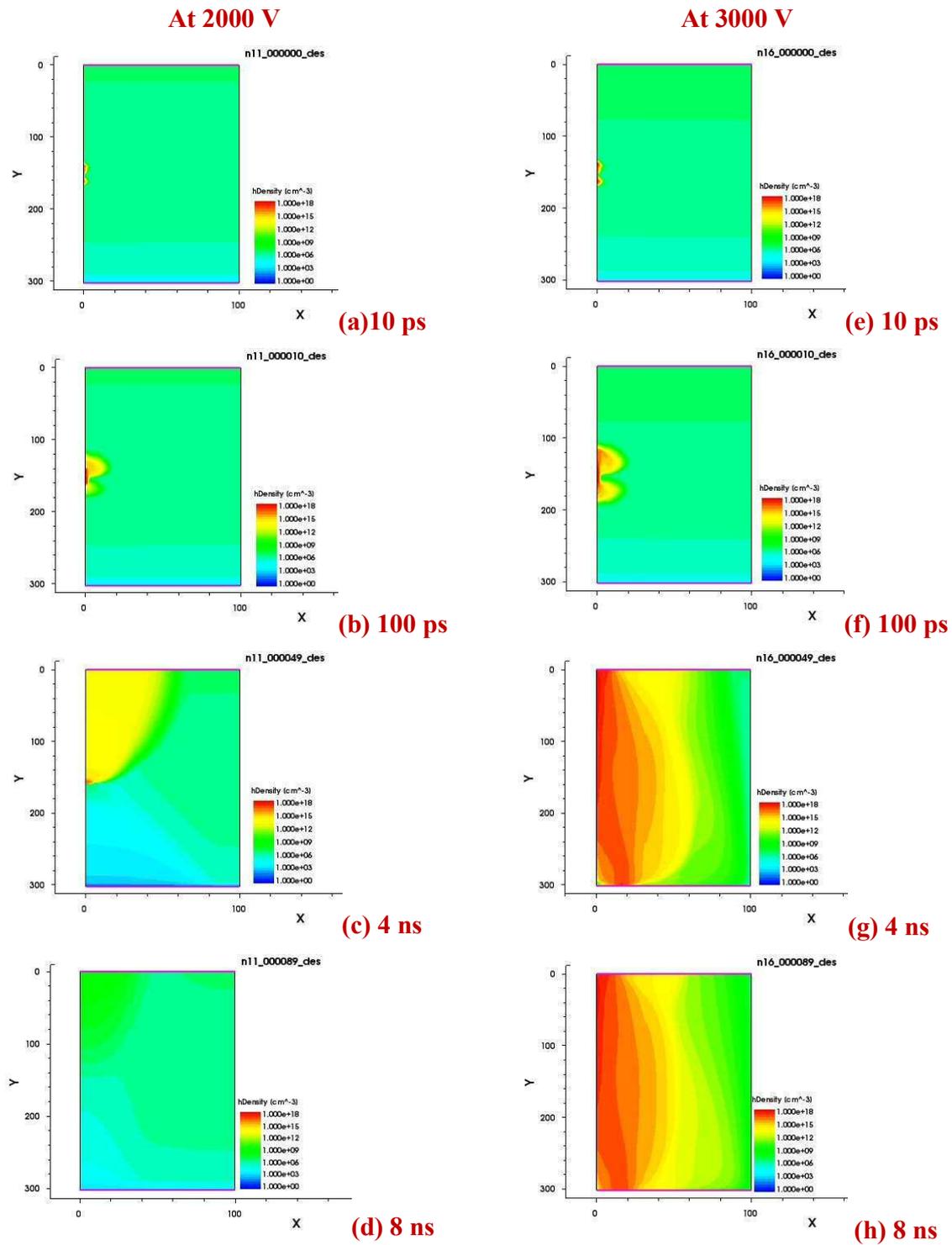
Figure 4-13: Hole density distribution in 300 µm (3 kV) PiN diode (a) ,(b), (c),(d) during 2000 V (e),(f),(g),(h) during 3000 V operation.

The simulation results are shown for two different operating voltages 2000 V and 3000 V to understand the failure phenomena. In case of 2000 V operation, the initial deposited holes starts moving towards anode contact due to the reverse biased operation as shown in Figure 4-13. However due to the absence of impact ionization at 2000 V, there is no further generation of holes takes place. Therefore, the initially deposited holes due to the neutron interaction diffuse away and the diode returns to blocking state at 8 µs. Therefore, the interaction of 300 MeV neutron at 141µm from anode contact result in no damage to PiN diode when operating at 2000 V. However, in case of 3000 V operation, the high electric field in the diode causes impact ionization. Therefore, this results in further generation of holes due to impact ionization and forms filament of holes between anode and cathode. The resulting short circuit between anode and cathode results in loss of blocking capability device destruction.

The temporal and spatial distribution of hole density at 2000 V shown in Figure 4-14. From the figure it is clear that, the initial deposited hole due to the interaction of 300 MeV neutron diffuse away and diode regains its blocking capability at 10 ns incase of 2000 V operation.
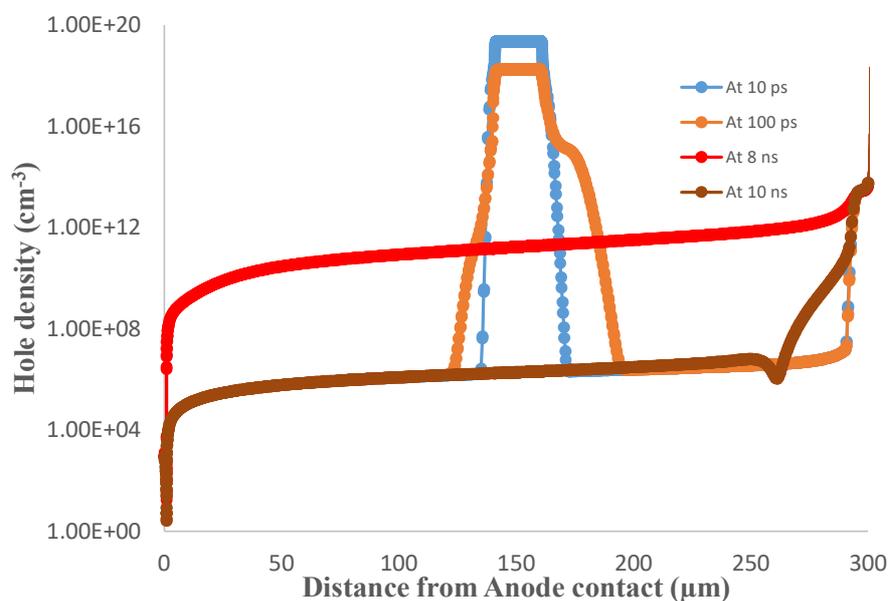
Figure 4-14: Temporal and Spatial distribution of Hole density in 300 µm (3 kV) PiN diode at 2000 V operation

The temporal and spatial distribution of hole density at 3000 V of device operation is shown in Figure 4-15 due to the impact of 300 MeV neutron at 141 μm from the anode contact. In this case, due to the presence of high electric field and resulting impact ionization, causes further generation of holes and results in the formation of hole filament between anode and cathode at 7 ns. The short circuit between anode and cathode results in device destruction at 3000 V of operation.
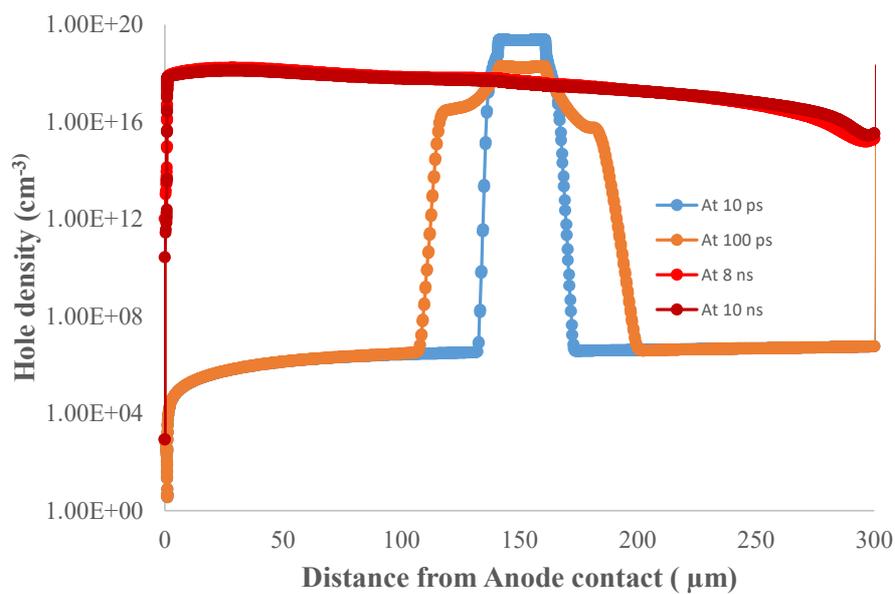
Figure 4-15: Temporal and Spatial distribution of Hole density in 300 μm (3 kV) PiN diode at 3000 V operation

The transient current due to the impact of 300 MeV neutron at 141 μm from anode contact is obtained at various operating voltages as shown in Figure 4-16. At 2000 V of reverse bias operation, due to the absence of impact ionization and subsequent non-multiplication event, the maximum transient current reaches mA level before decaying to normal value. Therefore, the transient current represents only the charge collection due to the neutron interaction and results in non-destructive event at 2000 V. However in case of 3000 V operation, the generation of further electron hole due to impact ionization results in very high current and destruction of device.

The generated charge is obtained from transient current waveforms and is shown in Figure 4-17. It is clear that, there is no significant generation of charge up to 3000 V due to the interaction of 300 MeV neutron at 141 μm from anode contact. However, at 3000 V, it shows

abrupt generation charge due to impact ionization. The operating voltage of the device at the instant of abrupt change in generating charge is the voltage corresponding to the device destruction and the corresponding charge is termed as destruction charge (Q_{dest}). This destruction charge is an important parameter in the proposed failure rate calculation method because destruction charge considered as failure criteria.
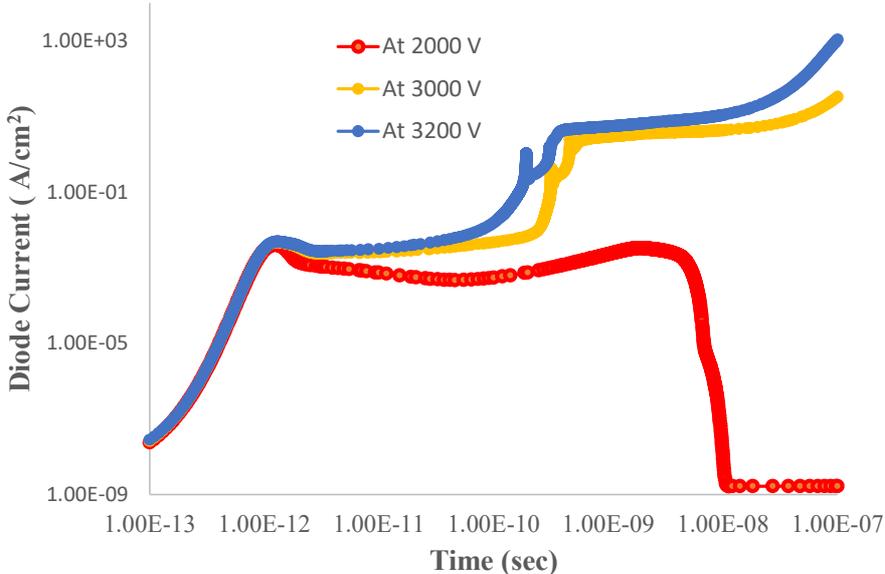
Figure 4-16: Transient current pulse induced by 300 MeV neutron in 300 μm (3 kV) PiN diode due to the impact at 141 μm from Anode contact

The generated charge profile is shown for 100 MeV and 500 MeV neutrons as well in the Figure 4-17 to show the destruction voltage dependence on neutron energy. It is clear that the for higher neutron energy, the device destruction takes place at lower operating voltage. If the neutron interaction takes place nearer than 141 μm from anode contact then, the presence of high static electric field at the position, compare to 141 μm results in initiation of impact ionization at lower voltage for the same neutron energy. In other words, the threshold charge for device destruction is low when the neutron interaction happens near to the PN junction and is increases as we move away from the junction. Therefore, the device is more sensitive to burnout failure when the impact happens near to the junction.
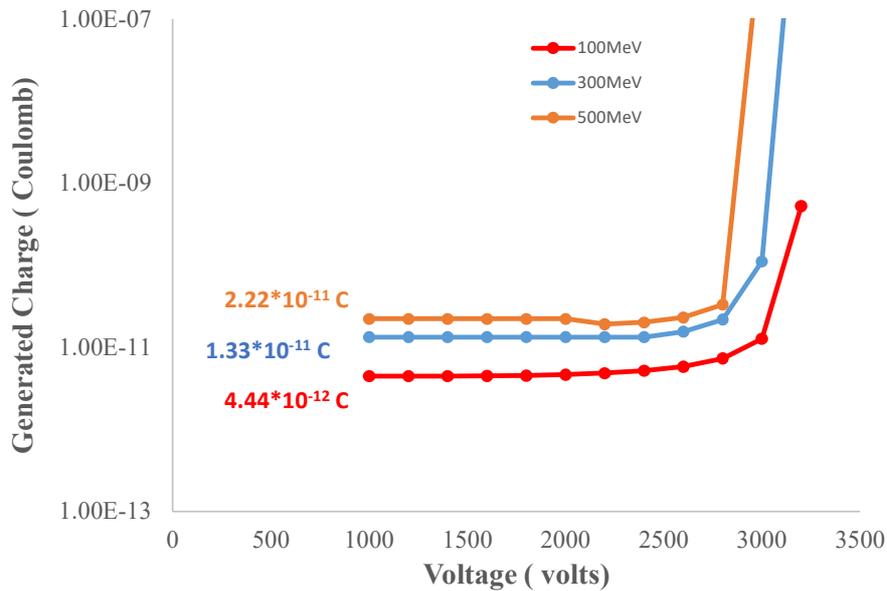
Figure 4-17: Charge generated by various energetic neutron in 300 μm (3 kV) PiN diode due to the impact at 141 μm from Anode contact

4.5 Simulated results for Burnout phenomena in 100 μm PiN diode

The phenomena for destructive failure due to the deposition of energy by the neutrons inside the 100 μm PiN diode is shown in this section. The initial energy deposited by the neutron inside the PiN diode is implemented in Sentaurus TCAD simulation using Heavy Ion model. The energy deposited by the neutron due to the interaction with the device material causes the generation of electron hole pairs. These charge carriers in presence of low electric field at low voltage operation simply diffuses away from the location of deposition. However, the presence of high electric field at high voltages and the resulting peak electric field due to the deposited charge results in further generation of electron hole pairs due to impact ionization and subsequent short circuit of anode and cathode contacts due to charge filamentation. The simulation results for the 100 μm PiN diode due to the interaction of 300 MeV neutron are shown for two different operation reverse voltage conditions i.e. at 800 V and 1200 V when the neutron interacts at 50 μm from anode contact.

The simulated results for electric field distribution inside the PiN diode during different instants after energy deposited by the 300 MeV neutron is shown in Figure 4-18 for both 800 V and 1200 V operation. In this case, we considered the impact location as center of the device, i.e. 50 μm from the anode contact.
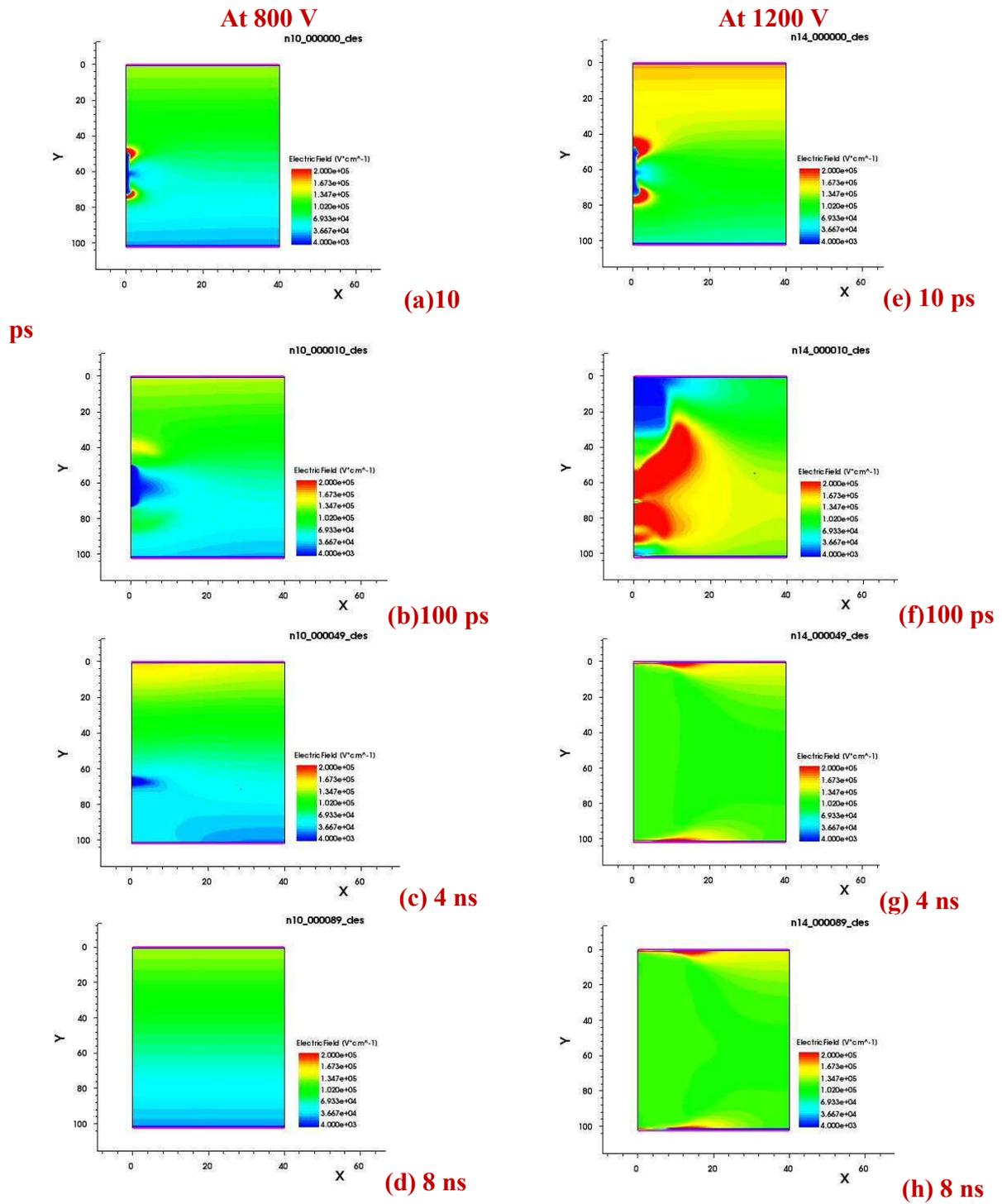
Figure 4-18: Electric Field distribution in 100 µm (1 kV) PiN diode (a) ,(b), (c),(d) during 800 V (e),(f),(g),(h) during 1200 V operation.

The initial deposited charge by the 300 MeV neutron shields its interior from the static electric field present in the device. Because of this, two peaks in the electric field appears at both ends of deposited charge plasma. With time, these electric field peaks moves towards anode and cathode junctions. In case of the 800 V of operation, the peaks in the electric field disappears as they move towards the anode and cathode junctions due to the absence of impact ionization. This results in the recovery of PiN diode and no resulting burnout in the PiN diode as shown in 8 ns. However, if higher energetic neutron interacts with the device at the same location, there may be chance of failure of device at 800 V. Therefore, the 100 µm PiN diode is resistive to failure due to the impact of 300 MeV neutron at the center when operating at 800 V.
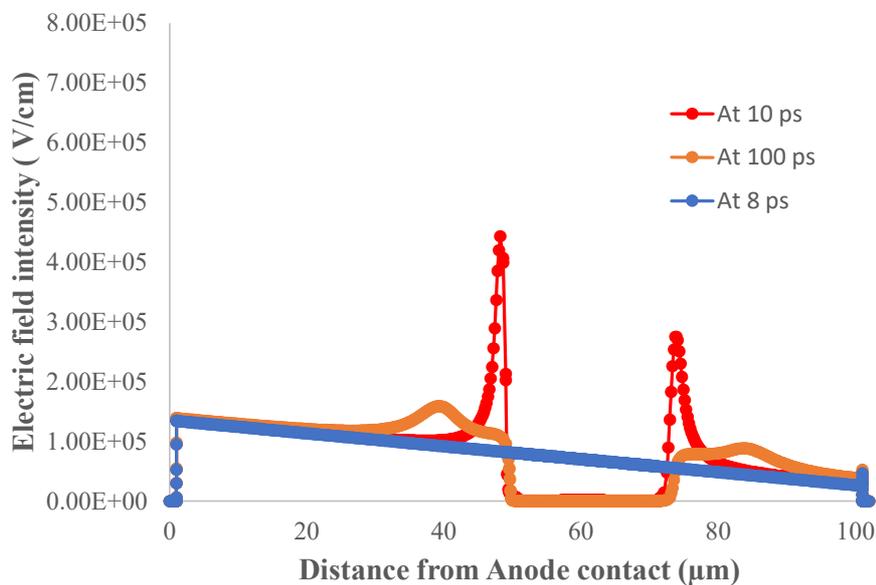
Figure 4-19: Temporal and Spatial distribution of Electric Field in 100 µm (1 kV) PiN diode at 800 V operation

However, different phenomena observed in case of 1200 V of operation. The impact ionization due to high electric field causes the generation of further electron hole pairs and resulting in increase in peak of electric field. This continues and the peak electric field moves to anode and cathode junctions with the generation of electron and holes. We can observe this condition at 8 ns incase of 1200 V operation as shown in Figure 4-18. The temporal and spatial electric field distribution at 800 V is shown in Figure 4-19 showing the extinction of peak in electric field at 8 ns and recovery of PiN diode.

The temporal and spatial electric field at 1200 V in Figure 4-20 shows increase in the peak of electric field as it moving towards anode and cathode junctions. The peak is greater than the critical electric field of silicon material at 8 ns. So impact ionization causes the further generation of electrons and holes and finally destruction takes place.
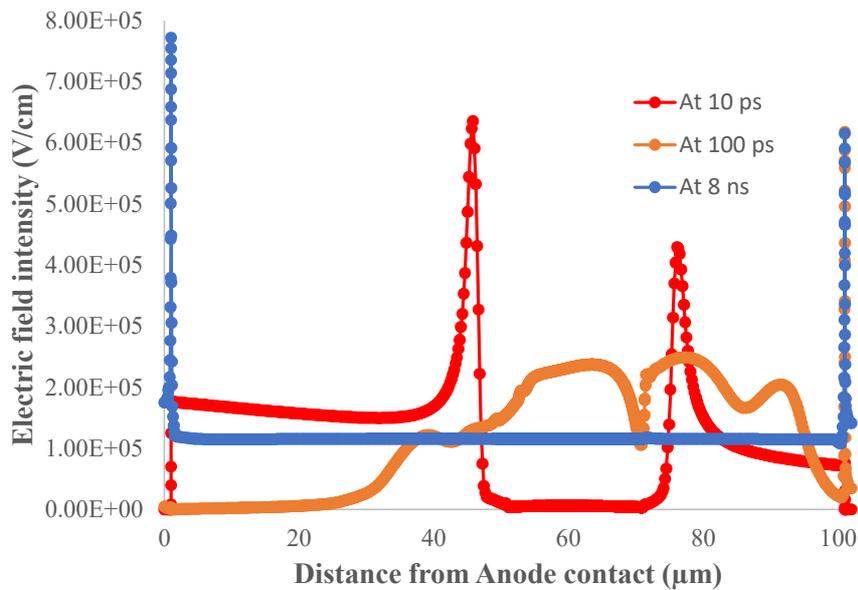
Figure 4-20: Temporal and Spatial distribution of Electric Field in 100 μm (1 kV) PiN diode at 1200V operation

The electron density profile is shown in Figure 4-21 at different instants after the interaction of 300 MeV neutron with 300 μm PiN diode. The results shown at 800 V and 1200 V to differentiate the burnout phenomena.

In case of 800 V operation, the deposited electrons by the 300 MeV neutron diffuses away from the deposition location because of absence of further generation of electrons. The devices regains its blocking capability at 8 ns as shown.

However, in case of 1200 V operation, the deposited electrons due to the impact of 300 MeV neutron shields its interior and results in electric field more than critical electric field of silicon. This results in impact ionization and further generation of electrons and holes. So the electron plasma extends from the impact location and short circuits the anode and cathode contact at 4 ns. The resulting high current through the diode causes the device destruction.

At 800 V　　　　　　　　　　　**At 1200 V**

(a) 10 ps　　　(e) 10 ps

(b) 100 ps　　　(f) 100 ps

(c) 4 ns　　　(g) 4 ns

(d) 8 ns　　　(h) 8 ns
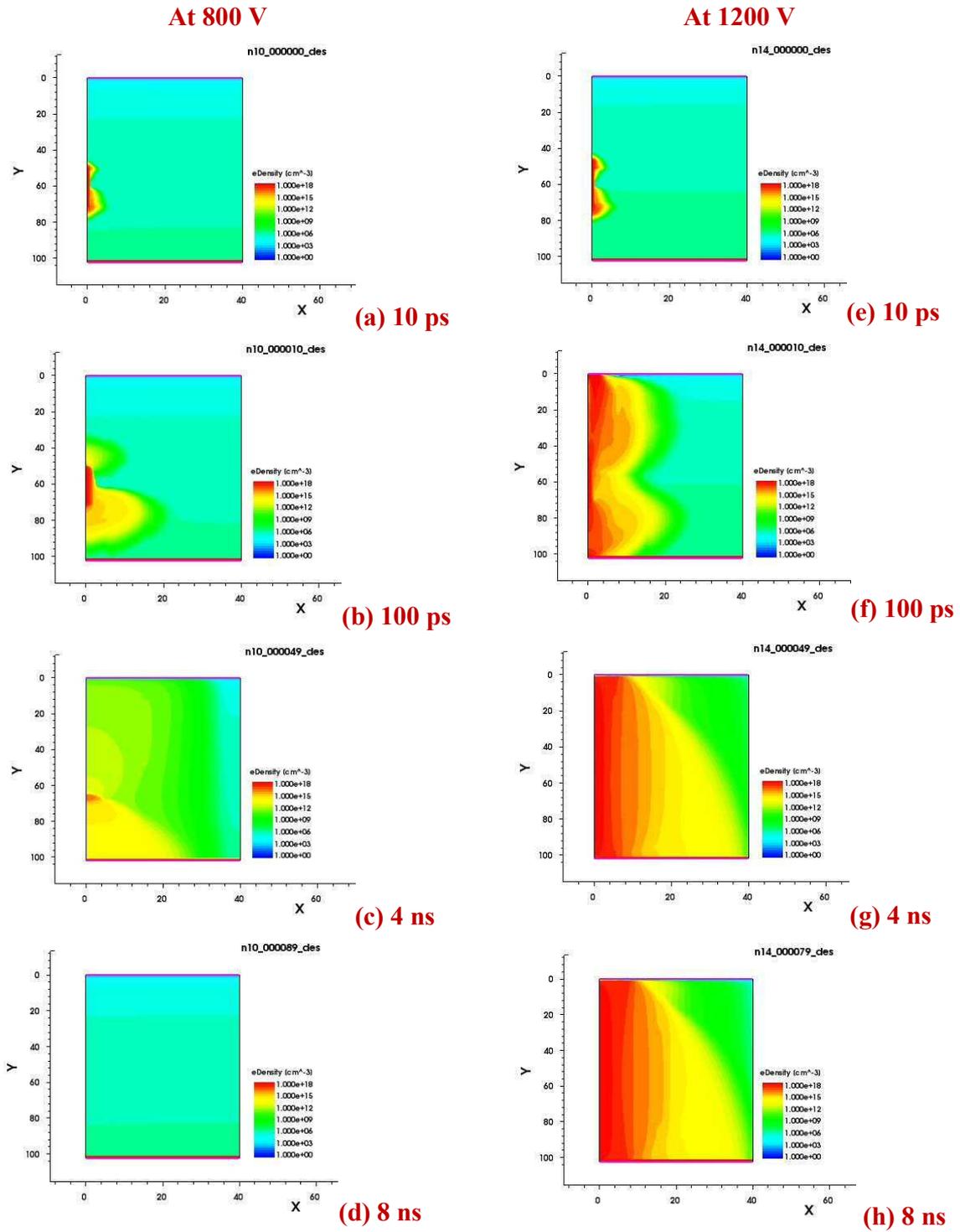
Figure 4-21: Electron density distribution in 100 µm (1 kV) PiN diode (a) ,(b), (c),(d) during 800 V (e),(f),(g),(h) during 1200 V operation.

The temporal and spatial distribution of electrons at 800 V and 1200 V is shown in Figure 4-22 and Figure 4-23 respectively.
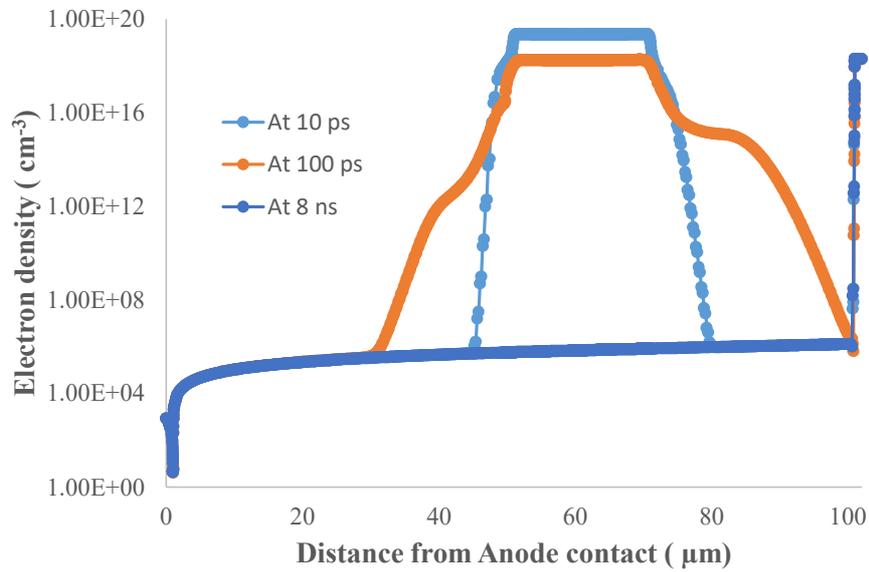
Figure 4-22: Temporal and Spatial distribution of Electron density in 100 μm (1 kV) PiN diode at 800 V operation
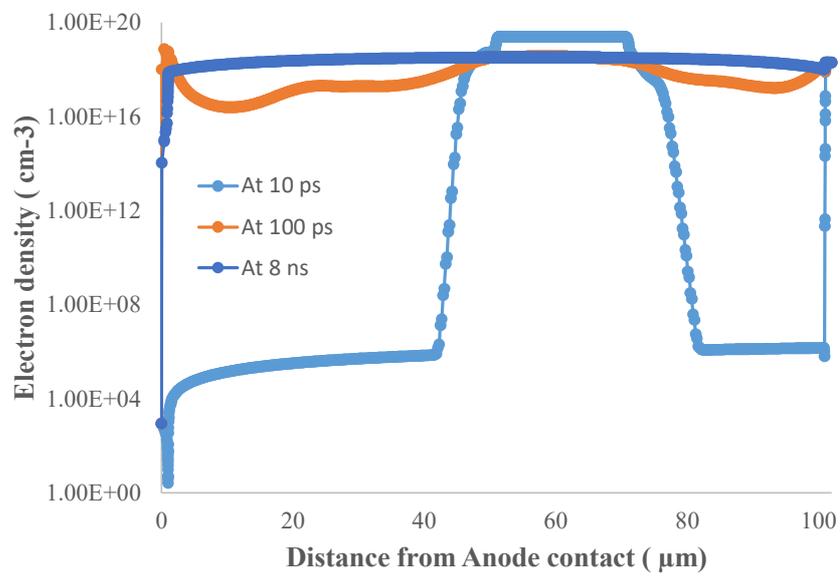
Figure 4-23: Temporal and Spatial distribution of Electron density in 100 μm (1 kV) PiN diode at 1200 V operation

Figure 4-22 clearly shows the diffusion of electrons away from the impact location and regaining the normal state at 8 ns in case of 800 V operation. However if neutrons with higher energy may result in destruction failure at the same voltage due to the deposition of more electrons by the energetic neutrons.

In case of 1200V operation as shown in Figure 4-23, the generation of further electrons adds to the deposited electrons. This is because of the impact ionization at high electric field. The generated electrons short circuits and anode and cathode contact at 8 ns and results in very high current. Therefore, the high temperature resulting from the high current melts the silicon in bulk and results in destructive failure.

The simulation results for holes generated inside the 100 μm PiN diode due to the interaction of 300 MeV neutron at the center of the device is shown in Figure 4-24 for both 800V and 1200V operation. In case of 800V operation, the initial deposited holes starts moving towards anode contact due to the reverse biased operation as shown. However due to the absence of impact ionization at 800V, there is no further generation of holes takes place. Therefore, the initially deposited holes due to the neutron interaction diffuse away and the diode returns to blocking state at 8 ns. Therefore, the interaction of 300MeV neutron at 51μm from anode contact result in no damage to PiN diode when operating at 800V.

However, completely different phenomena observed in 1200 V operation. The high electric field in the diode causes impact ionization. Therefore, this results in further generation of holes due to impact ionization and forms filament of holes between anode and cathode. The resulting short circuit between anode and cathode results in loss of blocking capability device destruction at 8 ns.

The temporal and spatial distribution of hole density at 800 V is shown in Figure 4-25. The deposited holes diffuse away from the impact location and diode regains the blocking capability at 8 ns. however, in case of 1200 V operation, the impact ionization results in further generation of holes and formation of hole filament between anode and cathode. This short circuits and anode and cathode contact and results in very high current and subsequent burnout of PiN diode takes place at 4 ns.

At 800 V   **At 1200 V**

(a) 10 ps

(b) 100 ps

(c) 4 ns

(d) 8 ns

(e) 10 ps

(f) 100 ps

(g) 4 ns

(h) 8 ns
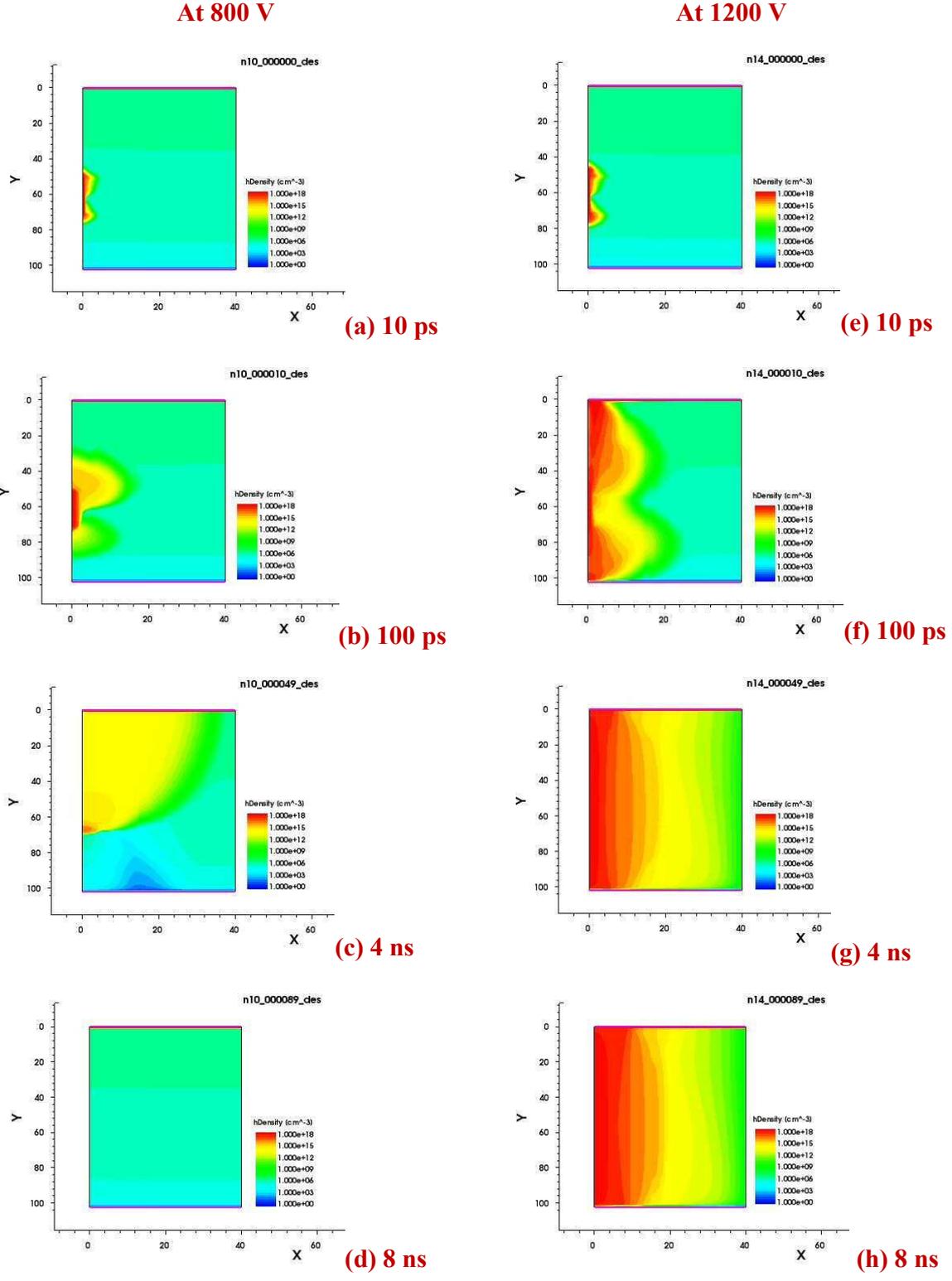
Figure 4-24: Hole density distribution in 100 μm (1 kV) PiN diode (a) ,(b), (c),(d) during 800 V (e),(f),(g),(h) during 1200 V operation.
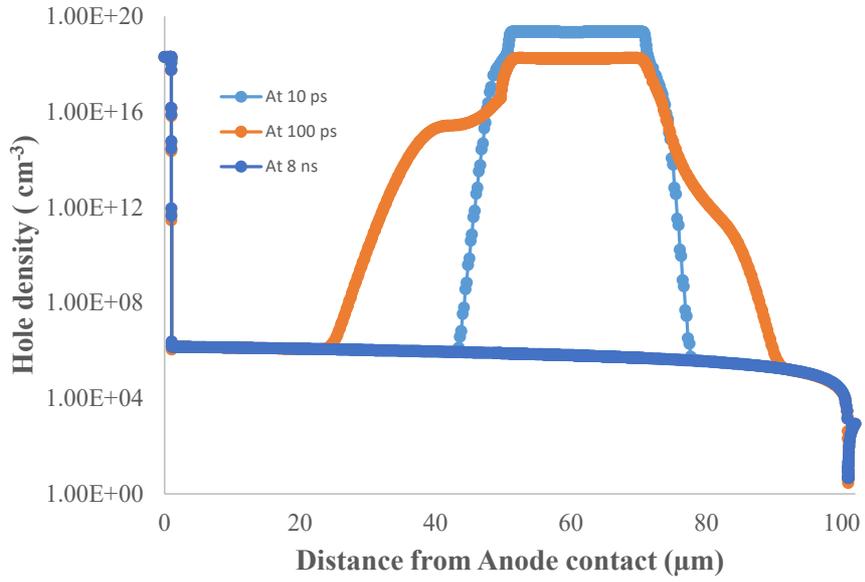
Figure 4-25: Temporal and Spatial distribution of Hole density in 100 µm (1 kV) PiN diode at 800 V
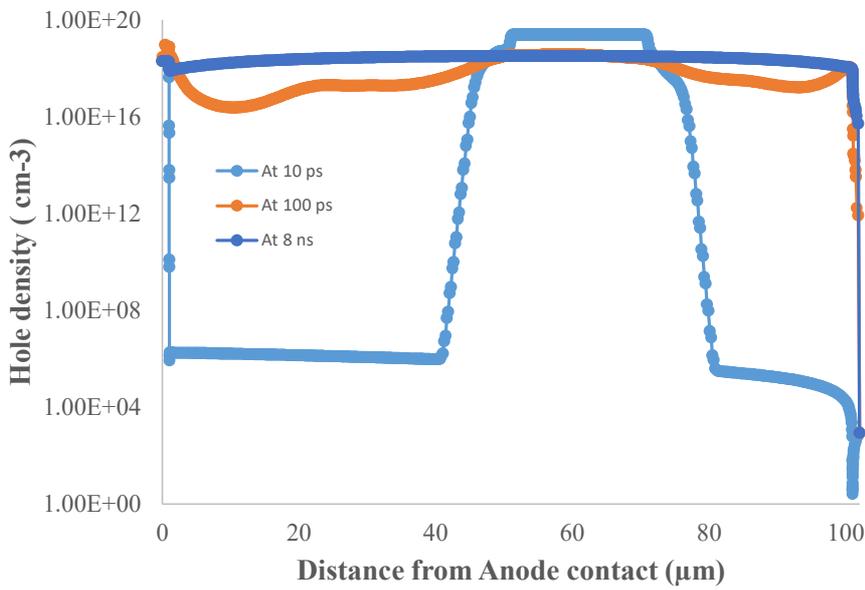
Figure 4-26:Temporal and Spatial distribution of Hole density in 100 µm (1 kV) PiN diode at 1200 V

The transient current flowing through the 100 µm PiN diode due to the impact of 300 MeV neutron at the center of the device is shown in Figure 4-27 for 800 V and 1200 V. In case of 800 V, the transient current corresponds to deposited charge carriers by the 300 MeV neutron. However, in case of 1200 V, the present of impact ionization and further generation of charge carriers results in high current that cause the destruction of the PiN diode.
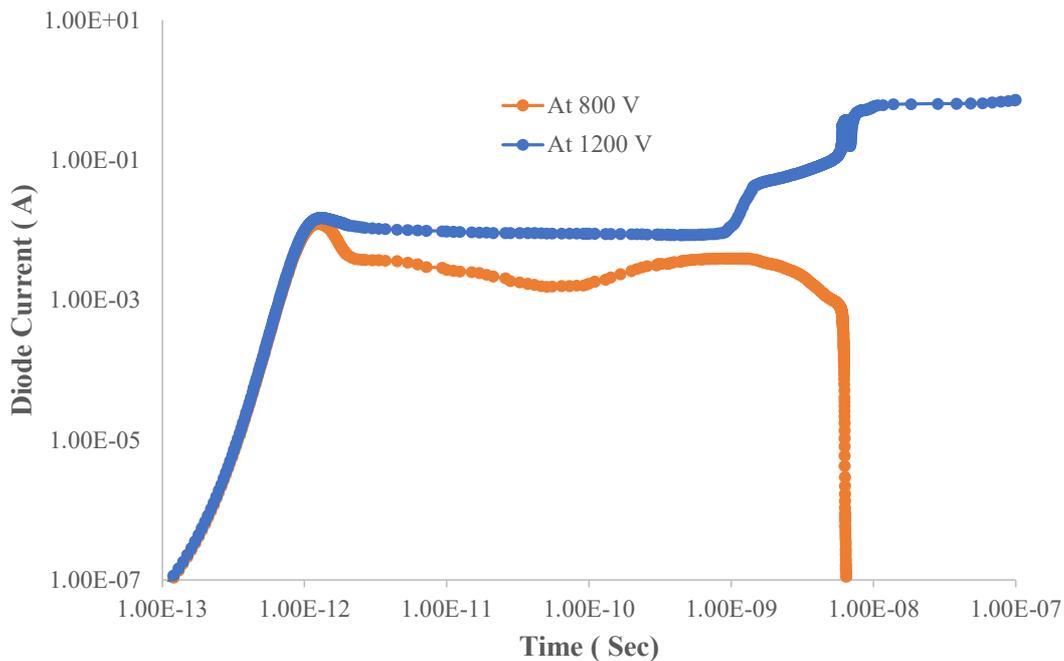
Figure 4-27: Transient current pulse induced by 300 MeV neutron in 100 µm (1 kV) PiN diode due to the impact at 50 µm from Anode contact

The generated charge is obtained from transient current waveforms and is shown in Figure 4-28. It is clear that, no significant generation of charge up to 800 V due to the interaction of 300 MeV neutron at 51 µm from anode contact. However, at 900 V, it shows abrupt generation charge due to impact ionization. The operating voltage of the device at the instant of abrupt change in generating charge is the voltage corresponding to the device destruction and the corresponding charge is termed as destruction charge (Q_{dest}). This destruction charge is an important parameter in our failure rate calculation because destruction charge considered as failure criterion in our proposed failure rate calculation method.

62
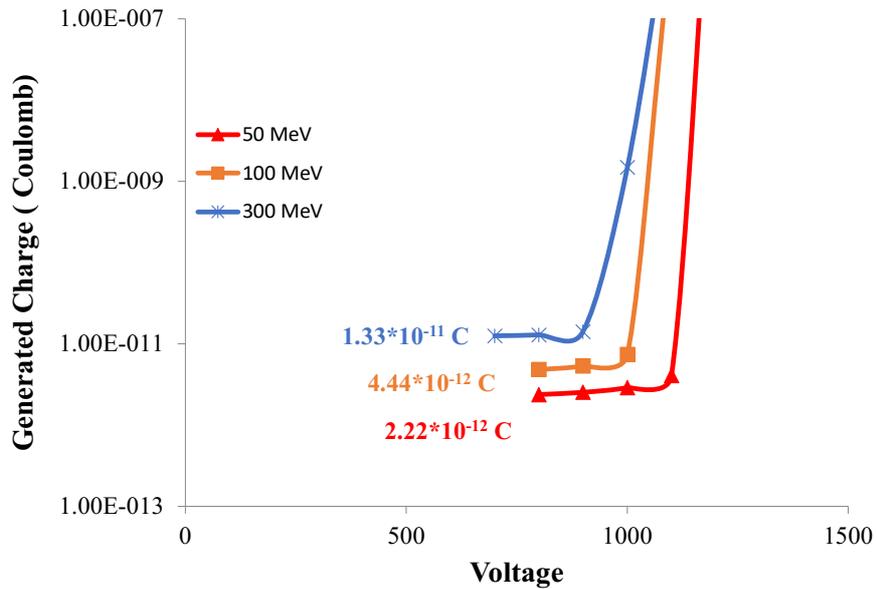
Figure 4-28: Charge generated by various energetic neutron in 100 μm (1 kV) PiN diode due to the impact at 50 μm from Anode contact

The generated charge profile is shown for 50 MeV and 100 MeV neutrons as well to show the destruction voltage dependence on neutron energy. It is clear that the for higher neutron energy, the device destruction takes place at lower operating voltage. If the neutron interaction takes place nearer than 51 μm from anode contact then, the presence of high static electric field at the position, compare to 51 μm results in initiation of impact ionization at lower voltage for the same neutron energy. In other words, the threshold charge for device destruction is low when the neutron interaction happens near to the PN junction and is increases as we move away from the junction. Therefore, the device is more sensitive to burnout failure when the impact happens near to the junction.

4.6 Conclusion

In this chapter, Sentaurus TCAD is introduced that used to model the single event burnout phenomena in the present work. The destruction results are shown due to the impact of 300 MeV neutron at the middle of the device for both 300 μm and 100 μm power diode. The simulation results are shown at two different voltages for each diode to differentiate the burnout and non-burnout events. Finally, the generated charge profiles are shown for the diodes due to the impact of 300 MeV neutron.

63

5 Proposed Universal SEB Failure rate calculation method

The previous chapter presented the simulation results obtained from TCAD simulation. In this section, various failure rate calculations methods are discussed briefly before introducing the proposed failure rate calculation method. The important factors in the proposed failure rate calculation method are, threshold charge for device destruction obtained from TCAD simulation, the probability function for energy deposition by the energetic neutron in silicon and the neutron flux spectrum at the device operating environment. These are discussed briefly in this chapter.

5.1 SEB failure rate calculation approaches

The continuous scaling down of semiconductor feature sizes raises reliability challenges in high power semiconductor devices. Smaller and faster semiconductor devices cause higher current densities and higher electric fields, which make the devices vulnerable to failure due to the radiation of operating environment. When the energetic particles interact with the device, deposits electron hole pairs along its track in the device. If the electric field peak is high enough to cause the impact ionization, then catastrophic failure of power device happens which is called the Single Event Burnout (SEB). The SEB failure rate can be obtained for the power device using Real life tests, Radiation testing and using the failure modeling approach of physics of failure phenomena.

5.1.1 Real-life tests

This is the most direct way to measure the failure rate of the device. The actual devices are exposed to natural radiation such as terrestrial, avionic altitude etc and obtain the failure rate of the device. Some interested works are presented by kabza etc al. [51] in the salt mine experiment.

The advantage of this method is the results are actual and trustworthy due to the fact the devices are exposed to actual radiation environment. However, the disadvantage is that large number of devices have to be exposed for a long period of time for obtaining the failure rate.

5.1.2 Radiation ground testing

In this method radioactive sources , particle accelerators and the laser beams are used to obtain the failure rate of the device in short period of time compare with real-life tests due to the

fact that the radiation flux is produced several orders of magnitude greater than the natural radiation flux.

- ➢ **Radioactive sources**

  A simple and inexpensive way to have a preliminary idea of semiconductor sensitivity is to use source of Californium 252. In this case, alpha particles and two types of heavy ions are emitted giving an LET of 45 and 46 Mev.cm^2/mg. the limitation of this is the low penetration depth (6 to 15 µm) of ions in the device compare to those found in space environment. A device with multiple surface layers, the ions may not reach to sensitive parts of the device. Waskiewicz etc al. observed a destructive latch up effect observed for the first time in n-type power MOSFET using Californium-252[27].

- ➢ **Particle accelerators**

  A particle accelerator is an apparatus that uses electric fields to propel charged particles to nearly speed of light while increasing their energy and magnetic field to contain them in a narrow beam. There are two main types of accelerators: straight-line accelerators where the particle beam travel from one end to other in straight line like Van de Graf accelerator, and circular accelerators where beam of particles travels repeatedly round a loop like cyclotrons.

  Accelerating tests are conducted to evaluate the SEB failure rate of power devices. Various accelerating facilities available with different cutoff energy such as, LANSCE facility has a maximum particle energy of 800 MeV, Tri-University Meson Facility has maximum energy of 520 MeV, Osaka research center for nuclear physics has facility of 400 MeV. Various researchers conducted experiments using particle accelerators to obtain the failure rate[46], [59], [60].

- ➢ **Laser beam**

  A laser is a device that emits light through a process of optical amplification based on the stimulated emission of electromagnetic radiation. Laser beams are present in thousands of applications in daily life including electronics, medicine, industry, military, entertainment, and they are a key technology in fiber-optic communications.

Laser beams are an important means for the characterization of power devices since they allow simulating Single Event Effects. Richer et al. conducted the SEB experiments on IRF 120 n-MOSFETS using pulsed Nd:Yg laser[32]. This technique permits to test devices rapidly for upsets focusing in very tiny spots of a device. The main advantage of laser beams consists in allowing the mapping of the sensitive zones of a device, which is not possible with particle accelerators since the particles reach the entire surface[67]. However, lasers have two main limitations: the beam reflection by the metallization layers, which is more problematic in complex components multi-layers, and the fact that deposited energy by photons during the test has no correlation with the LET of an energetic particle.

5.1.3 Failure rate modeling approaches

Failure rate can also be find using accurate mathematical approach utilizing the Physics of Failure (PoF) knowledge. Zeller[68], [69] proposed phenomenological expression for failure rate calculation using the accelerating experiment results at ground level. Hence, this method is only applicable for terrestrial failure rate calculation.

Availability of powerful and accurate device simulators makes it possible to develop the models using the knowledge of Physics of Failure. Electrical characteristics during SEB are obtained by solving poison's equation along with continuity equation for holes and electrons. The impact ionization model plays crucial role in describing ion-induced breakdown. First attempts of modeling SEB of power devices using numerical simulation was by Kabza et al[51] by depositing the radiation generated carriers along the diode axis. Kaindl et al[61] further simulation studies to obtain the failure criteria.

We proposed failure rate calculation based on failure modeling through simulation. In the proposed formula, we have considered the threshold charge for device destruction as a parameter for failure criteria. This threshold charge for device destruction is obtained from Sentaurus TCAD simulation using the Heavy Ion model.

5.2 Proposed failure rate calculation method

In the present research, we proposed a universal calculation method for failure rate of high power semiconductor devices applicable to any radiation environment[70]–[73]. The proposed formula based on single event burnout cross section or failure cross section and the neutron flux

spectrum. The proposed method has a unique advantage of decoupling between failure cross section and the neutron flux spectrum. The failure cross section is unique for a particular device and remains constant irrespective of operating radiation environment. Therefore, once the failure cross section of a device known, it is possible to calculate the failure rate of the device for any operating radiation environment like terrestrial, aviation or space environment.

The failure cross section calculation formula is given in equation 5.1. It depends on two functions; one is the threshold voltage for the device destruction, which we considered as a failure criterion for the power device in our method, and charge generation probability function in silicon by the heavy ion, which is considered from the literature.

$$\sigma(V_{DC}, E_p) = \frac{A}{l} \int_0^l \int_{Q_{dest}(V_{DC}, Z)}^{\infty} \tilde{\phi}_{E_p}(Q_d) dQ_d \, dz \qquad (5.1)$$

Where σ = Failure cross section in cm^2

V_{DC} = Applied voltage in Volts

E$_p$ = Energy of particle in MeV

A   = Device area in cm^2

l = i-layer thickness in μm

Q$_{dest}$ = Destruction charge for device burnout in C

$\tilde{\phi}_{E_p}$ = Deposited charge probability in silicon in C^{-1}cm^{-1}

z   = Position along depth direction in μm

The failure cross section calculated is unique for a particular device i.e. the failure cross section of the device remains same irrespective of operating radiation environment of the device. We have shown the results for failure cross section of two PiN diodes with 100 μm (1 kV) and 300 μm (3 kV) thickness. The convolution of the failure cross section with the neutron flux spectrum of the operating environment gives the failure rate of the device i.e. the failure rate of 100 μm PiN diode in avionics can be obtained by convolving the failure cross section of 100 μm

PiN diode with neutron flux spectrum at aviation altitude. The proposed decoupled formula for failure rate calculation is shown in equation 5.2.

$$\lambda = \int_{E_{min}}^{\infty} \int_{\Omega} \sigma(V_{DC}, E_p) Flux(E_p)\, d_\Omega\, d_{E_p} \qquad (5.2)$$

Where λ = Failure rate in FIT

Ω = solid angle in sr

Flux = particle flux in $MeV^{-1}s^{-1}cm^{-2}\ sr^{-1}$

E_{min} = minimum energy of particles in MeV

The solid angle taken as $2\boldsymbol{\pi}$ by considering the interaction of neutron particles coming from all directions. The block diagram representing the process of failure calculation using proposed method shown inFigure 5-1. The proposed method is established based on mainly three components. First, The destruction charge ($Q_{dest}(V_{DC},z)$) of the 100 µm and 300 µm PiN diode that obtained from TCAD simulation for various energies deposited by the incident neutrons at different operating voltages of the devices. Second, the energy deposition probability of neutrons inside the silicon is obtained from the literature. By using these two, we obtain the failure cross section of the 100 µm and 300 µm PiN diodes. Third, the neutron flux spectrum that is convolved with the obtained failure cross section of the device to obtain the failure rate of 100 µm and 300 µm PiN diode due to neutron interaction. In the present work, the neutron flux spectrum is obtained from EXPACS data base. The main components of failure rate calculation are explained in detail in the following section.
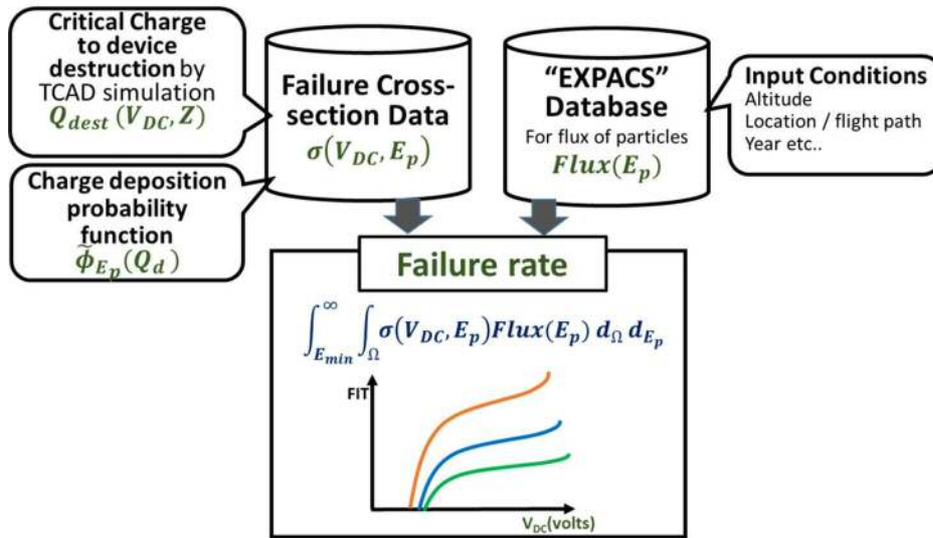
Figure 5-1: Block diagram representation of failure calculation process

5.3 Destruction charge from TCAD simulation

As shown in section 4.3, the neutron induced charge is deposited in PiN diode using Heavy ion model of TCAD simulation. The generated charge as function of voltage is obtained for different energies of neutron. As it is clear that, the region near to PN junction is very sensitive to nuclear induced breakdown due to the presence of high electric field near to junction. To clarify this, simulation is carried out by depositing the charge at various locations and obtained the generated charge to get destruction charge. The figures shows the generated charge inside the PiN diode due to the deposition of 50 MeV, 100 MeV and 150 MeV energy at the junction and 106μm from the junction.

High electric field present near the PN junction in PiN diode. When the neutrons interacts near the PN junction , the masking phenomena of deposited charge results in peak electric field more than critical electric field intensity of silicon for very lower voltage itself. The generated charge profile due to the impact at the PN junction 1 µm away from anode contact is shown in Figure 5-2. It is clear from the result that, when a 150 MeV neutron particle interacts near the junction, an abrupt increase in generated charge happens due to impact ionization near to 1000 V and which is corresponds to destruction charge. Charge generation also shown for the neutron energies of 50 MeV and 150 MeV. As the neutron energy increases, the voltage corresponding to the destruction charge decreases.

69

5.3.1 Destruction charge in 300 µm PiN diode

The generated charge profile due to the neutron interaction at 106 µm from anode contact is shown in Figure 5-3 for various energies of neutrons. In the figure, the charge generated due to 50 MeV, 100 MeV and 150 MeV neutron is shown. These are obtained by integrating the transient current waveform during the impact.
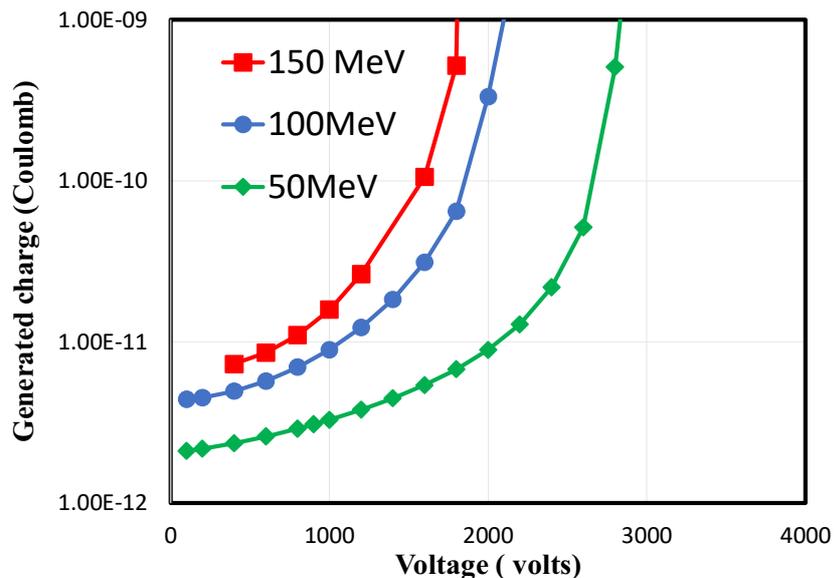
Figure 5-2: Generated charge in 300 µm PiN diode due to the impact of energetic neutron at the PN junction at 1 µm from Anode contact

When 150 MeV neutron interacts the device at 106 µm from the junction, the abrupt charge generation due to impact ionization happens at 2400 V. However, the corresponding voltage in case of impact at 1 µm is only 1000 V. This shows the decrease in operating voltage corresponding to the generation of destruction charge when the impact near to the junction. This concludes the fact that devices are more sensitive to single event burnout failure when impact happen near to the junction.

The simulation is carried out by depositing the various energies at 36µm, 71 µm, 176 µm, 246 µm and 281 µm from the anode contact to obtain the voltage corresponding to the generation of abrupt charge. This is called the destruction charge. The obtained destruction charge for 300 µm PiN diode is shown in Figure 5-5. We can observe the increase in threshold charge when the impact is happening away from the junction. Therefore, power devices are more hardened against the
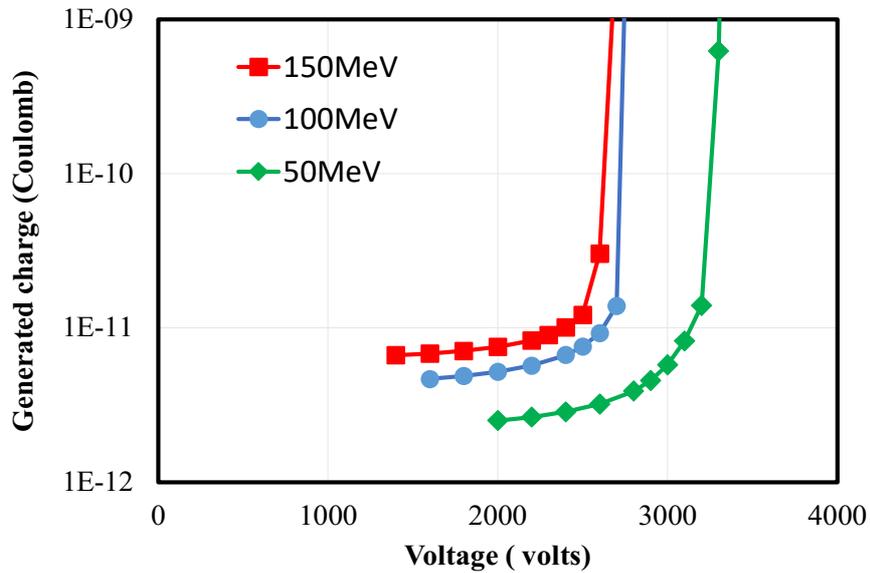
Figure 5-3: Generated charge in 300 μm PiN diode due to the impact of energetic neutron at 106 μm from Anode contact
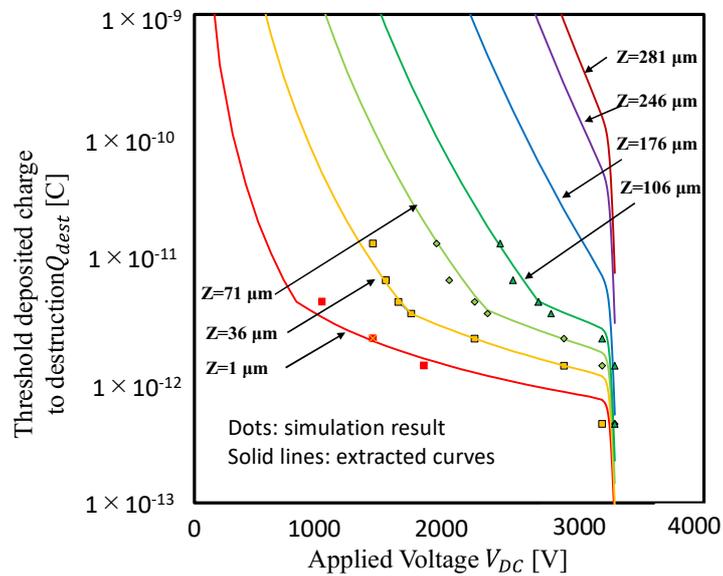
Figure 5-4: Threshold deposited charge corresponding to destruction at various points in 300 μm PiN diode

burnout failure if the neutron impact happens at low electric field region. In otherwords, the power device has to operate at reduced voltage in order to save the device from failure.

5.3.2 Destruction charge in 100 μm PiN diode

TCAD simulation is carried out by depositing the initial energy deposition by neutron at different locations along 100 μm PiN diode. The generated charge profile due to the energy deposition at 1 μm from anode contact is shown in Figure 5-5 for different neutron energies.
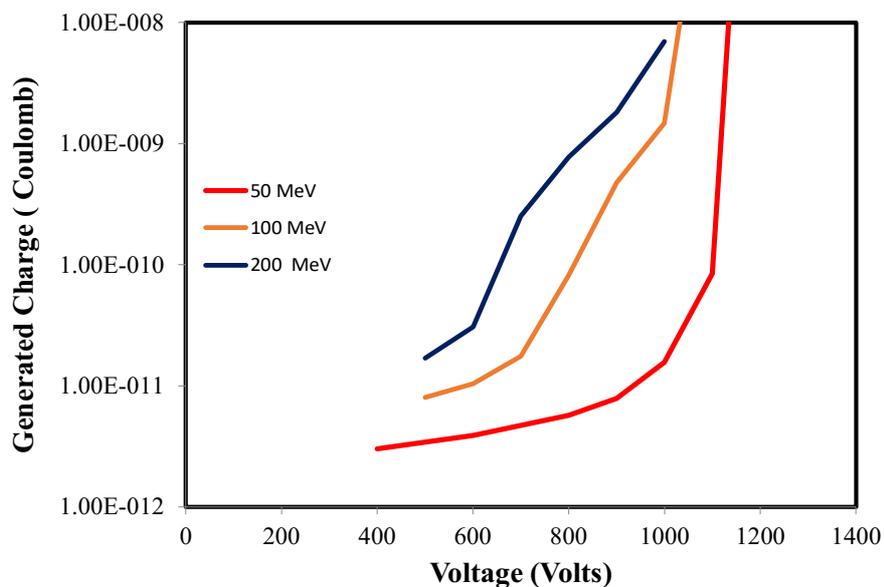
Figure 5-5: Generated charge in 100 μm PiN diode due to the interaction of energetic neutron at the junction 1 μm from Anode contact

Similarly, the generated charge profile due to the impact of energetic neutron at 21 μm from anode contact is shown in Figure 5-6. The voltage corresponding to the generation of destruction charge is 1100 V due to the impact of 50 MeV neutron at 1 μm. however, this increases to 1150 V when impact at 21 μm. This increase in voltage corresponding to abrupt charge generation is because the electric field at 21 μm is less than that of field at 1μm. similar increase in voltage corresponding to destruction charge generation for 100 MeV and 200 MeV at 21 μm compare to 1 μm is observed.

From the generated charge profile, the destruction charge as function of voltage and device location is obtained and shown in Figure 5-7. The charge corresponding to device destruction increases when the impact location is away from the PN junction. Moreover, the charge corresponding to device destruction decreases with increased voltage.
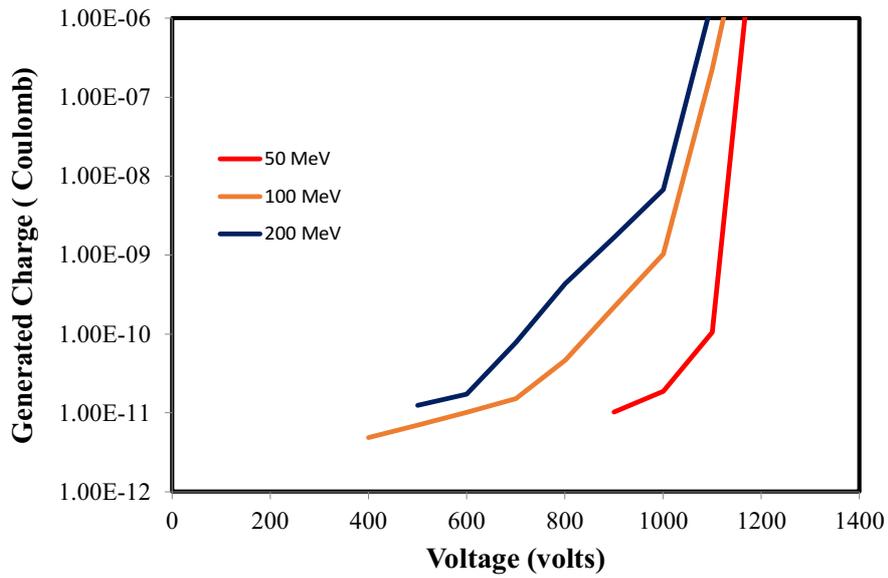
Figure 5-6: Generated charge in 100 μm PiN diode due to the interaction of energetic neutron at 10 μm from Anode contact
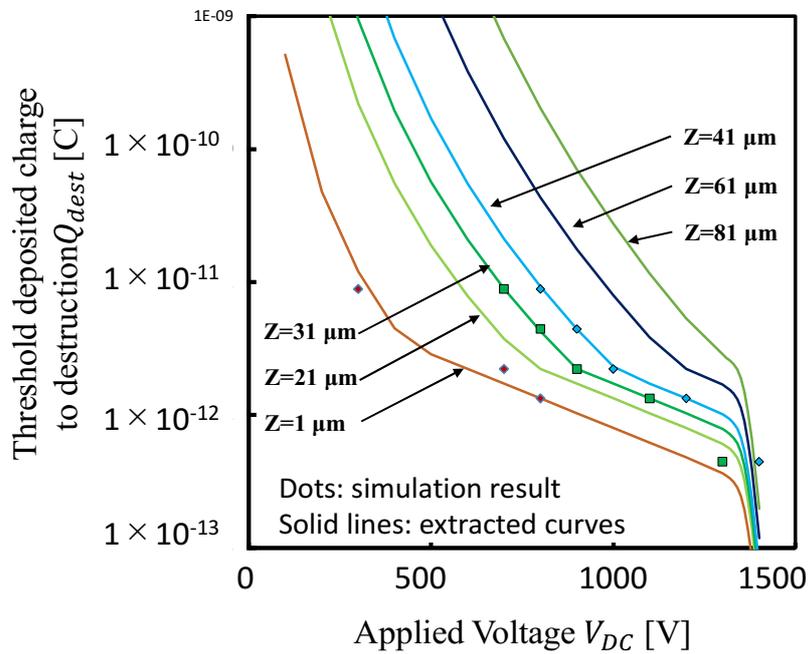
Figure 5-7: Threshold deposited charge corresponding to destruction at various points in 100 μm PiN diode

5.4 Probability of charge deposition by energetic neutron in silicon

During the energetic particle interaction with the semiconductor, the energetic particle deposits part of its energy into the semiconductor with certain probability. In this section, we will discuss about this probability of energy deposited by cosmic ray neutron in silicon in detail.

The energy W(Eg) required to create an electron- hole pair in semiconductor by an energetic particle traversing the medium majorly depends on the bandgap energy of the semiconductor material and given in eV. The measurement of this quantity shows a linear dependence on the bandgap energy which is shown in below equation. The mean energy required to create an electron-hole pair of $1.6* 10^{-19}$ Coulomb in silicon is 3.68 eV. The coefficient of $\alpha = 2.33*10^{13}$ MeV/C gives the relation between deposited energy by the energetic neutron partilcle to generated charge inside silicon.

$$W(Eg) = 1.76 + 1.84\, Eg \qquad (5.3)$$

The single event burnout initiated by the neutron inside the silicon is based on the fact that the secondary recoils induced by neutron silicon nuclear reactions are mainly responsible for device destruction. The energy lost by the neutron inside the silicon is very low to initiate the device destruction. The secondary recoil energies ranges from several KeV to several MeV, which in comparison to the energy lost by the primary energetic neutrons crossing the device. Based on this, in the present study we assumed that, deposited energy by the neutron completely generates the electron- hole pairs in silicon.

The important information needed is how much energy the energetic neutron deposits in silicon. The probability function of energy deposited by the energetic neutron inside the silicon obtained from Doucin et al.[74], [75] and is given in below equation.

$$\phi_{E_n}(E_d) = 10^{a_1(E_n)E_d + a_0(E_n)} + 10^{b_1(E_n)E_d + b_0(E_n)} \qquad (5.4)$$

$$\phi_{E_n}(E_d) = \phi_1(E_d) + \phi_2(E_d) \qquad (5.5)$$

The probability of energy deposition function consists of two decreasing exponential functions $\phi_1(E_d)$ and $\phi_2(E_d)$ as shown in above equation. The first term $\phi_1(E_d)$ corresponds to

deposited energy less than 2 MeV deposited by the neutrons. The second term $\phi_2(E_d)$ corresponds to energy deposition probability by the higher energetic neutrons. The higher energetic particles plays crucial role for the device failure when the semiconductor devices operated near to the breakdown voltage. Therefore, we are particularly interested in high energetic particles and the corresponding probability function for energy deposition minimized as shown below.

$$\phi_{E_n}(E_d) = 10^{b_1(E_n)E_d + b_0(E_n)} \qquad (5.6)$$

The parameter b1 and b0 are considered from Doucin et al.[74], [75] and the fitting functions are obtained for b1 and b0 as function of particle energy.

$$b_1(E_n) = \frac{-100}{(E_n + 15)^{1.80}} - 0.063 \quad \& \quad b_0(E_n) = \frac{200}{(E_n + 20)^{1.38}} - 4.2$$

The plot of b1(En) and b0(En) with the neutron energy is shown in Figure 5-8and Figure 5-9 respectively. And the data points from Doucin et al.[74] are shown for comparision.
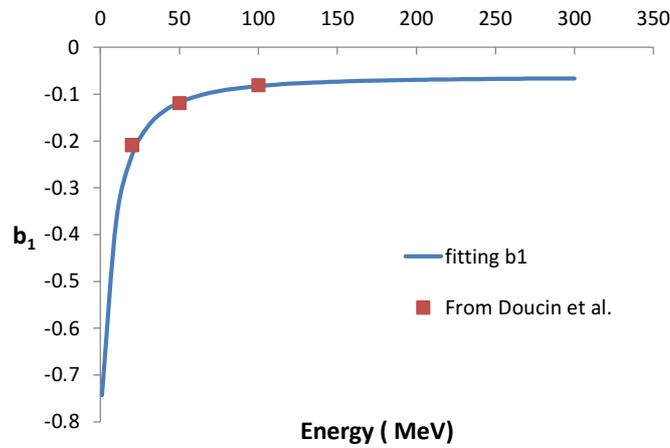
Figure 5-8: Fitting curve developed for b_1 and the comparison from Doucin et al.[74]
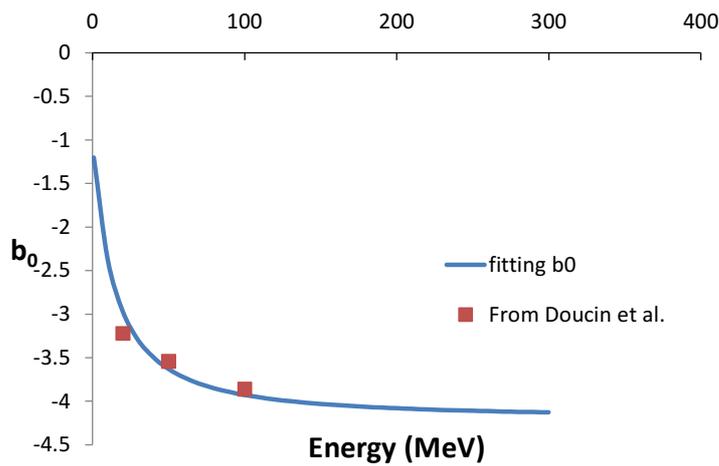
Figure 5-9: Fitting curve developed for b_1 and the comparison from Doucin et al.[74]

Using b1 and b0, the probability of energy deposition by the cosmic ray neutrons inside the silicon is obtained using equation 5.6 and is shown in Figure 5-10. The data from Truscott et al.[76] are shown for comparison.
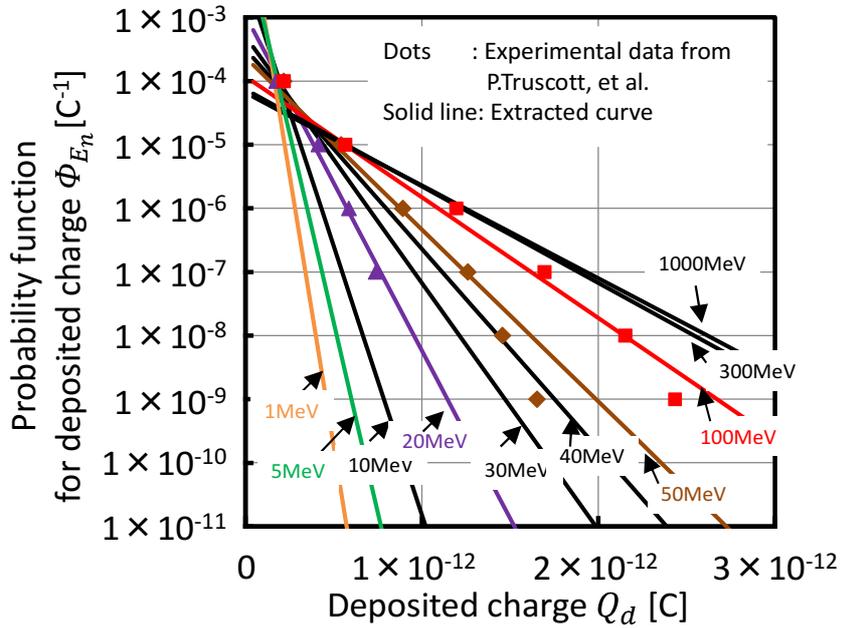
Figure 5-10: Evaluated probability function for energy deposition by neutron in silicon, dots shows data from Truscott et al.[76]

5.5 Neutron spectrum from EXPACS database

Galactic cosmic rays are continuously incident on earth and induce extensive air shower (EAS) by successively causing nuclear and atomic interactions in the atmosphere. Simulation of of EAS over a wide range of energy is essential not only for particle physics but also for single event studies in power devices. A number of studies evaluated the terrestrial cosmic ray fluxes based on analytical approaches and Monte Carlo methods. In general, Monte Carlo methods give better results compare to analytical calculations, but they require huge computational resources. This prevents the direct incorporation of Monte Carlo methods in to system for rapidly evaluating the cosmic ray fluxes at various altitudes.

Considering this situation, an analytical model is developed for estimating cosmic ray fluxes under any global condition, by modeling the result of an EAS simulation performed using Particle and Heavy Ion Transportation Code System (PHITS). This comprises several empirical equations with free parameters whose numerical values determined from least square fitting of EAS data. The fluxes of neutrons, protons, He ions, muons, electrons, positrons, and photons can

be obtained using the model with energy range from 1 MeV to 100 GeV. The model was designated PARMA: PHITS based Analytical model in the atmosphere, and its implementation called Excel based Program for calculating Atmospheric Cosmic ray Spectrum (EXPACS) was released to the public usage is shown in Figure 5-11.

Figure 5-11: User interface to access the EXPACS database[77]

PARMA and EXPACS have been extensively used in various research fields such as radiation protection, semiconductor design etc.
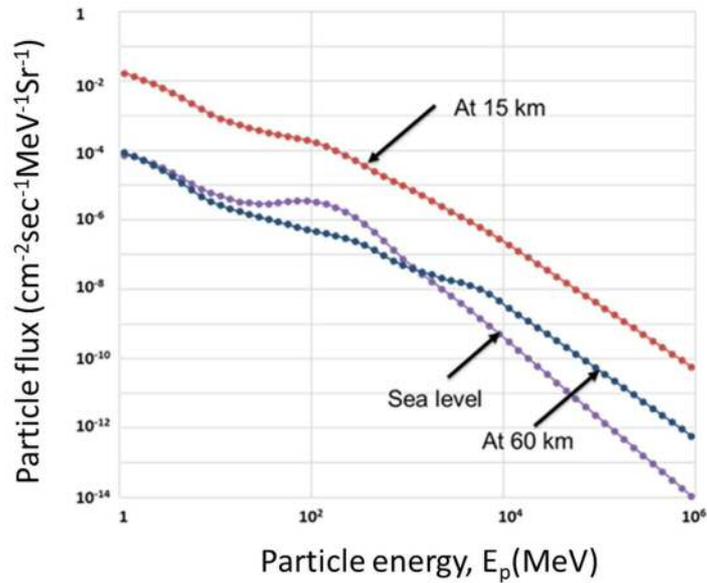
Figure 5-12: The neutron spectrum at different altitudes obtained from EXPACS database

5.6 Conclusion

In this chapter, we have discussed about various failure rate calculation methods available. Then, we introduced our proposed failure rate calculation method. The main parameters of failure rate calculation are threshold charge for device destruction, which is obtained from TCAD simulation, the probability function of energy deposition by neutrons in silicon developed from the available literature and the neutron spectrum of operating environment, which is obtained from EXPACS database. In the next chapter, we will show the results obtained from the proposed failure rate calculation method for 300µm and 100µm PiN diodes.

6 Failure rate calculation results

In this chapter, the calculated failure cross section shown for 300 μm and 100 μm PiN diode using the proposed method. This failure cross section is unique for the device and remains constant irrespective of operating radiation environment. By using this failure cross section, the failure rate is obtained as sea level and compared with phenomenological failure calculation method proposed by Zeller [68], [69]. More over altitude dependent failure is calculated up to an altitude of 60 km using the neutron flux spectrum from EXPACS database. In addition, the effect of maximum cutoff energy of neutron spectrum on accuracy of failure rate is obtained.

6.1 Results for failure cross section

The proposed failure rate cross section formula is shown in section 5.2. The failure cross section mainly depends on two factors. One is the threshold charge that causes the device failure that is the destruction charge (Q_{dest}) and the other is the probability function of deposited charge by the energetic neutron in silicon. We have evaluated the failure cross section for two PiN diode structures 100 μm and 300 μm. the failure cross section for the 300 μm PiN diode is shown in Figure 6-1.
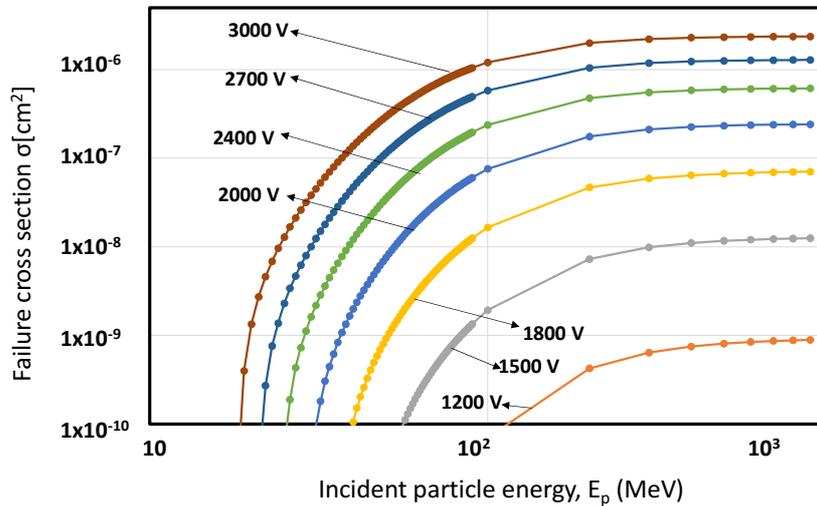
Figure 6-1: Failure cross section of 300 μm PiN diode obtained using proposed method

This failure cross section is unique for the 300 μm PiN diode. Using this failure cross section, it is possible to obtain the failure rate of 300 μm PiN diode at any radiation condition using equation.

80

Similarly, the obtained failure rate cross section from the proposed formula for 100 µm PiN diode is shown in Figure 6-2. The failure cross section is unique for 100 µm PiN diode and this can be used to evaluate the failure rate 100 µm PiN diode at any operating radiation environment.
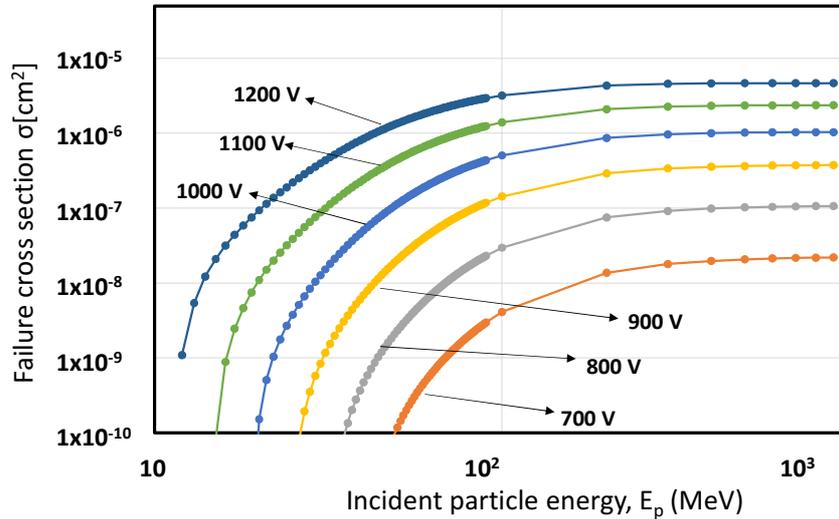
Figure 6-2: Failure cross section of 100 µm PiN diode obtained using proposed method

The important advantage of our proposed failure rate calculation method is the decoupling between failure cross section and neutron flux spectrum. We have evaluated the failure rate of 100 µm and 300 µm PiN diode at various location using the neutron flux spectrum from EXPACS database.

6.2 Failure rate at sea level

The failure rate is calculated using the proposed formula for 300 µm and 100 µm PiN diode using the flux spectrum from Gordon et al.,[23]. The evaluated failure rate is compared with the failure rate calculated by Zeller using the phenomenological failure rate expression[68], [69]. Zeller used the neutron spectrum at LANSCE in deriving the phenomenological failure rate formula in terms of device parameters and it is applicable only to sea level. However, our proposed method can be applicable to any radiation environment. The evaluated failure rate using the proposed failure rate method for 300 µm PiN diode is shown in Figure 6-3.
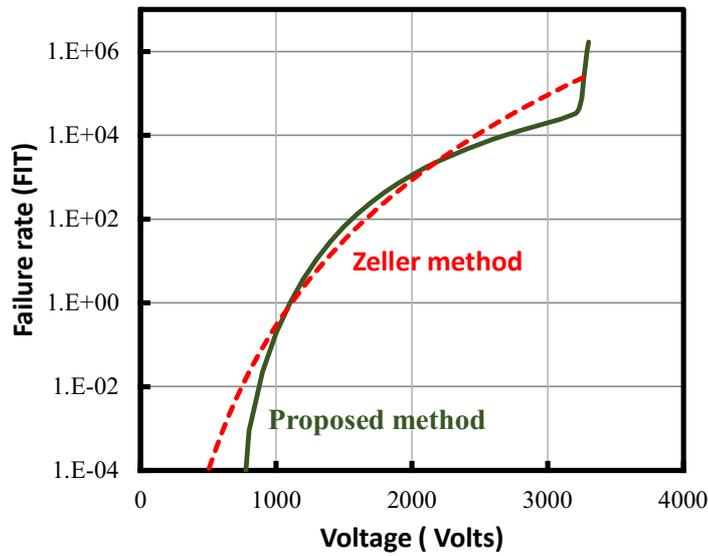
Figure 6-3: Failure rate of 300 μm PiN diode calculated using proposed method at sea level in comparison with Zeller method[68], [69]

The failure rate calculated for 300 μm diode using proposed method shows excellent agreement with the failure rate calculated from phenomenological expression proposed by Zeller. Similarly, the calculated failure rate at sea level for 100 μm PiN diode using proposed method is shown in Figure 6-5. The proposed failure rate also compared with the phenomenological expression by Zeller in terms of device parameters. The over estimation in case of Zeller method is expected to be due to the interpolation of failure rate to low voltage region. In our proposed method, the destruction obtained at even lower voltages of operation and evaluated the failure rate.
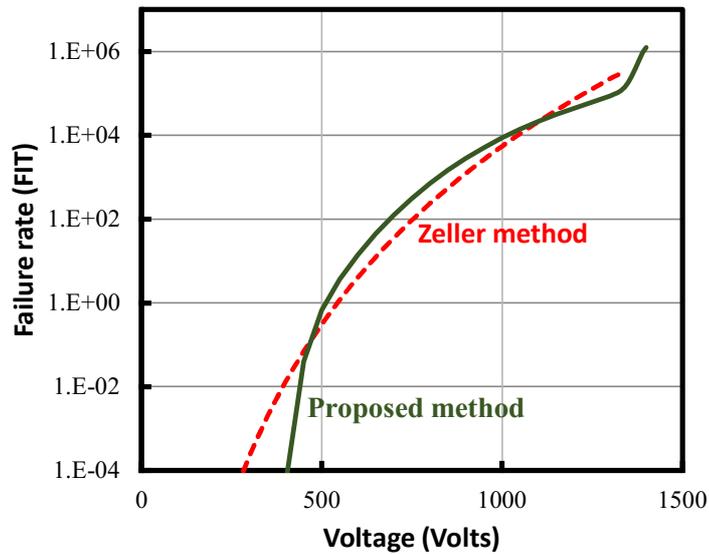
Figure 6-4: Failure rate of 100 μm PiN diode calculated using proposed method at sea level in comparison with Zeller method[68], [69]

6.3 Altitude dependent failure rate

The atmospheric radiation environment that affect the operation of power devices consists of neutrons, protons and pions. They are generated due to the interaction of galactic cosmic rays, which are 83 % protons, 16 alpha particles and 1 heavy ions[14] with the atmospheric atoms that consists of nitrogen (78%) and oxygen(21%)[15]. Every cosmic ray creates showers of secondaries due to this interaction and generates further cascades that results in complex radiation environment. The created secondary cascades do not continue to increase in number as they penetrate earth atmosphere because there is also absorption processes. Therefore, neutrons are the main particles that trigger the failure in high power semiconductor devices, as they indirectly ionize the atoms inside the device by nuclear reaction. The neutron flux for single event is considered above 10 MeV, as the cross section of most semiconductor devices are sensitive above this threshold energy of neutron. However, with technology scaling the devices upsets observed even for 1 MeV neutrons[78], [79]. In our study, we have considered the neutron energy as low as 1 MeV in evaluating the failure cross section of the device. According to IEC Standard 62396-2 [66] notes, the neutron flux at ground level in neutron is reported as 13 neutron/cm^2/ hr and is 300 times lower than the neutron flux at 12 km altitude where commercial

airplane usually travels. Altitude plays an important role in neutron fluxes that highest neutron flux is at 18.3 km altitude called Pfotzer maximum.

We have calculated the failure rate of the 300 μm and 100 μm PiN diodes due to the interaction of neutrons upto and altitude of 60 km. the neutron flux spectrum is obtained from EXPACS data base. By convolving the neutron flux spectrum with the failure cross section of the device the failure rate is obtained using the failure rate calculation equation.

The obtained altitude dependent failure rate as function of voltage is shown in Figure 6-5 for 300 μm PiN diode. These result shows increase in failure rate up to Pfotzer maximum due to the increased neutron flux and then decreases. This graph is very important in power electronic system prospective in selecting the proper device rating in order to keep failure rate with in permissible limits. According to IEC standard 62396-2, the maximum permissible failure rate of the power device should be within 100 FIT. Therefore, from the graph it is easy to know the maximum allowable voltage stress of the device at different altitudes to keep the failure rate within 100 FIT.
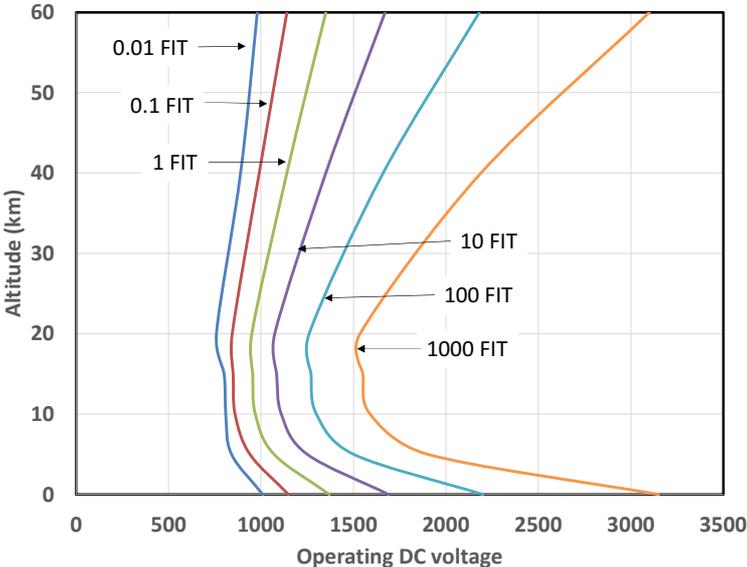
Figure 6-5: Altitude dependent failure rate as function of operating voltage in 300 μm PiN diode

From the results, it is clear that maximum operating voltage of the power device is 2250 V at sea level operation in order to limit the failure rate within 100 FIT, whereas the maximum operating voltage must not exceed 1250 V at 12 km altitude for the same FIT.

Similarly, the evaluated altitude dependent failure rate for 100 µm PiN diode is shown in Figure 6-6. From this, it is clear that, the maximum operating voltage of the diode should not exceed 1100 V in order to limit the failure rate to 100 FIT in sea level operation, whereas the voltage should not exceed more than 580 V at 12 km altitude where the most of the commercial airplanes travels. Therefore, the maximum voltage stress of the device should be around 50 % in the power devices used in avionics.
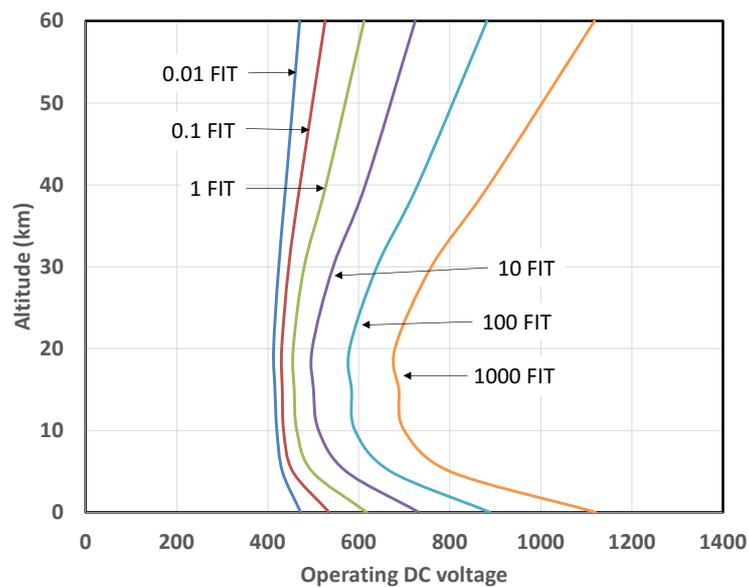
Figure 6-6: Altitude dependent failure rate as function of operating voltage in 100 µm PiN diode

6.4 Cutoff energy limitation on failure rate

Accelerating tests are one of the means to evaluate the SEB failure rate of power devices. The accelerating test facilities have the limitation of maximum energy of the particles, e.g. LANSCE facility has a maximum particle energy of 800 MeV, Tri-University Meson Facility has maximum energy of 520 MeV, Osaka research center for nuclear physics has facility of 400 MeV. The effect of low energy particles is critical to the failure when the power device operating near to breakdown voltage of device. However, when considering the de rating of power device in avionics, high-energy particles shown significant effect on failure rate. To clarify this, the effect maximum cutoff particle energy on failure rate of the 300 µm and 100 µm devices is evaluated by limiting the upper cutoff energy of neutron spectrum.

The failure rate of 300 μm diode is shown in Figure 6-7 due to neutron spectrum with various upper cutoff energies. The results indicates, the calculated failure rate is one order lower in case of 400 MeV cutoff compare to 1 GeV. However, for cutoff energy lower than 400 MeV, the calculated failure rate is two orders of magnitude lower near to breakdown voltage and more than three orders of magnitude away from breakdown voltage. This indicates the failure rate at low operating voltages are affected by the upper cutoff energy of neutron spectrum. A minimum of 200 MeV neutrons must be considered in order to evaluate the nearly acceptable results.
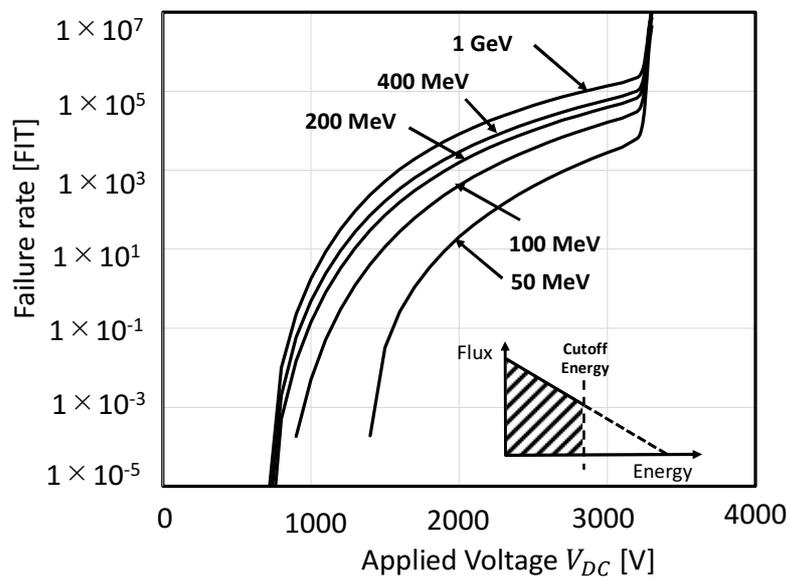
Figure 6-7: Failure rate of 300 μm PiN diode due to neutron spectrum with various cutoff energies

Similarly the failure rate of 100 μm PiN diode is shown for neutron spectrum with different cutoff energies. Upto 400 MeV cutoff energy, the calculated failure rate is below one order of magnitude lower than the spectrum with 1 GeV cutoff.
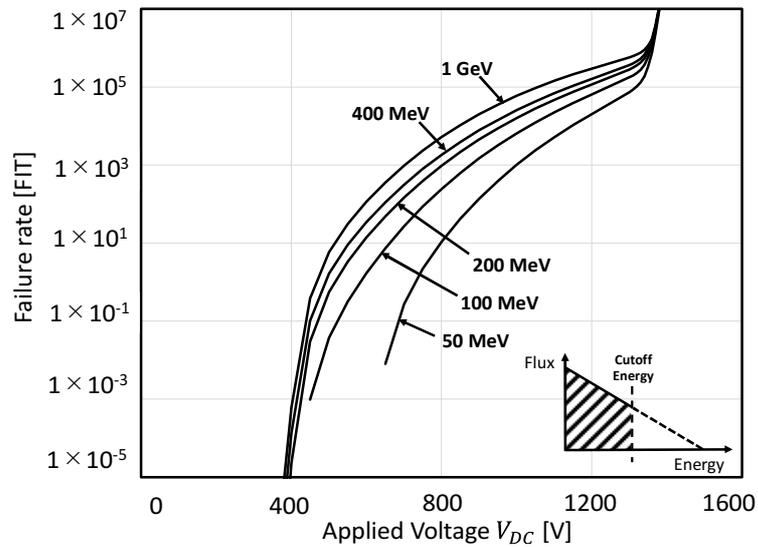
Figure 6-8: Failure rate of 100 μm PiN diode due to neutron spectrum with various cutoff energies

To understand the dependence of neutron cutoff energy on failure rate more clearly, the under estimation factor of failure rate is obtained. the failure rate due to the neutron spectrum shown in Figure 5-12 is taken as reference. The obtained failure rate underestimation factor for 300 μm PiN diode due to various cutoff energy is shown in Figure 6-9 . As shown in the results, the under estimation factor is lower than one order of magnitude up to 400 MeV cutoff in neutron spectrum. However, if the neutron spectrum is limited below 400 MeV, the under estimation factor increases more and at lower voltages it is near to 0.1 for 200 MeV cutoff. This estimation error increases rapidly for further decrease in cutoff energy at lower operating voltages.
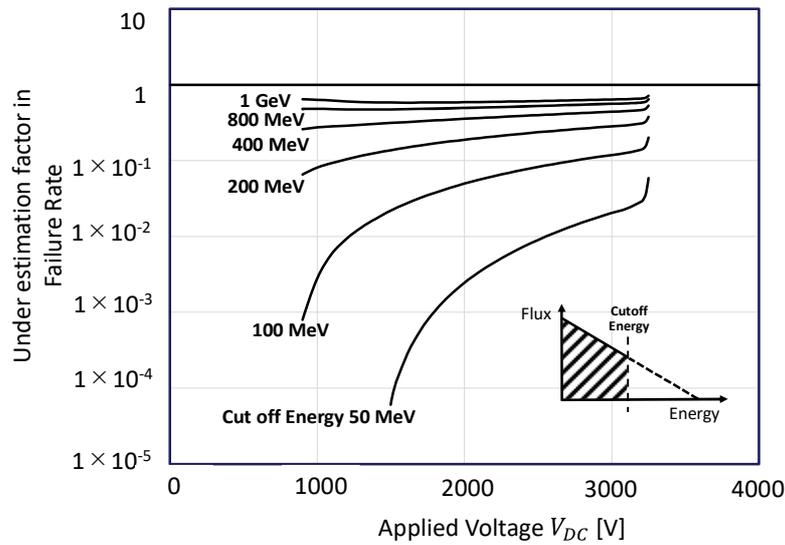
Figure 6-9: Failure rate under estimation factor in 300 μm PiN diode due to various neutron spectrum cutoff. The reference due to complete spectrum is taken as 1.

Similarly, the calculated under estimation factor in failure rate calculation for 100 μm PiN diode is shown in Figure 6-10. This also indicates the increase in failure rate calculation error due to the limitation of neutron spectrum cutoff energy to lower values. So, there is a limitation of neutron spectrum cutoff below which high deviation in calculated failure rate. The results shows that, if the neutron spectrum should have upper cutoff energy of at least 400 MeV to have closer failure rate calculation to actual value.

These results agrees with the cutoff energy limitations of various neutron irradiation facilities. LANSCE facility has a maximum particle energy of 800 MeV, Tri-University Meson Facility has maximum energy of 520 MeV, and Osaka research center for nuclear physics has facility of 400 MeV. Therefore, the evaluated failure rate using these is close to actual conditions. However, the limitation in the experimental facilities encourages in developing the proposed failure rate calculation method.
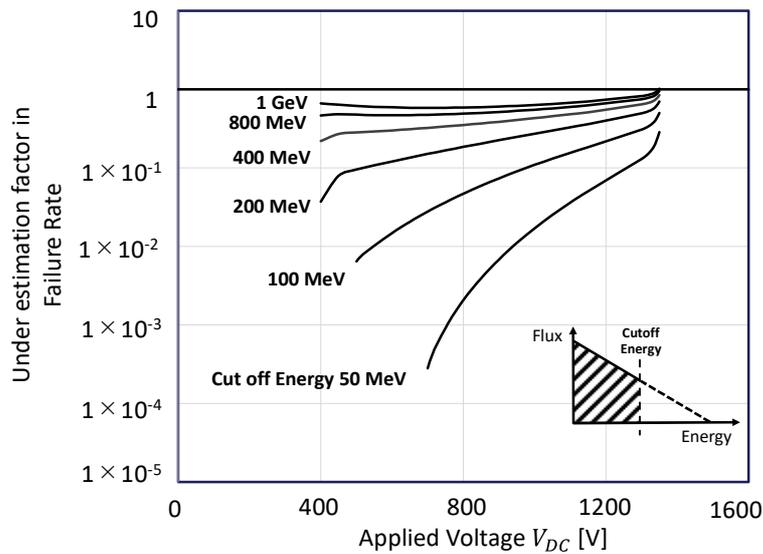
Figure 6-10: Failure rate under estimation factor in 100 µm PiN diode due to various neutron spectrum cutoff. The reference due to complete spectrum is taken as 1.

6.5 Conclusion

In this chapter, we shown the failure rate results obtained using the proposed method. Failure rate is calculated at sea level for 300 µm and 100 µm PiN diode and validated with the sea level failure rate calculated using Zeller phenomenological expression. Further, altitude dependent failure rate is calculated up to an altitude of 60 km using neutron spectrum from EXPACS data base. Moreover, the effect of upper cutoff energy in neutron flux spectrum on calculated failure rate is studied.

7 Conclusion

Power semiconductor devices are susceptible to catastrophic failures when exposed cosmic radiation. single event burnout (SEB) is the destructive phenomena that takes place due to this failure. SEB in terrestrial operating condition is a widely recognized problem due to the usage of high Power semiconductor devices in many terrestrial applications. However, the recent increase in the use of high power semiconductor devices in avionics shows the important of expanding the SEB study to higher altitudes. Our proposed universal failure calculation can be used in any radiation environment such as terrestrial, aviation, space environments to obtain the failure rate of all types of high power semiconductor devices.

Chapter 1 introduced the failure induced by the energetic particle of neutron and importance of failure rate calculation in system design stage. In addition, the objective of the present research work are presented.

Chapter 2 described the origin of radiation along with the radiation environment. The mechanism of interaction between radiation in matter are discussed. The early discovery of Single Event Effects in integrated electronic circuits is discussed. Moreover, the reason for considering the cosmic ray neutrons in the present work is discussed.

Chapter 3 presents the literature review about energetic particle interaction with the high power semiconductor devices and the subsequent research on understanding the failure phenomena. The physical phenomena leading to device destruction also discussed in various power devices in detail.

Chapter 4 describes the Single Event Burnout simulation of PiN diode. The physical process leading to the failure is shown for 300 μm and 100 μm PiN diode using the simulation results. The transient current waveforms shown at differentiate the burnout and non-burnout situations.

Chapter 5 introduces the proposed universal failure rate calculation method. Various components of the failure calculation method are discussed in detail. The threshold charge for device destruction obtained from simulation results is shown for 300 μm and 100 μm PiN diode.

Chapter 6 presents failure rate results obtained using the proposed method. The calculated failure rate at sea level is validated with the Zeller results. Further, altitude dependent failure rate

upto 60 km is obtained using the neutron spectrum from EXPACS database. In addition, the cutoff energy dependence on failure rate also briefly discussed.

List of Figures

References

[1] E. A. Underwood, "Wilhelm Conrad Röntgen (1845–1923) and the Early Development of Radiology," *Proceedings of the Royal Society of Medicine*, vol. 38, no. 12, pp. 697–706, Oct. 1945, doi: 10.1177/003591574503801214.

[2] J. T. Wallmark and S. M. Marcus, "Minimum Size and Maximum Packing Density of Nonredundant Semiconductor Devices," *Proceedings of the IRE*, vol. 50, no. 3, pp. 286–298, Mar. 1962, doi: 10.1109/JRPROC.1962.288321.

[3] D. Binder, E. C. Smith, and A. B. Holman, "Satellite Anomalies from Galactic Cosmic Rays," *IEEE Transactions on Nuclear Science*, vol. 22, no. 6, pp. 2675–2680, Dec. 1975, doi: 10.1109/TNS.1975.4328188.

[4] T. C. May and M. H. Woods, "Alpha-particle-induced soft errors in dynamic memories," *IEEE Transactions on Electron Devices*, vol. 26, no. 1, pp. 2–9, Jan. 1979, doi: 10.1109/T-ED.1979.19370.

[5] J. C. Pickel and J. T. Blandford, "Cosmic Ray Induced in MOS Memory Cells," *IEEE Transactions on Nuclear Science*, vol. 25, no. 6, pp. 1166–1171, Dec. 1978, doi: 10.1109/TNS.1978.4329508.

[6] C. S. Guenzer, E. A. Wolicki, and R. G. Allas, "Single Event Upset of Dynamic Rams by Neutrons and Protons," *IEEE Transactions on Nuclear Science*, vol. 26, no. 6, pp. 5048–5052, Dec. 1979, doi: 10.1109/TNS.1979.4330270.

[7] R. C. Wyatt, P. J. McNulty, P. Toumbas, P. L. Rothwell, and R. C. Filz, "Soft Errors Induced by Energetic Protons," *IEEE Transactions on Nuclear Science*, vol. 26, no. 6, pp. 4905–4910, Dec. 1979, doi: 10.1109/TNS.1979.4330248.

[8] W. A. Kolasinski, J. B. Blake, J. K. Anthony, W. E. Price, and E. C. Smith, "Simulation of Cosmic-Ray Induced Soft Errors and Latchup in Integrated-Circuit Computer Memories," *IEEE Transactions on Nuclear Science*, vol. 26, no. 6, pp. 5087–5091, Dec. 1979, doi: 10.1109/TNS.1979.4330278.

[9] "James Ziegler - SRIM & TRIM." http://srim.org/ (accessed Oct. 21, 2021).

[10] "The official FLUKA site: FLUKA home." http://www.fluka.org/fluka.php (accessed Oct. 21, 2021).

[11] J. Allison *et al.*, "Geant4 developments and applications," *IEEE Trans. Nucl. Sci.*, vol. 53, no. 1, pp. 270–278, Feb. 2006, doi: 10.1109/TNS.2006.869826.

[12] W. R. Leo and LEO, *Techniques for Nuclear and Particle Physics Experiments: A How-To Approach*. Springer Science & Business Media, 1994.

[13] T. Oldham and F. B. McLean, "Total ionizing dose effects in MOS oxides and devices," 2003, doi: 10.1109/TNS.2003.812927.

[14] J. F. Ziegler, "Terrestrial cosmic rays," *IBM J. Res. & Dev.*, vol. 40, no. 1, pp. 19–39, Jan. 1996, doi: 10.1147/rd.401.0019.

[15] "IEC 62396-1:2016 | IEC Webstore." https://webstore.iec.ch/publication/24053 (accessed Nov. 12, 2021).

[16] A. Taber and E. Normand, "Single event upset in avionics," *IEEE Transactions on Nuclear Science*, vol. 40, no. 2, pp. 120–126, Apr. 1993, doi: 10.1109/23.212327.

[17] E. S. Light, M. Merker, H. J. Verschell, R. B. Mendell, and S. A. Korff, "Time dependent worldwide distribution of atmospheric neutrons and of their products: 2. Calculation," *J. Geophys. Res.*, vol. 78, no. 16, pp. 2741–2762, Jun. 1973, doi: 10.1029/JA078i016p02741.

[18] E. Normand and T. J. Baker, "Altitude and latitude variations in avionics SEU and atmospheric neutron flux," *IEEE Trans. Nucl. Sci.*, vol. 40, no. 6, pp. 1484–1490, Dec. 1993, doi: 10.1109/23.273514.

[19] Y. Uwamino, T. Nakamura, and A. Hara, "Two types of multi-moderator neutron spectrometers: Gamma-ray insensitive type and high-efficiency type," *Nuclear Instruments and Methods in Physics Research Section A: Accelerators, Spectrometers, Detectors and Associated Equipment*, vol. 239, no. 2, pp. 299–309, Sep. 1985, doi: 10.1016/0168-9002(85)90730-2.

[20] P. Goldhagen, J. M. Clem, and J. W. Wilson, "The energy spectrum of cosmic-ray induced neutrons measured on an airplane over a wide range of altitude and latitude," *Radiation Protection Dosimetry*, vol. 110, no. 1–4, pp. 387–392, Aug. 2004, doi: 10.1093/rpd/nch216.

[21] P. Goldhagen *et al.*, "Measurement of the energy spectrum of cosmic-ray induced neutrons aboard an ER-2 high-altitude airplane," *Nuclear Instruments and Methods in Physics Research Section A: Accelerators, Spectrometers, Detectors and Associated Equipment*, vol. 476, no. 1–2, pp. 42–51, Jan. 2002, doi: 10.1016/S0168-9002(01)01386-9.

[22] F. Lei, A. Hands, S. Clucas, C. Dyer, and P. Truscott, "Improvement to and Validations of the QinetiQ Atmospheric Radiation Model (QARM)," *IEEE Transactions on Nuclear Science*, vol. 53, no. 4, pp. 1851–1858, Aug. 2006, doi: 10.1109/TNS.2006.880567.

[23] M. S. Gordon *et al.*, "Measurement of the flux and energy spectrum of cosmic-ray induced neutrons on the ground," *IEEE Trans. Nucl. Sci.*, vol. 51, no. 6, pp. 3427–3434, Dec. 2004, doi: 10.1109/TNS.2004.839134.

[24] T. Nakamura, T. Nunomiya, S. Abe, K. Terunuma, and H. Suzuki, "Sequential Measurements of Cosmic-Ray Neutron Spectrum and Dose Rate at Sea Level in Sendai, Japan," *Journal of Nuclear Science and Technology*, vol. 42, no. 10, pp. 843–853, Oct. 2005, doi: 10.1080/18811248.2005.9711035.

[25] M. Kowatari, Y. Ohta, S. Satoh, K. Nagaoka, J. Abukawa, and T. Nakamura, "Evaluation of Geomagnetic Latitude Dependence of the Cosmic-ray Induced Environmental Neutrons in Japan," *Journal of Nuclear Science and Technology*, vol. 44, no. 2, pp. 114–120, Feb. 2007, doi: 10.1080/18811248.2007.9711264.

[26] B. Wiegel and A. V. Alevra, "NEMUS—the PTB Neutron Multisphere Spectrometer: Bonner spheres and more," *Nuclear Instruments and Methods in Physics Research Section A: Accelerators, Spectrometers, Detectors and Associated Equipment*, vol. 476, no. 1–2, pp. 36–41, Jan. 2002, doi: 10.1016/S0168-9002(01)01385-7.

[27] A. E. Waskiewicz, J. W. Groninger, V. H. Strahan, and D. M. Long, "Burnout of Power MOS Transistors with Heavy Ions of Californium-252," *IEEE Trans. Nucl. Sci.*, vol. 33, no. 6, pp. 1710–1713, 1986, doi: 10.1109/TNS.1986.4334670.

[28] E. G. Stassinopoulos, G. J. Brucker, P. Calvel, A. Baiget, C. Peyrotte, and R. Gaillard, "Charge generation by heavy ions in power MOSFETs, burnout space predictions and dynamic SEB sensitivity," *IEEE Transactions on Nuclear Science*, vol. 39, no. 6, pp. 1704–1711, Dec. 1992, doi: 10.1109/23.211357.

[29] G. J. Brucker, P. Measel, D. Oberg, J. Wert, and T. Criswell, "SEU Sensitivity of Power Converters with MOSFETs in Space," *IEEE Transactions on Nuclear Science*, vol. 34, no. 6, pp. 1792–1795, Dec. 1987, doi: 10.1109/TNS.1987.4337556.

[30] D. L. Oberg and J. L. Wert, "First Nondestructive Measurements of Power MOSFET Single Event Burnout Cross Sections," *IEEE Trans. Nucl. Sci.*, vol. 34, no. 6, pp. 1736–1741, 1987, doi: 10.1109/TNS.1987.4337546.

[31] T. A. Fischer, "Heavy-Ion-Induced, Gate-Rupture in Power MOSFETs," *IEEE Transactions on Nuclear Science*, vol. 34, no. 6, pp. 1786–1791, Dec. 1987, doi: 10.1109/TNS.1987.4337555.

[32] A. K. Richter and I. Arimura, "Simulation of Heavy Charged Particle Tracks Using Focused Laser Beams," *IEEE Transactions on Nuclear Science*, vol. 34, no. 6, pp. 1234–1239, Dec. 1987, doi: 10.1109/TNS.1987.4337458.

[33] T. F. Wrobel, F. N. Coppage, G. L. Hash, and A. J. Smith, "Current Induced Avalanche in Epitaxial Structures," *IEEE Transactions on Nuclear Science*, vol. 32, no. 6, pp. 3991–3995, Dec. 1985, doi: 10.1109/TNS.1985.4334056.

[34] J. H. Hohl and K. F. Galloway, "Analytical Model for Single Event Burnout of Power MOSFETs," *IEEE Transactions on Nuclear Science*, vol. 34, no. 6, pp. 1275–1280, Dec. 1987, doi: 10.1109/TNS.1987.4337465.

[35] J. H. Hohl and G. H. Johnnson, "Features of the triggering mechanism for single event burnout of power MOSFETs," *IEEE Transactions on Nuclear Science*, vol. 36, no. 6, pp. 2260–2266, Dec. 1989, doi: 10.1109/23.45433.

[36] J. L. Titus, L. S. Jamiolkowski, and C. F. Wheatley, "Development of cosmic ray hardened power MOSFET's," *IEEE Transactions on Nuclear Science*, vol. 36, no. 6, pp. 2375–2382, Dec. 1989, doi: 10.1109/23.45451.

[37] J. L. Titus, G. H. Johnson, R. D. Schrimpf, and K. F. Galloway, "Single-event burnout of power bipolar junction transistors," *IEEE Transactions on Nuclear Science*, vol. 38, no. 6, pp. 1315–1322, Dec. 1991, doi: 10.1109/23.124111.

[38] S. Kuboyama, S. Matsuda, T. Kanno, and T. Ishii, "Mechanism for single-event burnout of power MOSFETs and its characterization technique," *IEEE Trans. Nucl. Sci.*, vol. 39, no. 6, pp. 1698–1703, Dec. 1992, doi: 10.1109/23.211356.

[39] R. J. McNulty, W. J. Beavais, and D. R. Roth, "Determination of SEU parameters of NMOS and CMOS SRAMs," *IEEE Transactions on Nuclear Science*, vol. 38, no. 6, pp. 1463–1470, 1991.

[40] F. W. Sexton, "Microbeam studies of single-event effects," *IEEE Transactions on Nuclear Science*, vol. 43, no. 2, pp. 687–695, Apr. 1996, doi: 10.1109/23.490912.

[41] H. Asai *et al.*, "Tolerance Against Terrestrial Neutron-Induced Single-Event Burnout in SiC MOSFETs," *IEEE Trans. Nucl. Sci.*, vol. 61, no. 6, pp. 3109–3114, Dec. 2014, doi: 10.1109/TNS.2014.2371892.

[42] A. F. Witulski *et al.*, "Single-Event Burnout Mechanisms in SiC Power MOSFETs," *IEEE Transactions on Nuclear Science*, vol. 65, no. 8, pp. 1951–1955, Aug. 2018, doi: 10.1109/TNS.2018.2849405.

[43] D. R. Ball *et al.*, "Ion-Induced Energy Pulse Mechanism for Single-Event Burnout in High-Voltage SiC Power MOSFETs and Junction Barrier Schottky Diodes," *IEEE Transactions on Nuclear Science*, vol. 67, no. 1, pp. 22–28, Jan. 2020, doi: 10.1109/TNS.2019.2955922.

[44] Q. Li *et al.*, "Study on single-event burnout of SiC VDMOSFET: failure mechanism and influence factors," in *2019 20th International Conference on Electronic Packaging Technology(ICEPT)*, Aug. 2019, pp. 1–5. doi: 10.1109/ICEPT47577.2019.245733.

[45] X. Zhou *et al.*, "Single-Event Effects in SiC Double-Trench MOSFETs," *IEEE Transactions on Nuclear Science*, vol. 66, no. 11, pp. 2312–2318, Nov. 2019, doi: 10.1109/TNS.2019.2944944.

[46] C. Martinella *et al.*, "Impact of Terrestrial Neutrons on the Reliability of SiC VD-MOSFET Technologies," *IEEE Transactions on Nuclear Science*, vol. 68, no. 5, pp. 634–641, May 2021, doi: 10.1109/TNS.2021.3065122.

[47] P. T. McDonald, B. G. Henson, W. J. Stapor, and M. Harris, "Destructive heavy ion SEE investigation of 3 IGBT devices," in *2000 IEEE Radiation Effects Data Workshop. Workshop Record. Held in conjunction with IEEE Nuclear and Space Radiation Effects Conference (Cat. No.00TH8527)*, Jul. 2000, pp. 11–15. doi: 10.1109/REDW.2000.896262.

[48] T. Shoji *et al.*, "Neutron induced single-event burnout of IGBT," in *The 2010 International Power Electronics Conference - ECCE ASIA -*, Sapporo, Japan, Jun. 2010, pp. 142–148. doi: 10.1109/IPEC.2010.5543845.

[49] M. Zerarka, P. Austin, and M. Bafleur, "Cosmic ray immunity of new IGBT structures for aerospace application," in *CAS 2011 Proceedings (2011 International Semiconductor Conference)*, Sinaia, Romania, Oct. 2011, pp. 305–308. doi: 10.1109/SMICND.2011.6095800.

[50] L. L. Foro, A. D. Touboul, F. Wrobel, and F. Saigne, "Development of Monte Carlo Modeling for Neutron-Induced Failures of Trench FieldStop IGBT," *IEEE Trans. Nucl. Sci.*, vol. 58, no. 6, pp. 2748–2754, Dec. 2011, doi: 10.1109/TNS.2011.2172631.

[51] H. Kabza *et al.*, "Cosmic radiation as a cause for power device failure and possible countermeasures," in *Proceedings of the 6th International Symposium on Power Semiconductor Devices and Ics*, Davos, Switzerland, 1994, pp. 9–12. doi: 10.1109/ISPSD.1994.583620.

[52] H. Matsuda, T. Fujiwara, M. Hiyoshi, K. Nishitani, A. Kuwako, and T. Ikehara, "Analysis of GTO failure mode during DC voltage blocking," in *Proceedings of the 6th International Symposium on Power Semiconductor Devices and Ics*, Davos, Switzerland, 1994, pp. 221–225. doi: 10.1109/ISPSD.1994.583727.

[53] H. R. Zeller, "Cosmic ray induced breakdown in high voltage semiconductor devices, microscopic model and phenomenological lifetime prediction," in *Proceedings of the 6th International Symposium on Power Semiconductor Devices and Ics*, Davos, Switzerland, 1994, pp. 339–340. doi: 10.1109/ISPSD.1994.583762.

[54] P. Voss *et al.*, "Irradiation experiments with high-voltage power devices as a possible means to predict failure rates due to cosmic rays," in *Proceedings of 9th International Symposium on Power Semiconductor Devices and IC's*, Weimar, Germany, 1997, pp. 169–172. doi: 10.1109/ISPSD.1997.601462.

[55] G. Busatto, F. Iannuzzo, J. Wyss, D. Pantano, and D. Bisello, "Effects of heavy ion impact on power diodes," in *1999 Fifth European Conference on Radiation and Its Effects on Components and Systems. RADECS 99 (Cat. No.99TH8471)*, Sep. 1999, pp. 205–209. doi: 10.1109/RADECS.1999.858581.

[56] K. H. Maier, A. Denker, P. Voss, and H.-W. Becker, "Single event burnout of high-power diodes," *Nuclear Instruments and Methods in Physics Research Section B: Beam Interactions with Materials and Atoms*, vol. 146, no. 1–4, pp. 596–600, Dec. 1998, doi: 10.1016/S0168-583X(98)00436-4.

[57] G. Soelkner, P. Voss, W. Kaindl, G. Wachutka, K. H. Maier, and H.-W. Becker, "Charge carrier avalanche multiplication in high-voltage diodes triggered by ionizing radiation," *IEEE Trans. Nucl. Sci.*, vol. 47, no. 6, pp. 2365–2372, Dec. 2000, doi: 10.1109/23.903778.

[58] E. Normand, J. L. Wert, D. L. Oberg, P. R. Majewski, P. Voss, and S. A. Wender, "Neutron-induced single event burnout in high voltage electronics," *IEEE Transactions on Nuclear Science*, vol. 44, no. 6, pp. 2358–2366, Dec. 1997, doi: 10.1109/23.659062.

[59] E. Normand, J. L. Wert, P. P. Majewski, and P. Voss, "Neutron-Induced Single Event Burnout in High Volta," p. 9.

[60] A. Hallen, H. Bleichner, and K. Nordgren, "Cosmic ray-induced DC-stability failure in Si diodes," in *Proceedings of 9th International Symposium on Power Semiconductor Devices and IC's*, Weimar, Germany, 1997, pp. 121–124. doi: 10.1109/ISPSD.1997.601450.

[61] W. Kaindl, G. Solkner, and G. Wachutka, "Analysis of charge carrier multiplication events in NPT and PT-diodes triggered by an ionizing particle," in *2003 IEEE Conference on Electron Devices and Solid-State Circuits (IEEE Cat. No.03TH8668)*, Dec. 2003, pp. 383–386. doi: 10.1109/EDSSC.2003.1283555.

[62] H. Egawa, "Avalanche characteristics and failure mechanism of high voltage diodes," *IEEE Transactions on Electron Devices*, vol. ED-13, no. 11, pp. 754–758, Nov. 1966, doi: 10.1109/T-ED.1966.15838.

[63] A. M. Albadri, R. D. Schrimpf, D. G. Walker, and S. V. Mahajan, "Coupled electro-thermal Simulations of single event burnout in power diodes," *IEEE Trans. Nucl. Sci.*, vol. 52, no. 6, pp. 2194–2199, Dec. 2005, doi: 10.1109/TNS.2005.860691.

[64] H. Asai *et al.*, "Terrestrial Neutron-Induced Single-Event Burnout in SiC Power Diodes," *IEEE Trans. Nucl. Sci.*, vol. 59, no. 4, pp. 880–885, Aug. 2012, doi: 10.1109/TNS.2012.2203145.

[65] T. Shoji, S. Nishida, K. Hamada, and H. Tadano, "Experimental and simulation studies of neutron-induced single-event burnout in SiC power diodes," *Jpn. J. Appl. Phys.*, vol. 53, no. 4S, p. 04EP03, Jan. 2014, doi: 10.7567/JJAP.53.04EP03.

[66] "IEC 62396-2:2017 | IEC Webstore." https://webstore.iec.ch/publication/27921 (accessed Nov. 12, 2021).

[67] S. P. Buchner *et al.*, "Laser Simulation of Single Event Upsets," *IEEE Transactions on Nuclear Science*, vol. 34, no. 6, pp. 1227–1233, Dec. 1987, doi: 10.1109/TNS.1987.4337457.

[68] H. R. Zeller, "Cosmic ray induced failures in high power semiconductor devices," *Microelectronics Reliability*, vol. 37, no. 10–11, pp. 1711–1718, Oct. 1997, doi: 10.1016/S0026-2714(97)00146-7.

[69] H. R. Zeller, "Cosmic ray induced failures in high power semiconductor devices," *Solid-State Electronics*, vol. 38, no. 12, pp. 2041–2046, Dec. 1995, doi: 10.1016/0038-1101(95)00082-5.

[70] E. Dashdondog, S. Harada, Y. Shiba, and I. Omura, "Failure rate calculation method for high power devices in space applications at low earth orbit," *Microelectronics Reliability*, vol. 64, pp. 502–506, Sep. 2016, doi: 10.1016/j.microrel.2016.07.114.

[71] Y. Shiba, E. Dashdondog, M. Sudo, and I. Omura, "Formulation of single event burnout failure rate for high voltage devices in satellite electrical power system," in *2017 29th International Symposium on Power Semiconductor Devices and IC's (ISPSD)*, Sapporo, Japan, May 2017, pp. 167–170. doi: 10.23919/ISPSD.2017.7988937.

[72] M. Sudo, T. Nagamatsu, M. Tsukuda, and I. Omura, "Calculation of single event burnout failure rate for high voltage devices under satellite orbit without fitting parameters," *Microelectronics Reliability*, vol. 100–101, p. 113396, Sep. 2019, doi: 10.1016/j.microrel.2019.07.001.

[73] S. Gollapudi and I. Omura, "Altitude dependent failure rate calculation for high power semiconductor devices in aviation electronics," *Jpn. J. Appl. Phys.*, vol. 60, no. SB, p. SBBD19, Apr. 2021, doi: 10.35848/1347-4065/abebc0.

[74] B. Doucin *et al.*, "Characterization of proton interactions in electronic components," *IEEE Trans. Nucl. Sci.*, vol. 41, no. 3, pp. 593–600, Jun. 1994, doi: 10.1109/23.299805.

[75] B. Doucin, T. Carriere, C. Poivey, P. Garnier, J. Beaucour, and Y. Patin, "Model of single event upsets induced by space protons in electronic devices," in *Proceedings of the Third European Conference on Radiation and its Effects on Components and Systems*, Arcachon, France, 1996, pp. 402–408. doi: 10.1109/RADECS.1995.509810.

[76] P. Truscott, C. Dyer, A. Frydland, A. Hands, S. Clucas, and K. Hunter, "Neutron Energy-Deposition Spectra Measurements, and Comparisons with Geant4 Predictions," in *2005 8th European Conference on Radiation and Its Effects on Components and Systems*, Cap d'Agde, France, Sep. 2005, pp. LN11-1-LN11-6. doi: 10.1109/RADECS.2005.4365664.

[77] "EXPACS Homepage in English." https://phits.jaea.go.jp/expacs/ (accessed Feb. 03, 2021).

[78] M. Cecchetto *et al.*, "SEE Flux and Spectral Hardness Calibration of Neutron Spallation and Mixed-Field Facilities," *IEEE Trans. Nucl. Sci.*, vol. 66, no. 7, pp. 1532–1540, Jul. 2019, doi: 10.1109/TNS.2019.2908067.

[79] H. Quinn, A. Watkins, L. Dominik, and C. Slayman, "The Effect of 1–10-MeV Neutrons on the JESD89 Test Standard," *IEEE Trans. Nucl. Sci.*, vol. 66, no. 1, pp. 140–147, Jan. 2019, doi: 10.1109/TNS.2018.2884908.

List of Publications

1. S. Gollapudi and I. Omura, "Altitude dependent failure rate calculation for high power semiconductor devices in aviation electronics," *Jpn. J. Appl. Phys.*, vol. 60, no. SB, p. SBBD19, Apr. 2021, doi: 10.35848/1347-4065/abebc0.

2. S. Gollapudi and I. Omura, "Cosmic ray failure rate calculation for Power semiconductor devices for Aircraft applications", The Paper of Joint Technical Meeting on "Electron Devices" and "Semiconductor Power Converter", EDD-20-069, SPC-20-219, pp.25-28 in Japanese (2020).

3. S. Gollapudi and I. Omura, "Altitude dependent failure rate calculation for high power semiconductor devices in aviation electronics", International conference on Solid State Devices and Materials, D9-06, pp. 275-276, 2020.

4. S. Gollapudi and I. Omura, "SEB Failure rate calculation for High Power Semiconductor Devices due to neutrons at aviation altitude", 8th International Symposium on Applied Engineering and Sciences, C000193, 2020.

5. S. Gollapudi and I. Omura, "Influence of maximum cutoff energy of neutron spectrum on SEB failure rate", 9th International Symposium on Applied Engineering and Sciences, ET36, 2021.

About the author

Srikanth gollapudi was born in Andhra Pradesh, India on 18 November 1988. He received Bachelor degree in Electrical and Electronics engineering from Jawaharlal Nehru Technological University, Kakinada, Andhra Pradesh in 2009 and Master degree in Electrical Machines and Drives from Indian Institute of Technology, Banaras Hindu University (IIT-BHU) in 2012. He worked as lecturer in Mangalayatan University, Aligarh until April 2013. After that worked as Assistant professor in Vellore Institute of Technology, Chennai from May 2013 to March 2019. From April 2019, he has been a doctoral student in Graduate School of Life Sciences and Systems Engineering, Kyushu Institute of Technology in Japan.